POLITECNICO DI MILANO

Scuola di Ingegneria dell'Informazione

Corso di Laurea Magistrale in
Ingegneria dell'Automazione

Modelling and simulation of desiccant wheels for the design and control of energy efficient air handling units

Modellistica e simulazione di ruote entalpiche per il progetto e il controllo di unità di trattamento aria energeticamente efficienti

Relatore: Prof. Alberto LEVA
Correlatore: Ing. Marco BONVINI

Tesi di Laurea Magistrale di:
Erica ZAVAGLIO
Matr. 770085

Anno Accademico 2011 - 2012

Ringraziamenti

Desidero ringraziare quanti hanno contributo direttamente o indirettamente alla realizzazione di questo lavoro.

In particolare ringrazio il Professor Alberto Leva per avermi dato la possibilità di impegnarmi in questo progetto e per la sua disponibilità, e l'Ingegner Marco Bonvini che è stato per me un punto di riferimento durante il lavoro e si è dimostrato sempre presente e disponibile.

Inoltre ringrazio la mia famiglia, i miei amici e i miei compagni di corso che hanno condiviso con me parte di questa esperienza e mi hanno sempre sostenuta.

Contents

Abstract

This dissertation, that is part of a longer-term research on energy efficiency, deals with dynamic modelling and simulation of desiccant wheels, having as primary (yet in principle not exclusive) goal that of employing such devices to improve the efficiency of air handling units.

To this end, first the theory of operation of desiccant wheels is analyzed, having however in mind that the particular purpose of the presented research requires dynamic models oriented to system-level studies, that will eventually come to comprise and consider also the control system. In other words, a peculiarity of the model developed herein, thus a contribution of the presented work, is that the developed model has to find a suitable compromise among several different - and sometimes conflicting - objectives, such as accuracy, ease of parametrization with design/nominal data, which incidentally calls for a first-principle approach, and numerical efficiency.

The results obtained in this work can be briefly summarized as follows.

- A dynamic model for a desiccant wheel is proposed that overcomes some limitations of these available to date in the literature, and a discussion is reported - based on a convenient brief review of related work - to justify the statement above.
- A Modelica implementation of that model is presented and validated against data available in the literature. Also, the so obtained simulation model allows to investigate some aspects of the wheel operation that are exquisitely dynamic, thereby paving the way to the control-oriented studies sketched out below.
- Some possibilities are envisioned for the use of desiccant wheels in air handling units, viewing the addition of the wheel - that quite intuitively is not a novelty *perse* - from an essentially control-centric standpoint. This allows to sketch out some guidelines, to be further investigated in future works, for an objective assessment of the achievable energy efficiency improvements.

Sommario

Questa tesi, che fa parte di una ricerca più ampia e di lungo periodo sull' efficienza energetica, si occupa di modellistica dinamica e simulazione di ruote entalpiche, avendo come obiettivo primario (ma in linea di principio non unico) quello di impiegare tali dispositivi per migliorare l'efficienza delle unità di trattamento aria (UTA).

A tale scopo, per prima cosa viene analizzata la teoria di funzionamento delle ruote entalpiche, avendo però presente che il particolare ambito della ricerca presentata richiede modelli dinamici per studi a livello di sistema che includono anche il sistema di controllo. In altre parole, una peculiarità del modello qui sviluppato, quindi un contributo del lavoro presentato, è che tale modello deve trovare un adeguato compromesso tra diversi - e talvolta contrastanti - obiettivi, quali la precisione, la facilità di parametrizzazione utilizzando dati di progetto e/o nominali, il che richiede un approccio basato su principi primi, e l'efficienza numerica.

I risultati ottenuti in questo lavoro possono essere brevemente riassunti come segue.

• Viene proposto un modello dinamico per una ruota entalpica che permette di superare alcuni limiti dei modelli disponibili fino ad oggi in letteratura, e viene riportata una discussione - sulla base di una breve revisione del lavoro già esistente - per giustificare la realizzazione di un nuovo modello.

• Una implementazione Modelica del modello proposto è presentata e validata con i dati disponibili in letteratura. Il modello così ottenuto permette di approfondire alcuni aspetti del funzionamento della ruota che sono squisitamente dinamici, preparando così il terreno per studi orientati al controllo qui di seguito introdotti.

• Vengono discusse alcune possibilità per l'uso di ruote entalpiche in unità di trattamento aria, considerando l'aggiunta della ruota - che intuitivamente non è una novità di per sé - da un punto di vista essenzialmente di controllo. Questo permette di delineare alcune linee guida, che saranno ulteriormente approfondite nei lavori futuri, per una valutazione oggettiva dei miglioramenti ottenibili dal punto di vista dell' efficienza energetica.

In particolare, nel primo capitolo viene introdotto il contesto in cui questo lavoro si inserisce e vengono presentati in maniera sintetica i sistemi di condizionamento dell'aria usati negli edifici e il loro funzionamento. Viene inoltre messo in evidenza il possibile risparmio energetico dato dall'uso delle ruote entalpiche. Nel secondo capitolo viene illustrato il funzionamento delle ruote entalpiche e sono presentate alcune configurazioni di unità di trattamento aria che prevedono l'uso di tali elementi.

Il terzo capitolo è dedicato a una breve presentazione di alcuni modelli di ruote entalpiche presenti in letteratura, in particolare vengono presi in considerazione alcuni modelli di primo principio implementati in linguaggio Modelica e alcuni modelli empirici. Il quarto capitolo illustra il modello proposto in questo lavoro mettendo in evidenza le principali scelte modellistiche che lo differenziano dai modelli finora proposti. Particolare attenzione viene posta alla rappresentazione del movimento della ruota che risulta essere un elemento particolarmente importante per l'aderenza del modello alla realtà fisica. La scelta della modellizzazione della velocità della ruota mediante un "flusso di materiale", ci permette inoltre di tenere conto in maniera semplice ed intuitiva di fenomeni fisici altrimenti difficilmente rappresentabili. Tale modello è validato attraverso dati sperimentali presenti in letteratura (quinto capitolo) con i quali viene riscontrata una buona aderenza.

Nel sesto capitolo vengono presentati alcuni risultati di simulazioni per mettere in evidenza la bontà del modello. In particolare, viene illustrata la distribuzione spaziale dei parametri di interesse (temperatura e umidità) e viene inoltre riportata un' analisi parametrica atta a identificare la variazione del comportamento della ruota al variare delle condizioni di funzionamento.

Il tema del risparmio energetico è trattato nello specifico nel settimo capitolo, in cui vengono messi a punto i sistemi di controllo sia per l' UTA standard che per quella con ruota entalpica in modo da poter confrontare la domanda energetica delle due configurazioni nelle stesse condizioni operative. Nell'ottavo capitolo vengono illustrate alcune possibilità di controllo alternative che prevedono l'uso della velocità della ruota come variabile di controllo. Nello stesso capitolo viene anche proposta una strategia di controllo di temperatura basata sull'utilizzo, come variabile manipolabile, della velocità della ruota.

Nel nono capitolo sono presentati alcuni risultati di simulazione che illustrano i consumi energetici dell'UTA in funzione della velocità della ruota in varie condizioni operative. Viene quindi proposto un metodo per la scelta della velocità della ruota in modo da minimizzare il consumo energetico dell'UTA, sia nel caso generale che in quello in cui si possa usufruire di fonti di calore di bassa qualità e/o a basso costo, come per esempio quelle legate a recuperi di calore "di scarto" oppure alle sorgenti rinnovabili.

L'ultimo capitolo è dedicato alle conclusioni e agli sviluppi futuri.

1 Background and motivation

The aim of this chapter is to introduce the reader to the HVAC (Heating, Ventilating and Air Conditioning) systems context, and to show the possible energy saving that can be obtained by using the desiccant wheel (DW) technology. In particular, this work is a part of a long-term research dealing with HVAC systems in buildings. Thus, a system level view on HVAC systems is enough to understand the motivation of our work. Energy saving is a crucial issue in the addressed context, and thus the use of new technologies to improve it, is increasing in interest. Desiccant wheel elements are one of the most promising technologies dealing with energy saving in HVAC systems. Thus, the need of a model of such an element, that is suitable for system design and diagnosis, appears clear. In the last part of this chapter, some simulations are shown to prove the possible energy saving with DWs.

1.1 Heating, Ventilating and Air Conditioning systems in buildings

The aim of HVAC systems in buildings is to preserve comfort conditions for human beings, a suitable operating environment for machines such as computers, or any combination thereof.

However, particularly when human comfort plays a relevant role, these conditions reveal a somehow subjective character, as they also depend on each single person's feelings, which in turn may be time-varying. In any case, comfort depends mainly on air temperature and humidity. Said quantities, thus need controlling, so as to fulfill constraints expressed in terms of the so-called PMV (predicted mean vote) index. The most typical constraint takes the form of (1.1):

$$-0.5 \leq PMV \leq 0.5 \tag{1.1}$$

The PMV index is defined by the ISO 7730 standard, and the comfort is maximum if its value is 0. If PMV is less than 0, a person tends to perceive the ambient as "cold", while if it is greater than 0, a person perceives the ambient as "warm". Hence, a comfort air conditions area can be defined as it is shown on the Psychrometric Chart in Fig. 1.1.

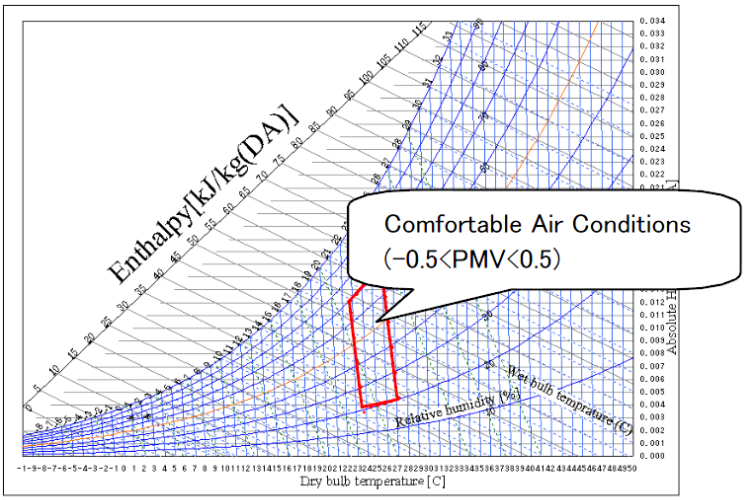

Figure 1.1: Comfort air conditions area on Psychrometric Chart.

There are many types of HVAC systems, and the choice of the best type for the particular case at hand, is a very important phase for the success of a project.

More specifically, when distinguishing types of HVAC systems, very important components from the viewpoint of both comfort and energy efficiency are the AHUs (Air Handling Units), on which we mainly concentrate.

1.2 Conventional Air Handling Unit

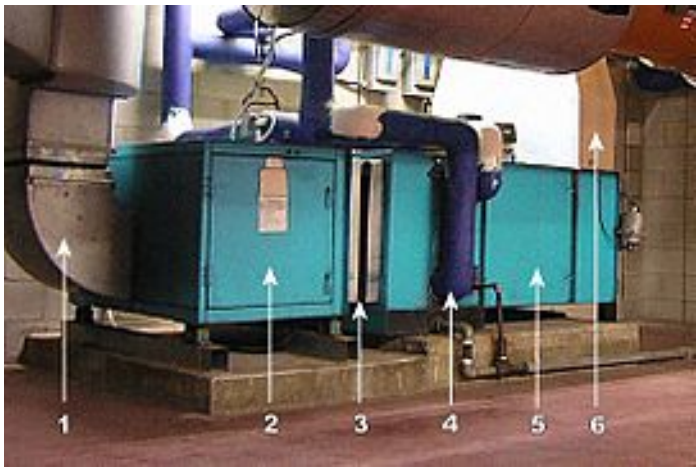

Figure 1.2: Air handling unit.

For our purpose, we first need to describe the structure and operation of "traditional" AHUs, i.e., in our context, of AHUs not comprising a DW. Such units are composed

of several elements, as shown in Fig. 1.2. The main elements are:

1. Supply duct
2. Fan compartment
3. Vibration isolator ("flex joint")
4. Heating and/or cooling coil
5. Filter compartment
6. Mixed (recirculated + outside) air duct

As shown in Fig. 1.3 in *conventional* AHUs (as opposite to *twin coil* ones described rater on) there exists only one cooling coil. This coil is devoted to heat exchange between chilled water and the heated air. The aim of this element is to remove sensible and latent heat from the air. Thus, the chilled water used for this purpose, has to be brought at a quite low temperature (typically around 7°C).

It should be noted that such a low temperature is required only for dehumidification. In fact, to remove moisture, the air has to be brought at a temperature lower than its dew point one. Thus, the chilled water temperature has to be considerably low. Conversely, to obtain the desired air temperature without condensation, a higher-temperature (around 15°C) chilled water would be enough. Therefore, a conventional AHU deals with very low chilled water temperature because of the condensation process. Clearly, after passing through the cooling coil, the air is at an excessively low temperature, and it has to be heated before entering the room.

In order to reduce energy consumption, due to the cooling of the water and the need to heat the cold air after the condensation process, there are several solutions that can be used.

One of such solutions consists of the use of a twin coil AHU, which is presented in the next section, but, as will be shown later on, the use of a desiccant wheel brings advantages also for the problem just mentioned.

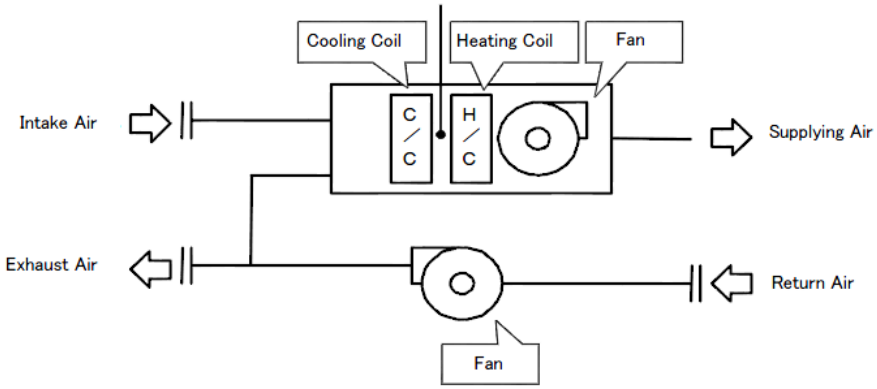

Figure 1.3: Conventional AHU plant scheme.

1.3 Twin Coil AHU

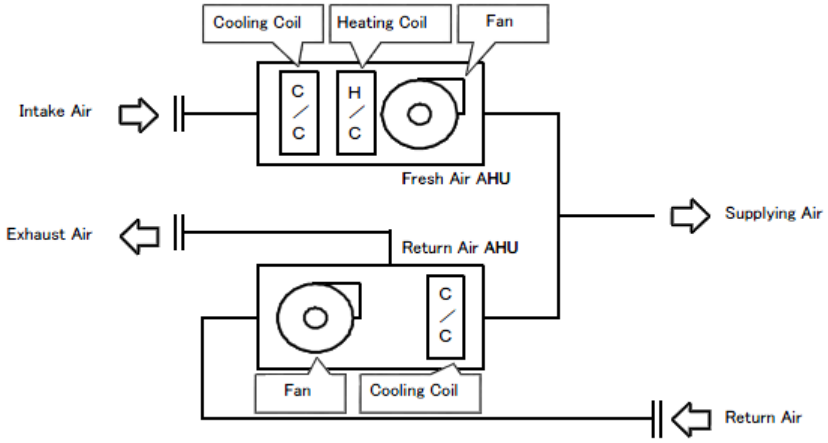

Figure 1.4: Twin coil AHU plant scheme.

The twin coil AHU structure is presented in [10] and shown in Fig. 1.4. With respect to the single coil (or conventional) one, the presence of a second cooling coil allows to use each coil with different purposes. One coil cools and dehumidifies the fresh air, using lower temperature chilled water, while the other coil is used to cool the room air, using higher temperature chilled water. As such, the most of the chilled water used here is at higher temperature with respect to that required by a conventional AHU. Thus, with the twin coil configuration we can obtain a smaller energy consumption according to the refrigeration cycle principle.

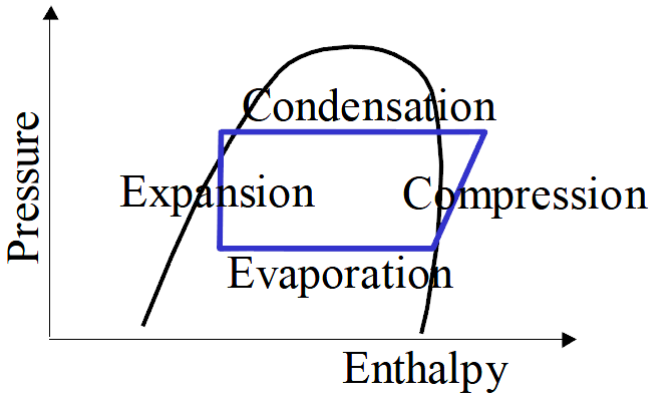

Figure 1.5: Refrigeration cycle.

In this respect, Fig. 1.5 shows the refrigeration cycle that is composed by four steps: compression, condensation, expansion and evaporation. The energy performance of such a cycle is typically quantified by the COP (Coefficient of Performance), defined as:

$$COP = \frac{Q_L}{W_{net,in}} \tag{1.2}$$

where Q_L is the cooling effect and $W_{net,in}$ is work input.

The amount of energy consumed in the process is approximately proportional to the difference between the evaporation and condensation pressures. It is also proportional to the temperature difference between the same two cycle phases. Thus, the energy consumption becomes smaller if the temperature difference between evaporation and condensation decreases. The condensation temperature is related to the cooling water temperature, while the evaporation temperature is related to the chilled water temperature. This implies that the higher the chilled water temperature is, and the lower the cooling water temperature is, then the smaller the energy consumption is.

1.4 AHU with desiccant wheel

The use of desiccant wheels in HVAC systems brings some relevant advantages:

- reduction of the refrigerating machine power;
- increase of the refrigerating machine evaporation temperature and COP;
- reduction of the thermal power consumption because the post-heating coil is not necessary anymore;

- reduction of the presence of microorganisms (like e.g. bacteria and fungi) because condensed water is absent;
- possibility to use low-temperature heat (50–60 °C) to activate the dehumidification process;
- improved flexibility in the use of renewable energies.

The DW behavior and the possible AHU configurations, comprising a DW, will be discussed more in detail in chapter 2. In this chapter, we only want to synthetically justify the increasing interest in the DW's technology, and underline the considerable energy saving that can be obtain with the use of a DW. To this end, we present in the next section, some simulation results from [13].

1.5 System energy performance

In this section, to show the relevance of the energy saving that can be obtained by using a DW, the performance of a standard AHU and that of a AHU with a DW are compared in reasonably realistic and operating conditions. The considered scenario is illustrated in [13]: the AHU is used for the air conditioning of an office (volume of 300 m^3: $10 \times 10 \times 30m$).

The external ambient and indoor air conditions can be viewed in this context as disturbances, which the control system has to reject. One of the most important specifications on the HVAC systems deals with the number of the air renewal per hour. In the presented configuration the AHU has to guarantee 4 air renewal per hour, thus, only one third of the return air has to be recirculated. The aim of the control system (working from 6:00 AM to 9:00 PM) is to maintain the air temperature at 26° C, and satisfy a variable requirement for the absolute humidity (between $12 - 14 g_{H2O}/kg_{DryAir}$). The external air temperature and humidity profiles are shown in Fig. 1.6 and Fig. 1.7, respectively the same figures also report the temperature and humidity set points. The air recirculated from the office has a temperature of 27° C, and its absolute humidity is $15 g_{H2O}/kg_{DryAir}$.

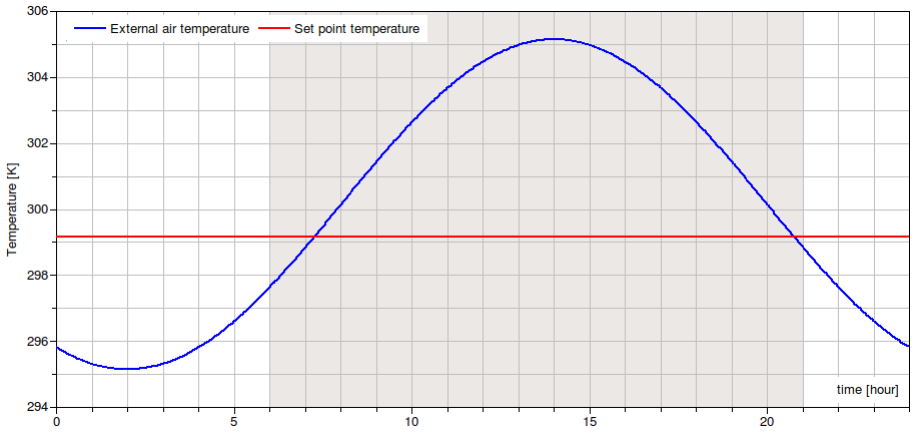

Figure 1.6: External air temperature and set point signal.

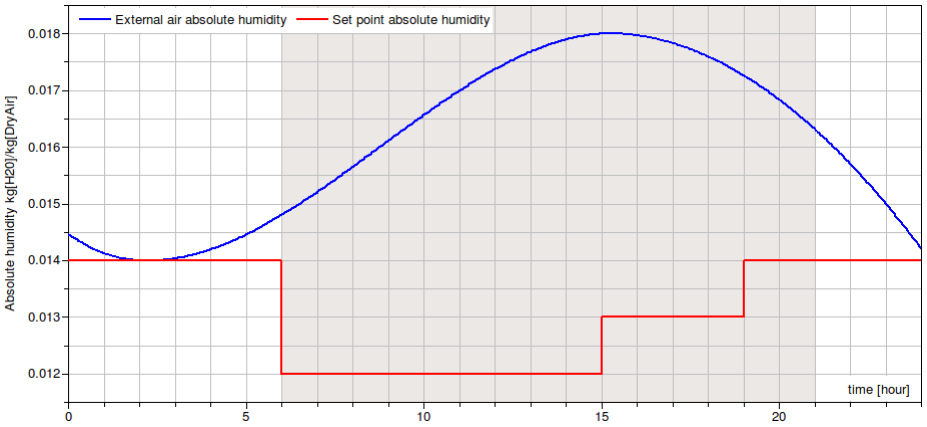

Figure 1.7: External absolute humidity and set point signal.

1.5.1 Traditional AHU

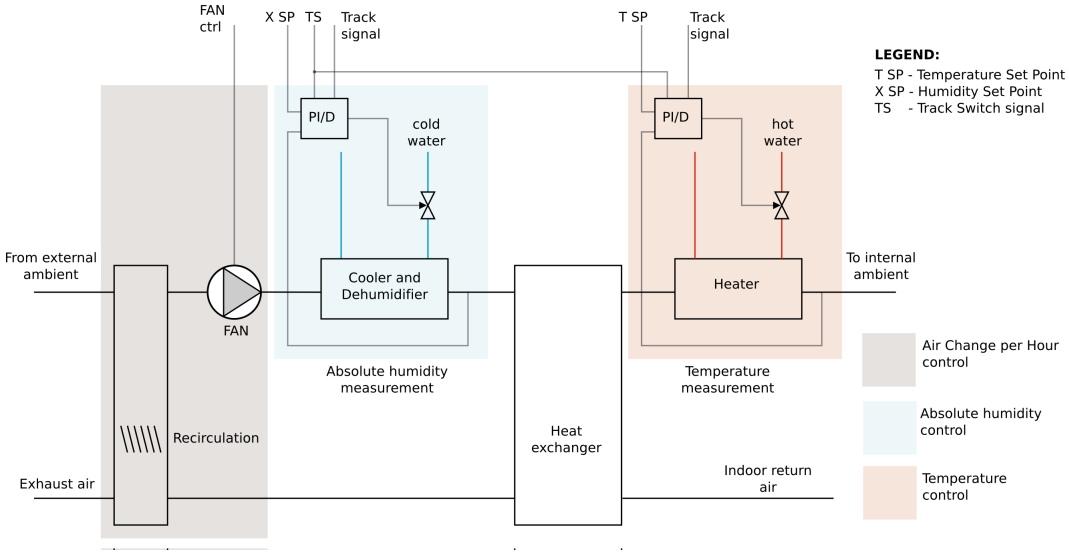

Figure 1.8: Scheme of a standard AHU with absolute humidity and temperature control loops.

In Fig. 1.8, the control scheme of a standard AHU is presented: the left (blue) and right (red) boxes respectively represent the humidity and temperature control systems.

The air from the external ambient is first cooled and dehumidified by a coil (with chilled water at 4° C). The absolute humidity is controlled by acting on the mass flow rate of chilled water used in that coil. The air, once it exits the cooler, has the desired moisture amount (thanks to the humidity control just mentioned), and its water vapor content remains the same while the air subsequently passes through a rotary heat exchanger. Then the air is heated with a second coil and, in the considered case, a temperature controller regulates the mass flow rate of hot water at 45° C. As shown before, humidity and temperature control can be treated separately (although they need addressing in the correct order), as the controlled system is triangular: after been dehumidified, the air is only heated until entering the room. In the presented configuration two PI controllers have been used, but is clear that humidity control affects temperature control.

1.5.2 AHU with desiccant wheel

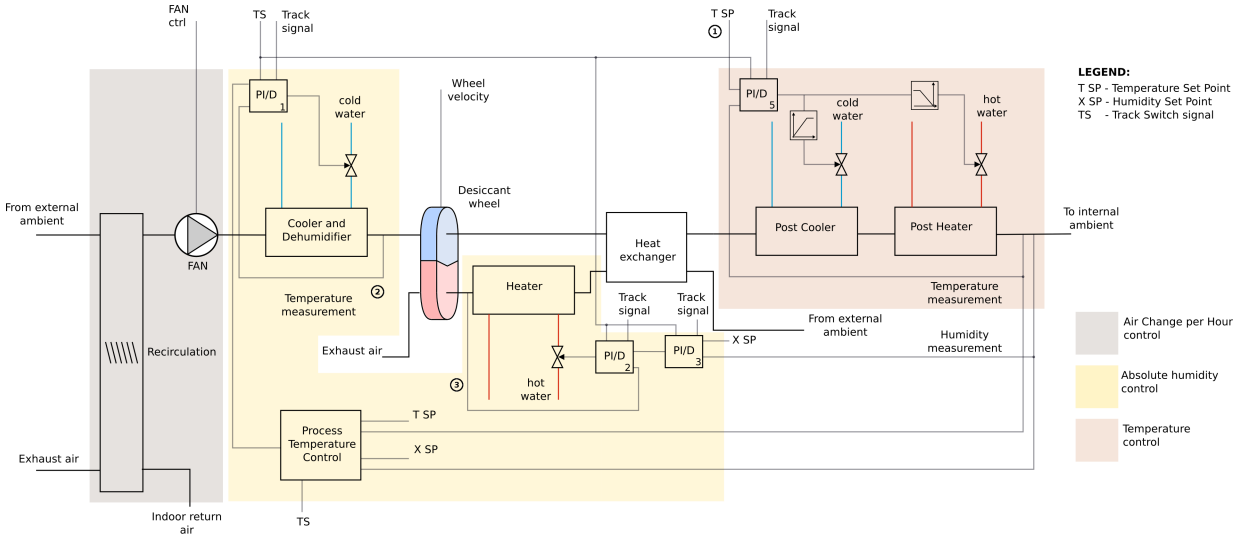

Figure 1.9: Control scheme for humidity and temperature control of an AHU with a DW.

In Fig. 1.9, an AHU configuration with a DW is shown. The external ambient air, mixed with some recirculation air, is first pre-cooled in a cooler/dehumidifier, and than enters the DW, where it is dehumidified and heated. Downstream the wheel, the air passes through a heat exchanger, and then, it is post-cooled/heated depending on the desired conditions. A second airflow is necessary to regenerate the wheel, as will be discussed in sec. 2.2. This regeneration air, coming from the internal ambient, first passes through the heat exchanger, and then is heated before entering the wheel. The L-shaped (yellow) box identifies the humidity control system, which regulates both the process and regeneration air temperature. This is because the desorption capacity of the wheel depends on both temperatures. The right (red) box identifies the air temperature control. The wheel velocity is considered as a parameter, and set to 3rev/hour . The AHU with DW configuration will be discussed more in detail in the following chapters.

1.5.3 Energy consumptions

With both the configurations (standard AHU and AHU with DW) we can obtain good results for set point tracking, as shown in [13].

Unfortunately, however, the second layout has some small drawbacks:

- the system is higher in complexity;
- the AHU closed-loop response is slower with respect to the previous case, due to the inertia introduced by the wheel.

Nevertheless, the important advantage of the DW configuration appears evident if we consider the energy consumption. In the standard AHU, the air dehumidification is performed through condensation, and to this end, the air temperature has to be pulled down considerably. Thus, the standard AHU is quite energy demanding because both the cooling energy, used by the condenser, and the heating energy, used to heat the air after dehumidification, are relevant. The DW configuration can reduce such a problem, because the dehumidification process is performed by the wheel through the desiccant material adsorption process. To maximize the advantages, as will be shown more in detail in the following chapters, the rationale is to cool down the process air and heat the regeneration one.

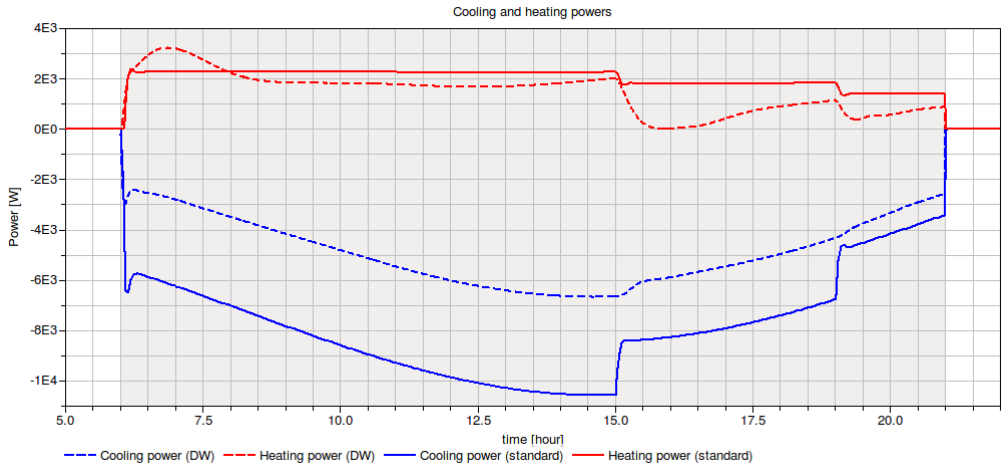

Figure 1.10: Energy consumption in the two cases: standard and DW layout.

In Fig. 1.10, where the dotted lines represent the DW-based solution, the energy consumptions of the two configurations is compared. It is clear that DW configuration reduces the total energy consumption, and in particular the cooling energy demand. Results, listed in Tab. 1.1, confirm that the total energy consumption can be reduced up to 37%.

Energy consumptions	standard AHU	AHU with DW
Cooling energy [kWh]	116.94	72.1
Heating energy [kWh]	30.34	21.8
Total energy [kWh]	147.28	93.9

Table 1.1: Energy consumptions in the presented test. Comparison between standard AHU and AHU with DW.

2 Air conditioning systems based on desiccant wheels

In the previous chapter, we have illustrated why the use of DWs is of increasing interest for energy saving purposes in HVAC systems. In this chapter, the physical structure and the operation of a DW are presented. Furthermore, some desiccant air conditioning system configurations are illustrated, to show how DWs can be used in the context of air conditioning.

2.1 Physical model of the desiccant wheel

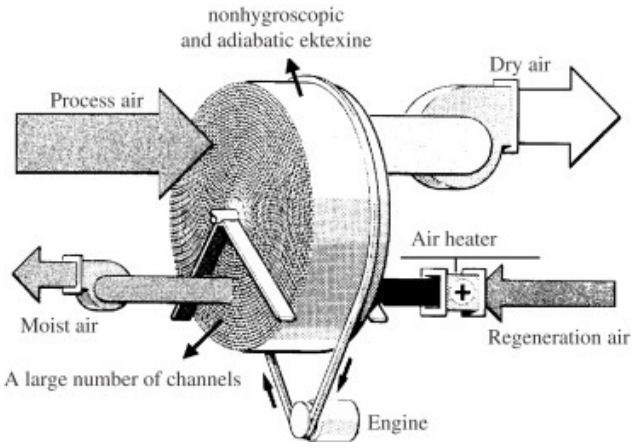

Figure 2.1: Desiccant wheel.

As said in sec. 1.2, in conventional AHUs the dehumidification and temperature regulation process is based on a cooling coil and a heating one: the air is first cooled below its dew point temperature, and then heated until the desired temperature is reached. This overall process can however be realized through more efficient HVAC systems based on the use of DWs.

A desiccant wheel is composed by a large number of channels, each one made by a supporting material (*matrix*) coated with desiccant. The wheel is also angularly partitioned by a clapboard in two different areas, the *process area* and the *regeneration* one, and driven by a motor which imposes a desired angular velocity, as shown in Fig. 2.1.

2.2 Working behavior of the wheel

While the wheel is rotating, it is also traversed by two different airflows in opposite directions: these are the process airflow and the regeneration one, as shown in Fig. 2.1.

Process air, humid and at ambient temperature, flows through the so-called process area, where a part of the water vapor contained in it, is adsorbed by the desiccant material of the wheel.

Regeneration air flows through a usually smaller (or at most equal) area, called the regeneration area. Before the regeneration air passes through the wheel, it is heated up. During the regeneration process, water contained in the wheel is extracted from the desiccant by the airflow, and the desiccant is regenerated.

The wheel rotation brings the desiccant material alternatively in the process area and in the regeneration one. Passing through the regeneration area, the desiccant material is brought back to the condition it had when last entering the process area, and the adsorption/desorption cycle can start again.

The adsorption capacity is thus intuitively foreseen to be a function of desiccant material, angular speed of the wheel, process and regeneration areas ratio, geometry of the wheel, and of course temperature, humidity and velocity of the airflows.

Therefore, the choice of the desiccant material plays a crucial role in the design of the wheel, and significantly affects the performance of the whole air conditioning system.

2.2.1 Desiccant material

Almost all materials have the capability to adsorb and hold water vapor. There are however some, the so-called *desiccant* materials, in which said capability is particularly relevant; among these are e.g. activated carbon, activated alumina, silica gel, lithium chloride, and calcium chloride. The most commonly used adsorbent for DWs is silica gel, i.e., a porous, amorphous form of silica (SiO_2). Silica gel has a great affinity for water vapor due to the enormous quantity of microscopic pores: the internal surface area of pores is in fact several orders of magnitude larger than the outer surface area of the adsorbent.

Adsorption of water vapor involves two different processes: *chemical sorption* and *physical adsorption*. The first process is permanent, and cannot be reverted by regenerating the silica gel, while the physical adsorption is a reversible process, driven by the intermolecular forces of attraction called Van Der Wall forces, that hold water molecules on the pores surface. Thus, it is the physical adsorption that plays a crucial role in dehumidification process involving DWs.

An important characteristic of a desiccant material is its *adsorption isotherm,* which determines its water vapor adsorption capacity as a function of temperature and vapor pressure.

We can classify a desiccant material according to the average diameter of the pores, but also, and more interesting for our purpose, according to its adsorption isotherm.

Some types of adsorption isotherms are shown below in Fig. 2.2, where the normalized loading fraction (NLF: actual desiccant water content at corresponding RH/maximum desiccant water content at RH=100%) is a function of relative humidity (RH), defined as the vapor pressure in moist air over the vapor saturation pressure at the same temperature, i.e., $RH = P_v/P_{vs}(t)$.

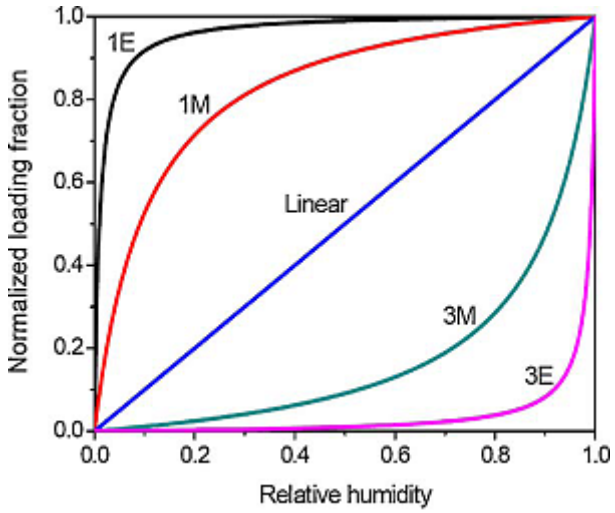

Figure 2.2: Adsorption isotherms.

As shown in Fig. 2.2, each material has its own adsorption isotherm, defined for a prescribed temperature. In this section, we consider adsorption isotherms to analyze the adsorption capacity of the corresponding material. It is clear that curves with great slope at low RH, e.g. 1E, correspond to materials that have a great adsorption power at low relative humidity, but saturated faster, i.e. their adsorption power increases "fast" and then "slower" with the increase of RH. For this type of materials, as shown in Fig. 2.2, the NLF reaches almost the maximum value at low RH (e.g. $RH \simeq 0.3$ for type 1E isotherm refers to $NLF \simeq 0.98$). On the contrary, materials with e.g. type 3E isotherm, do not have much adsorption power at low values of RH, but they express all their adsorption capacity when dealing with high RH (e.g. for type 3E, for $RH \geq 0.8$ the adsorption capacity increases "faster" with the RH).

Quite intuitively, thus, in the DW context it is also necessary a desiccant material should possess large saturated adsorption amount, but it is also necessary to take into account that this material has to be easily reactivated during the regeneration precess. The energy performance of a DW depends mainly on the power used for the regeneration process. Thus, the desorption process of the desiccant has to be

considered. Referring to Fig. 2.2, type 1E materials, because of its nearly complete loading at low RH, are more difficult to regenerate. Thus the adsorption performance of the desiccant material should approach type 1M adsorption isotherm.

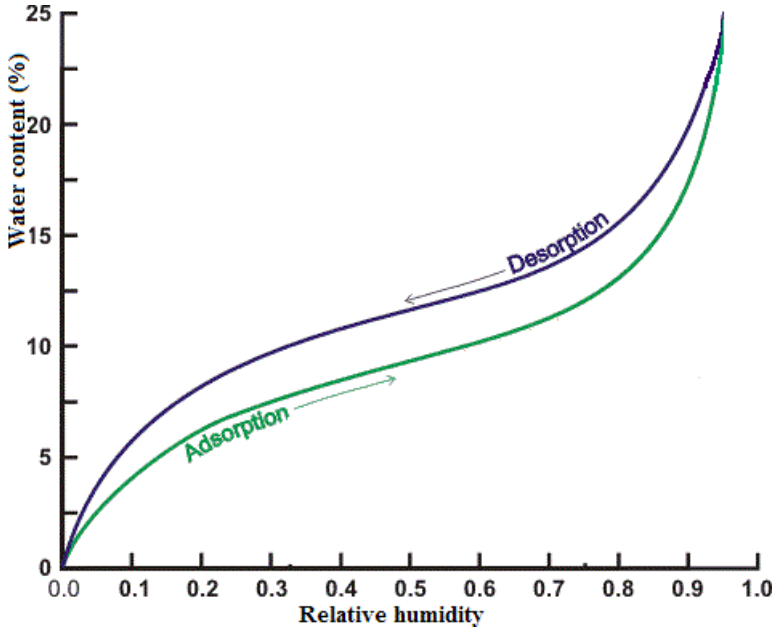

Figure 2.3: Adsorption isotherm hysteresis.

In Fig. 2.3, the typical adsorption/desorption process of a desiccant material is shown. This process exhibits an hysteresis, as the adsorption behavior of the material is different from its desorption behavior. In other words, the amount of energy that the material needs to be reactivated, depends on the desorption process. Thus, it is clear that the adsorption and desorption processes - rigorously speaking - require a different amount of energy. However, in this work we neglect the hysteretic behavior of the desiccant material owing to its tendentiously modest entity.

As said before, the choice of the desiccant material is very important, and thus, there are several researches under way to find the desiccant material that best approaches type 1M in its adsorption performance. At present, commonly used desiccant materials exhibit some drawbacks. For example, the silica gel adsorption performance decreases quickly with the rise of temperature, while lithium chloride has a higher adsorption capacity, but it also shows the lyolysis phenomenon, which leads to the loss of desiccant material and may reduce the performance of the entire system.

2.2.2 Rotating speed

Another element that affects the wheel operation is the rotating speed. At the same process and regeneration air inlet conditions, process air outlet humidity depends on

the wheel velocity, as shown in Fig. 2.4. We can identify two main different working behaviors of the wheel, depending on its velocity.

First, it is clear that at low speed the desiccant material remains for a long time in the process area, and its dehumidification capacity is exhausted before the material comes into contact with the regeneration air. Increasing the rotating speed, the adsorption capacity is better exploited, and water content in outlet process air reaches a minimum. If however we continue to further increase the speed, desiccant material comes to not use all its adsorption capacity, because the time spent in the process area is too short with respect to the adsorption time constant. In such a case, the process is dominated by heat transfer, and the dehumidification rate decreases.

In Fig. 2.4, we show an example of such a behavior. Note that there is an optimal rotating speed for dehumidification, corresponding at the minimum water content in the outlet process air. For different operating conditions the optimal wheel velocity can be found and exploited to maximize the wheel efficiency.

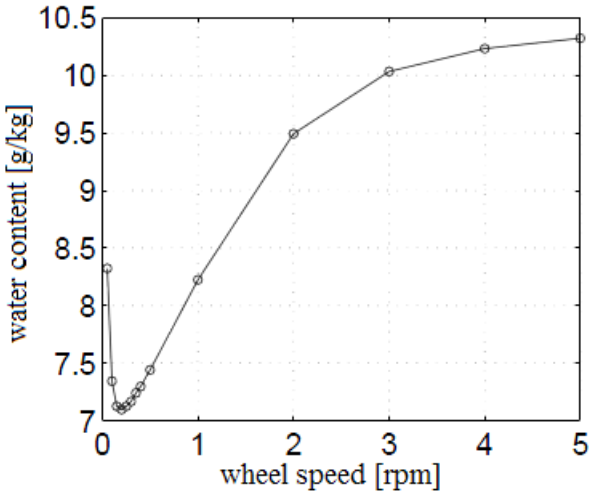

Figure 2.4: Air outlet water content for different desiccant wheel rotating speeds.

2.3 System Configurations

In order to reach the optimum operating conditions, and thus the highest performance of the whole air conditioning system, the system configuration is another crucial issue. In this section, we synthetically present some commonly used configurations, and we underline some advantages and drawbacks of them. For this purpose, it seems interesting to show, for each system configuration, both the plant scheme and the physical transformations undergone by air, using the Psychrometric chart. It should be noted that the dehumidification process in the DW is close to a isenthalpic transformation, as shown in Fig. 2.5 (1-2). So, additional air conditioning equipments must be introduced in order to reach the desired air conditions.

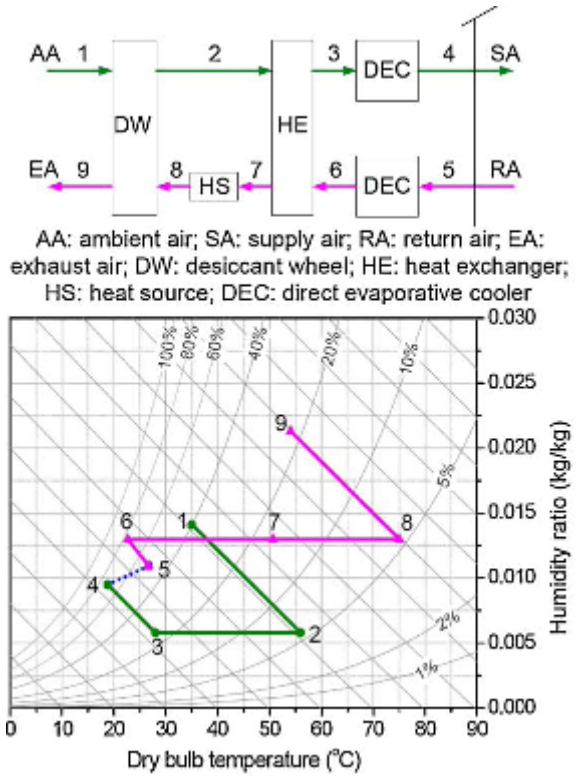

Figure 2.5: Pennington cycle.

The first patent on rotary desiccant air conditioning cycle was introduced by Pennington in 1955 [14]. In Fig. 2.5 the *Pennington cycle*, also known as ventilation cycle, is presented. The ambient air, at state point 1, is directly used as process air for the DW. The air, passing through the DW, decreases its moisture content and increases its temperature, because of the adsorption heat effect, until it reaches the state point 2. Then, this hot dry air is sensibly cooled, from state point 2 to 3, in a heat exchanger (HE). The process air is evaporatively cooled, from 3 to 4, by passing through a direct evaporative cooler (DEC). Then, the air can enter the room in the desired conditions, represented by state point 4. On the regeneration air side, return air, which is taken from the inlet ambient at state point 5, is cooled and humidified in another DEC, from state point 5 to 6. This air exchanges sensible heat with the process air, from 6 to 7, to precool the process air and pre-heat itself. Then the regeneration airflow is heated, from state point 7 to 8, by the heat source (HS). This air, at state point 8, can finally be used to regenerate the DW. After the regeneration, the air is exhausted and can be released at state point 9.

There are some variations of Pennington cycle, introduced in order to improve the performance of the system and to make it more suitable to the desired operating conditions. For example, the *Recirculation cycle* (Fig. 2.6) reuses return air as process air, to increase the cooling capacity, as the internal ambient air is at humidity and temperature conditions that are closer to the desired ones, if compared to the

external ambient air. This fact is evident, if one compares stare point 1 in Fig. 2.5 and the same point in Fig. 2.6. Thus, with a recirculation cycle, the variation of the air conditions requires less energy consumption. In Recirculation cycle the ambient air is used for regeneration purpose with the same advantages shown for the process airflow. The main disadvantage of this cycle is however some lack in fresh air. In HVAC systems the renewal of internal air with external ambient air is very important for human health, as already noted, and there are several regulations in this regard.

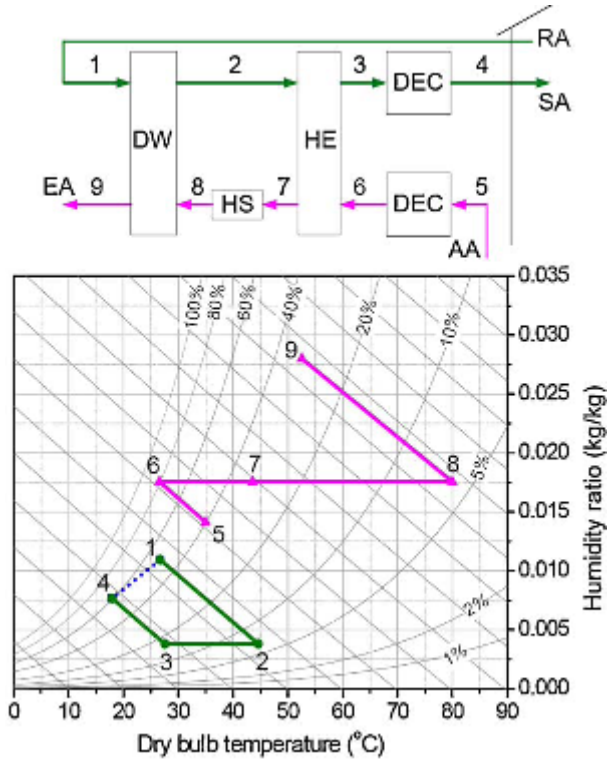

Figure 2.6: Recirculation cycle.

Another way to improve the thermal performance of rotary desiccant air conditioning systems is the *staged regeneration.* The basic idea was proposed by Glav in 1966, [8], and then rearranged in the presented context for desiccant regeneration. As illustrated in Fig. 2.7, the particularity of the Staged Regeneration Cycle, lies in the regeneration side of the DW, which is divided in pre-regeneration side and regeneration side. After being pre-heated in the HE, from state point 6 to 7, only a fraction of the regeneration air is heated by the HS, from state point 7 to 8, while most of the regeneration air is directly introduced to the pre-regeneration area of the DW. The advantage of this configuration is that the desiccant is first pre-regenerated with a low temperature airflow, and then is further regenerated with a much smaller amount of high temperature heat. This configuration thereby allows less energy consumption for the regeneration process.

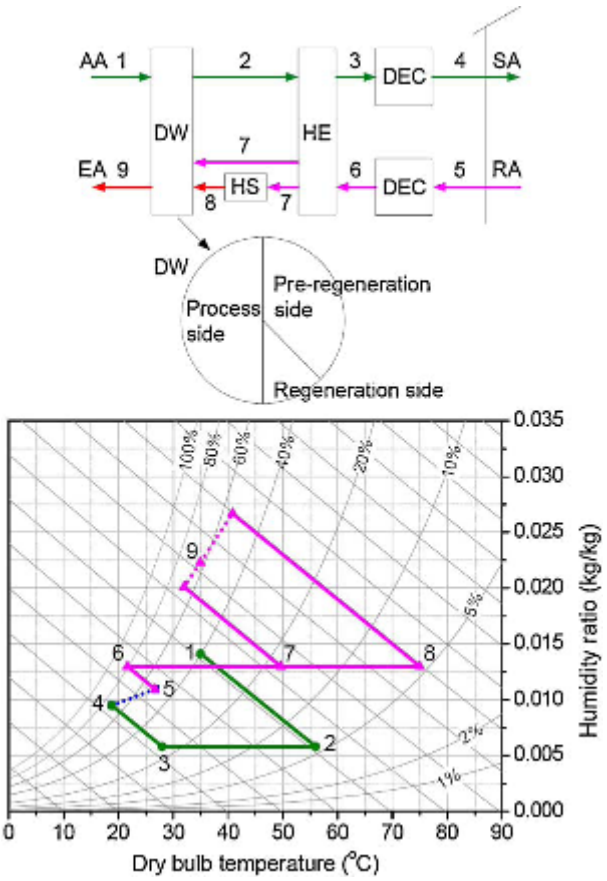

Figure 2.7: Staged regeneration cycle.

Several other configurations are presented in [9], and the choice of which is the best of them depends on the particular application context we do not delve into. Further details, however, as doing so would substantially stray from the scope of this dissertation.

3 Literature review

In HVAC systems based on DWs, the performance of the wheel is a critical issue for a satisfactory behavior of the whole system. Thus, a mathematical model for such a component can be extremely useful in system design, but also in analyzing experimental results, and all in all to find the optimal wheel operation for the envisioned working conditions.

In the literature, some DW models are presented and classified, as shown in [16]. Mathematical models can be divided into two main categories: first principle models and empirical models.

3.1 First principle models

First principle models are based on equations that represent the physical phenomena involved in the wheel operation. They can have a different level of accuracy, depending on how said phenomena are represented. In particular, sticking to the purpose of this work, if we want to investigate the operation of the wheel for a system level study, a very accurate description is not required.

The physical phenomena involved in the wheel behavior deal with heat and mass transfer principles, but some of them are of non trivial modelling at all. Thus, in order to obtain a simple enough model, some ideality assumptions are in order and advisable for example, some factors that do not significantly affect the wheel behavior, as seen in the context of the complete AHU, can be often neglected, thus reducing the complexity of the model.

First principle mathematical models are composed by partial differential equations, based on the mass and energy balances, and involving mass and heat transfers. In addiction, the initial conditions of airflows and desiccant material and the boundary conditions have to be determined so as to close the model. As said in sec. 2.2.1, the adsorption/desorption process is the key element on which the wheel operation is based. Thus, this process has to be represented with a specific equation. How to model this phenomenon is not a trivial matter, however in the literature, some semi-empirical models are presented and used to predict the adsorption capacity of the material, e.g. [5].

There are several methods to solve the differential equations used to describe the physical phenomena. One of them is the *characteristic potentials method.*

3.1.1 Characteristic potentials method

The basic idea of the characteristic potentials method is to transform the coupled non-linear partial differential equations into a set of decoupled differential equations. For this purpose, new independent variables (which are called characteristic potentials, whence the method's name), are used. These are associated with new parameters, which can in turn be related with convenient specific-heat ratios. The new set of equations is analogous to the heat transfer equations in a rotary heat exchanger. Thus, the problem con be solved with the analogy method, drawing e.g. from the solution of Kays and London [18] for a rotary heat exchanger.

This method has some relevant advantages. First, from the analogy with a rotary heat exchanger follows a simplified solution, requiring a low computation time. Then, the performance prediction is based on parameters, and relationships similar to those used for heat exchangers, and the model operation can be easily understood with the use of psychrometric charts.

However, the parametrization of the model is not a trivial matter. To partially overcome this problem, the method can be simplified, e.g. one can assume the effectiveness of the two characteristic potentials as constant, and the potentials can be described by analytical formulae (for silica-gel, for example, those defined by Jurinak [11]). The most relevant drawback of this (further) simplified model, is that default values for the effectiveness should be used, as they are generally unknown. Since no model completely fulfils the requirements defined above, a new model has been developed based on the method of characteristics. The model has been adapted in order to be parametrized only with the data provided by desiccant wheel manufacturers.

3.1.2 Wheel motion representation

Another critical issue for first principle DW modelling is how to represent the wheel motion. There are several works dealing on this problem. The aim of this subsection is to present three different modelling approaches, based on Object Oriented Modelling (OOM), i.e. the context in which the present work takes place.

In our work, we decided to use the Finite Volumes approach, that is a suitable method for the model implementation using the available software paradigm (the Modelica language, applied with the Dymola translator).

The Finite Volumes approach is based on control volumes (CVs) for which balance equations are written. In DW modelling, said volumes represent wheel "pie slices" and they are alternatively traversed by the process and regeneration airflows, depending on their position during the DW rotation. However, Modelica can only handle ordinary differential equations with respect to time, however, and to overcome this problem, there are some different approaches.

In Casas et all. ([17]), a variable transformation is used to express the position of the volume in terms of time instead of angular position. This is possible under the assumptions that the velocity of the wheel is constant and the boundary conditions do not change during the differential model's integration time. The wheel is split in two shares, one for each airflow, as shown in Fig. 3.1. The referring volume is composed by two opposite pie slices, one in part I and the other in part II. At the end of half a rotation period, the boundary conditions of the two slices are switched.

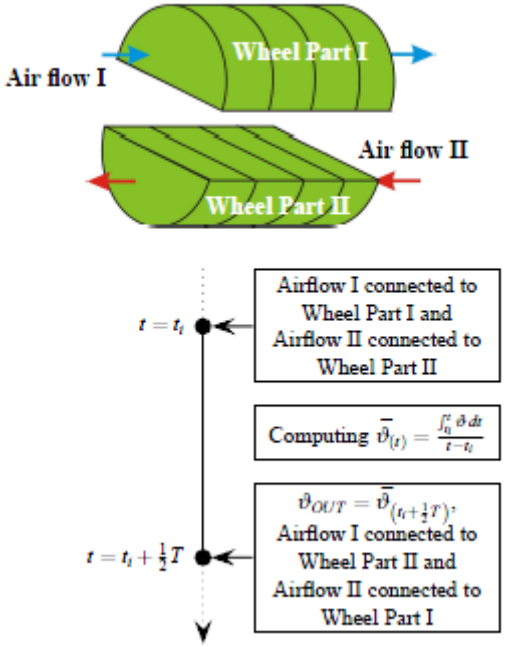

Figure 3.1: Wheel motion representation for Casas et all.

This model has two relevant drawbacks. First, the physical process is continuous, but owing to the abruptly described (switching) slice transition just mentioned, the model ends up producing discrete output variables even from continuous input values. Second, the model computing time is quite large, because (referring to the typical solvers used in OOM tools, that exploit variable-step integration to improve efficiency) it causes a state event every half a revolution time. To overcome said problems, another approach is presented in [1]. As shown in Fig. 3.2, the wheel motion is represented by the use of a so called *desiccant flow,* which flows in angular direction. Control volumes are spatially fixed (i.e., the model refers to portions of the fixed ambient space and not of the wheel moving in it) and composed by an *Air CV* and a *Desiccant CV*. Said volumes interact by exchanging heat and moisture for modelling the adsorption/desorption process. The DW velocity is thus related to the desiccant mass flow rate through the *Desiccant CV*.

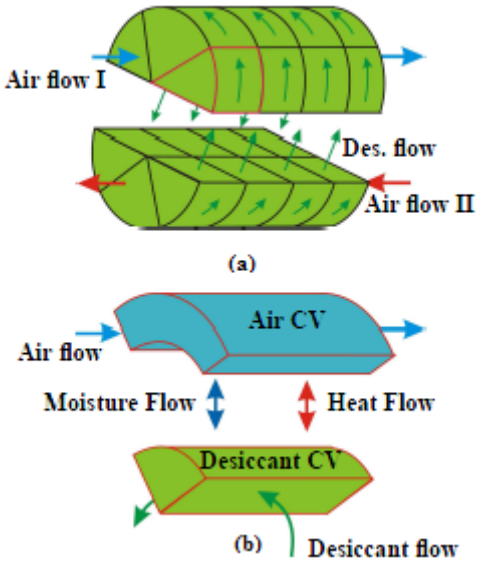

Figure 3.2: Wheel motion representation for Joos et al..

The last model presented in this subsection, see [13], is based on the use of hydraulic valves to represent the wheel motion. Each pie slice of the wheel is fixed in space, and alternatively traversed by the two airflows depending on the wheel motion. As shown in Fig. 3.3, the airflow (non abrupt) switching is represented by the opening and closure of four valves, and the time at which valves change state is related on the wheel rotation speed.

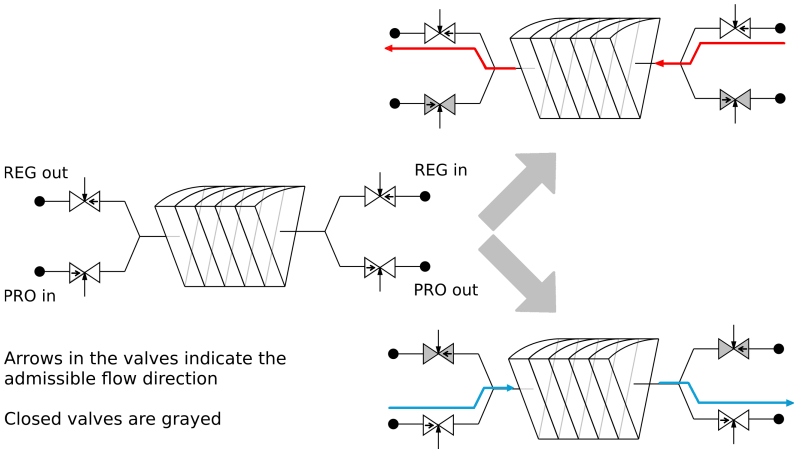

Figure 3.3: Wheel motion from a thermo-hydraulic viewpoint.

This model is quite accurate for control purposes, but introduces some additional elements that make the representation of the wheel motion very different from the physical phenomenon. Also, due to the periodical behavior of the model, the drawbacks already mentioned for the Casas et all. model ([17]) appear again.

3.2 Empirical models

Models based on heat and mass transfer phenomena are sometimes considered too complex for a system analysis, because solving differential equations is complicated and very time-consuming. A different approach was thus followed by Beccali et all. in [12], in which an empirical model for evaluating the performance of a DW was proposed. Using a set of equations, based on second-order polynomials, they provided outlet air temperature and humidity as a function of the inlet regeneration and process airflows. Using the available experimental data, they could define a set of parameters (with no direct physical meaning), however which could be used to predict the performance of the wheel. The simulation results obtained with this model are very close to the experimental data, but obviously, if the physical system changes, parameters have to be recalculated, and there is no way to simulate a wheel that thus not yet exist, as it is being designed and there is obviously no experimental data on it. Further, other works provide simplification for the model presented in [12], devoted mainly to reduce the number of parameters.

4 Desiccant wheel model

Progressively restricting the focus to first principle models as the scope of this research includes design, we can further (and in some sense alternatively with respect to the view point of chapter 3) divide the DW literature works in two main categories:

- complex ones, that describe DW in a very detailed manner, but are computationally intensive and time demanding, thus not suitable for a study that requires a huge number of simulations;
- simple ones, that are longer usable, but natively created for steady-state studies and their parameters have no direct physical meaning.

The aim of the present work is to propose an innovative model that has the main advantages, and overcomes the most relevant drawbacks, of both categories. Therefore, the new DW model is based on first-principle equations (thus with physically meaningful parameters) and includes spatial discretisation at a system level, as shown in Fig. 4.1.

The wheel has length L and radius R and it is split in M slices (radial direction) each one divided in N control volumes (axial direction); each slice has a corresponding angle $\theta = 360/M$ and a length $dl = L/N$. As shown in sec. 2.1, each slice is composed by several channels.

In this chapter, we first focus on the single channel, to understand in detail the physical phenomena involved in DW operation. Then, we introduce the used control volume, and the balance equations used in the presented model.

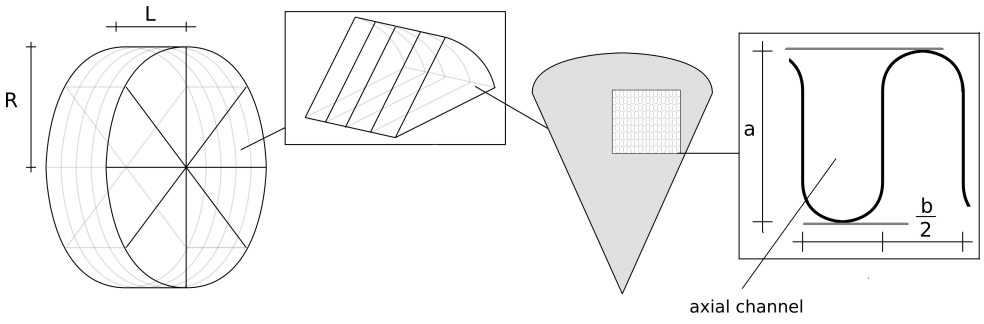

Figure 4.1: Wheel structure and spatial discretisation.

4.1 Preliminary assumptions

As said at the beginning of this chapter, the proposed model deliberately does not take into account some phenomena which would make it too complex for our purposes. Thus, before introducing the governing equations for the single channel, it is required to underline the preliminary assumptions on the base of the model construction. These assumptions are listed below.

- Axial heat conduction and water vapor diffusion in the air are neglected;
- hysteresis in the sorption isotherm for the desiccant, shown in sec. 2.2.1, is neglected, and the heat of sorption is constant;
- all channels are identical, with constant heat and mass transfer surface areas, adiabatic, and impermeable;
- the matrix thermal and moisture properties are constant, as are the mass and heat transfer coefficients, and the adsorption heat per unit mass of adsorbed water;
- mixing between the process and the regeneration airflows is neglected.

4.2 Single channel

4.2.1 Structure

There are several studies about the features of the channel used in the DW structure. Most of them aim at analyzing the possible geometries for the duct, to find advantages and disadvantages that different choices of the channel characteristics yield; for example in [6] the authors take into account three different channel shapes: square, triangular and circular. In our case, the wheel channels have the shape shown in Fig. 4.2 and can be described by two scalars, a and b, that define respectively the height and the length of the channel. Note however that the proposed modelling approach is general, and according for other channel shapes is totally straightforward.

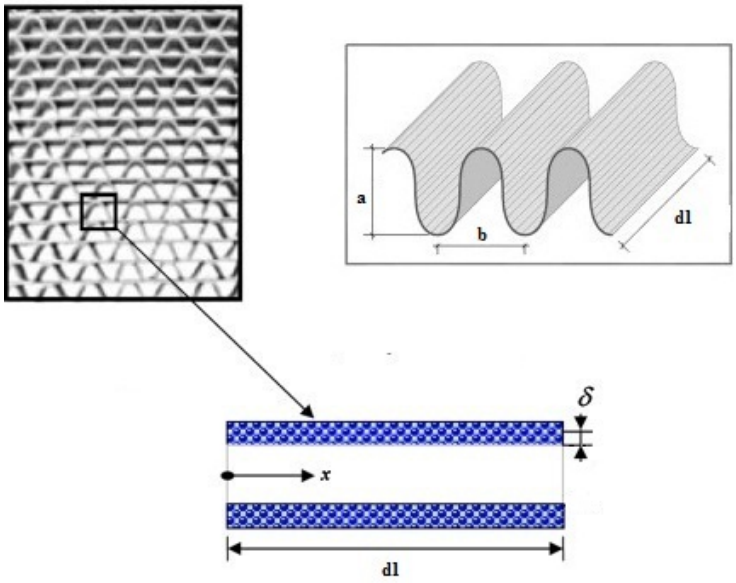

Figure 4.2: Single channel structure.

First of all, for a single channel, two areas of interest need defining, namely the effective area, A_{eff}, and the lateral area, A_{xcg}.

The effective area represents the wheel frontal area subtracted by the area occupied by the support matrix, thus it is the frontal area through which the airflows actually traverse the wheel, and is defined as:

$$A_{eff} = ab - \left(\pi\frac{b}{2} + 2\left(a - \frac{b}{2}\right)\right) 2\delta \tag{4.1}$$

where 2δ is the thickness of the matrix structure (with the desiccant).

The lateral area represents the contact area between air and desiccant material that is involved in the heat exchange and humidity adsorption/desorption processes, and it is defined as:

$$A_{xcg} = 2\left(\pi\frac{b}{2} + 2\left(a - \frac{b}{2}\right)\right) dl \tag{4.2}$$

where dl is the channel element length.

4.2.2 Physical phenomena

After defining the channel dimensions of interest, we have to consider the physical phenomena involved in the DW behavior.

First, we define the water mass flow rate adsorbed by the desiccant material, positive if adsorbed, as a function of the adsorption isotherm of the desiccant material, see [5], as shown in sec. 2.2.1.

$$w_{ad} = \frac{M_d}{\tau}\left(0.24\phi^{\frac{2}{3}} - X_d\right) \tag{4.3}$$

where M_d is the mass of the desiccant material, ϕ is the air relative humidity, τ is a discharge time constant and X_d is the desiccant water content.

The time constant τ is defined as:

$$\tau = \frac{M_d}{A_{xcg} h_m} \tag{4.4}$$

where h_m is a mass transfer coefficient, while the desiccant water content X_d is defined as:

$$X_d = \frac{M_{wd}}{M_d} \tag{4.5}$$

where M_{wd} is the mass of water inside the desiccant material.

Associated to such an adsorption/desorption process, there is a heat flow from the air to the desiccant material due to thermal convection, i.e.,

$$q_{cam} = h_t A_{xcg}\left(T_a - T_m\right) \tag{4.6}$$

where h_t is the convective heat transfer coefficient and T_a , T_m are respectively the air and matrix material temperature.

In addition, there is a power associated to the water mass flow rate adsorbed/released by the desiccant material, defined as:

$$Q_{wam} = w_{ad}\begin{cases} h_{wv}, & w_{ad} \geq 0 \\ h_{wm}, & w_{ad} < 0 \end{cases} \tag{4.7}$$

where h_{wv} is the water vapor specific enthalpy and h_{wm} is the specific enthalpy of water in the desiccant material.

Another phenomenon, that we need to take into account, is the water vapor diffusion in the desiccant material: this it is particularly relevant at slow wheel velocity in the angular direction, but has some relevance also in axial direction because of the spatial discretisation used in the model.

We define the water mass flow rate in the desiccant material between two different volumes as:

$$w_{in2} = G\left(X_{d1} - X_{d2}\right) \tag{4.8}$$

where w_{in2} is the water mass flow rate from the first to the second volume, X_{d1} , X_{d2} are respectively the desiccant water content in the first and in the second volume, and G is a diffusive coefficient.

The diffusive coefficient G is defined as:

$$G = coef\left(\frac{A_d}{dx}\right) \tag{4.9}$$

where $coef$ is a diffusivity-related constant depending on the desiccant material and A_d and dx are the crossing area and the distance between the two regions. These parameters are defined, for a single channel, as:

$$A_d = 2\delta_d dl \tag{4.10}$$

$$dx = \pi\frac{b}{2} + 2(a - \frac{b}{2}) \tag{4.11}$$

where δ_d is the only desiccant thickness, if we deal with water vapor diffusion in desiccant material in angular direction or

$$A_d = \frac{A_{xcg}}{dl}2\delta_d \tag{4.12}$$

$$dx = dl \tag{4.13}$$

if the axial direction is being considered.

4.3 Wheel motion representation

A major innovation in the presented model, lies in the choice of how to represent the wheel rotation. In the literature there are several DW models that use different modelling approach in this regard, as shown in sec. 3.1.2.

To represent the wheel motion, we suppose that there is a *desiccant flow* that flows through the wheel in angular direction, according to the wheel speed. Such a flow is composed by the desiccant (with its water content) and the matrix material. Each control volume is thus spatially fixed (i.e., it does not move with the wheel), and it is traversed by either the process or the regeneration airfolw (depending on its angular position) in axial direction , and by the desiccant flow in angular direction (Fig. 4.3).

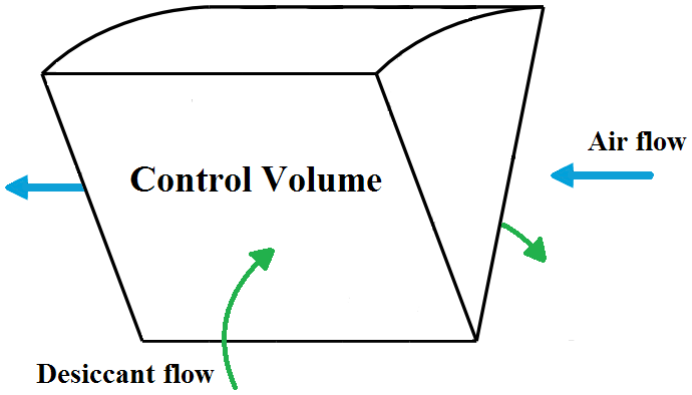

Figure 4.3: Desiccant flow.

4.4 Equations

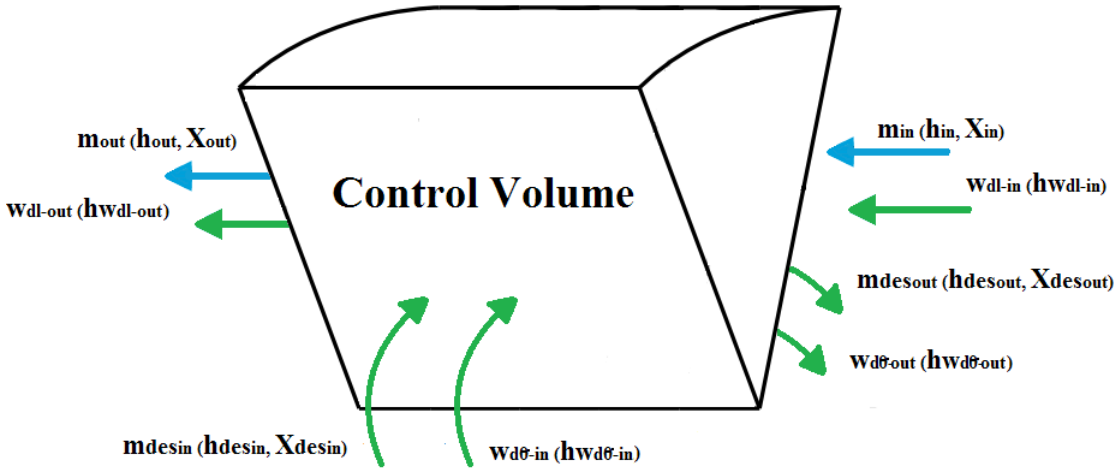

Figure 4.4: Air, water and desiccant mass flows for the control volume

In the presented model we define a control volume, one volume of the slice, with respect to which the mass and energy balances can be defined. Obviously, the physical phenomena in the control volume are structurally the same as those of a single channel, discussed in sec. 4.2.2, which is rigorous as long as one considers the number of channel in a volume to be given by:

$$n = \frac{\vartheta \pi R^2}{ab \cdot 360^\circ} \tag{4.14}$$

where ϑ is the angle of the slice and R is the wheel radius.

4.4.1 Balance equations

Once the mass and heat flows are defined, we can write the balances below for the control volume shown in Fig. 4.4.

- Mass balance of desiccant and matrix (solid) material:

$$\dot{M_d} = mdes_{in} - mdes_{out} = 0 \tag{4.15}$$

where M_d is the mass of desiccant material and $mdes_{in}$, $mdes_{out}$ are respectively the incoming and outgoing desiccant mass flow rates.

- Mass balance of moist air:

$$\dot{M_a} = m_{in} - m_{out} - w_{ad} \tag{4.16}$$

where M_a is the mass of moist air, m_{in}, m_{out} are respectively the incoming and outgoing moist air mass flow rates and w_{ad} is the water mass flow rate adsorbed by the desiccant material and defined in 4.3.

- Mass balance of water in the desiccant material:

$$\dot{M_{wd}} = mdes_{in}Xdes_{in} - mdes_{out}Xdes_{out} + w_{ad} + w_{dl-in} - w_{dl-out} + w_{d\theta-in} - w_{d\vartheta-out} \tag{4.17}$$

where M_{wd} is the mass of water vapor in desiccant material, $mdes_{in}$and $mdes_{out}$ are the incoming and outgoing desiccant material mass flow rates, while $Xdes_{in}$, $Xdes_{out}$ are the water vapor mass fraction respectively associated to said flow rates, w_{dl-in}, w_{dl-out}, $w_{d\theta-in}$, $w_{d\vartheta-out}$ are the incoming and outgoing water vapor mass flow rates, in the dl and $d\theta$ directions, due to the diffusion in desiccant material and defined in 4.8.

- Mass balance of water in the moist air:

$$\dot{M_{wa}} = m_{in}X_{in} - m_{out}X_{out} - w_{ad} \tag{4.18}$$

where M_{wa} is the mass of water vapor in the air and X_{in}, X_{out} are the water vapor mass fraction associated to m_{in} and m_{out}.

- Energy balance in the moist desiccant material:

$$\dot{E_m} = mdes_{in}hdes_{in} - mdes_{out}hdes_{out} + w_{dl-in}hw_{dl-in} - w_{dl-out}hw + \tag{4.19}$$
$$+ w_{d\theta-in}hw - w_{d\vartheta-out}hw_{d\vartheta-out} + Q_{wam} + q_{cam}$$

where E_m is the energy of the matrix and desiccant material, $hdes_{in}$, $hdes_{out}$ are the specific enthalpies associated to m_{in} and m_{out}, $Q_{wam}$is the power associated to the water mass flow rate adsorbed/released by the desiccant material defined in 4.7, and q_{cam} is the heat flow from the air to the desiccant material due to thermal convection, and defined in 4.6.

- Energy balance in the moist air:

$$\dot{E_a} = m_{in}h_{in} - m_{out}h_{out} - Q_{wam} - q_{cam} \tag{4.20}$$

where E_a is the energy of the moist air contained inside the volume.

4.4.2 Desiccant flow equation

As said in sec. 4.3, we want to represent the wheel motion by means of a desiccant flow in the angular direction. More in detail, said desiccant flow is represented with the relation below:

$$mdes_{out} = \left(\frac{R^2}{2} \cdot dl \cdot \omega \cdot (\rho_D + \rho_M)\right) \cdot \left(1 + \frac{Mwm}{(M_D + M_M)}\right); \tag{4.21}$$

where ω is the angular velocity of the wheel [rad/sec], ρ_D and ρ_M are respectively the desiccant material and the matrix densities, Mwm is the water content in the desiccant material, M_D and M_M are the mass of desiccant and matrix material in the control volume.

Equation 4.21 expresses the mass flow rate of the desiccant flow moving into the wheel as two components:

- a constant part of solid desiccant material, $\frac{R^2}{2} \cdot dl \cdot \omega \cdot (\rho_D + \rho_M)$;
- a quantity depending on the water content in the solid desiccant,

$\left(\frac{R^2}{2} \cdot dl \cdot \omega \cdot (\rho_D + \rho_M)\right) \cdot \left(\frac{Mwm}{M_D + M_M}\right)$.

5 Model validation

In this chapter, the proposed model is validated against experimental data available in the literature [2, 3, 4, 5]. The desiccant wheel used for the comparison has the characteristics listed below.

- desiccant material: *silica gel*;
- radius: $R = 1m$;
- thickness: $L = 0.2m$.
- channel dimensions: $a = 3.2mm$, $b = 1.8mm$;

Referring to Fig. 5.1, the input data are the inlet air humidity of the process and regeneration airflows ($Xpro, in$, $Xreg, in$), and the inlet air temperatures of the same air streams ($Tpro, in$ and $Treg, in$). In the simulations, said inputs have been set according to the experimental data, as shown in detail in the next section. In all the case studies, the inlet humidity of the process air is equal to the inlet humidity of the regeneration air, and the velocity of both air flows is equal to $1m/s$.

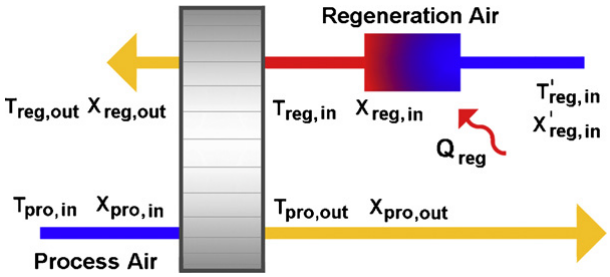

Figure 5.1: Process and regeneration air flow scheme.

5.1 Comparison between simulation results and experimental data

In [7], a validation for a DW model is presented, using a set of experimental data. We decided to use the same data to provide our model validation. Tab. 5.1 shows the inputs used for the comparison between simulated and experimental data.

EXP/SIM	$Xpro/reg, in[g/kg]$	$Tpro, in$[°C]	$Treg, in$[°C]	$\frac{Apro}{Areg}[m^2/m^2]$
expA	4.4-5.0	18.0	100	1
expB	13.2-13.8	25.0-27.0	60	1
expC	7.8	24.9	140	3.3
simA	4.4	18.0	100	1
simB	13.5	25.0	60	1
simC	7.8	24.9	140	3

Table 5.1: Input data used in the comparison between simulation results (sim) and experimental data (exp).

Fig. 5.2 shows the fractional residue of water vapor $Xpro, out/Xpro, in$, at steady state, against the wheel rotating speed and can be compared with Fig.5 in [7].

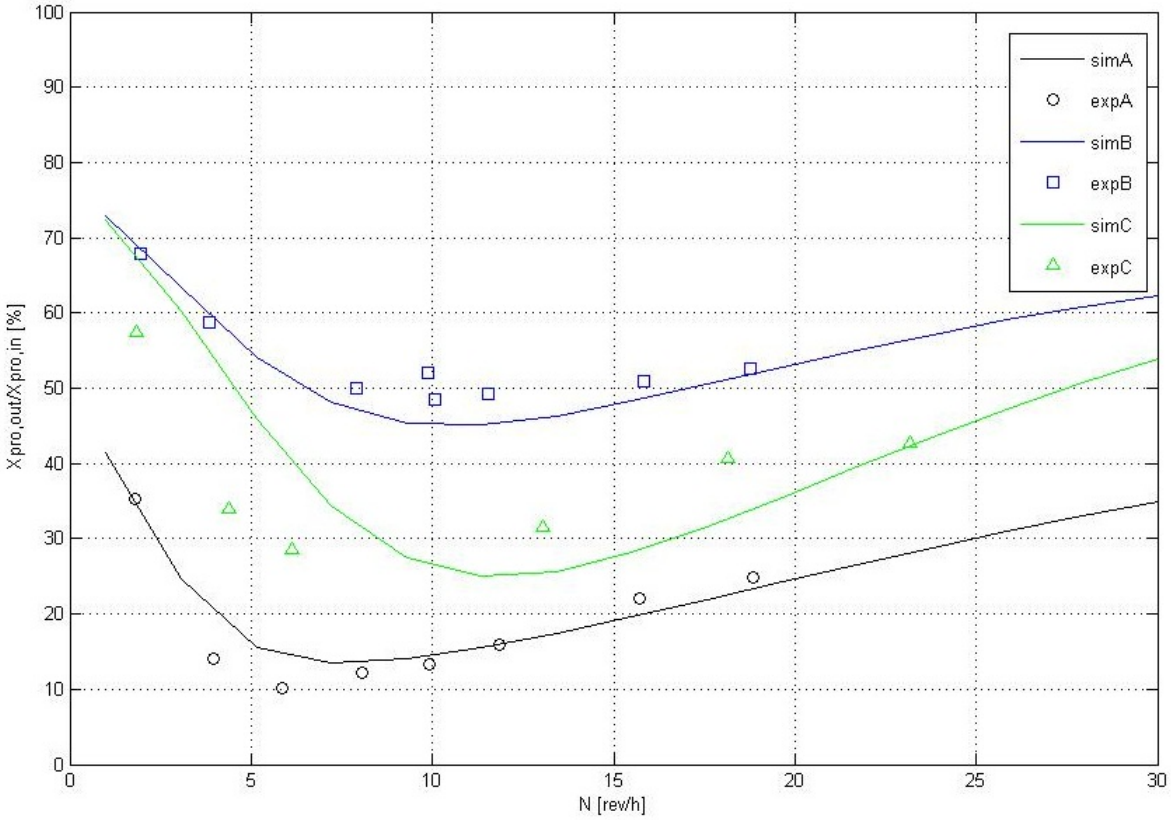

Figure 5.2: Comparison between experimental and simulated process outlet humidity for different working conditions (wheel rotation speed).

Simulation results are generally in good agreement with experiments, and in particular, the effect of the wheel velocity on the outlet conditions of the process air, is caught and reproduced, consistently with the discussion of sec. 2.2.2. At "low"

rotation speed, any given portion of the wheel matrix remains in contact with both the process and the regeneration air streams for a "long" time. As a consequence, the desiccant water vapor content has the time to reach the maximum value made possible by the operating conditions, before the wheel portion carrying that desiccant, is led by rotation back to the regeneration area. Thus, there is a limit on how much drying can be exerted on the process air. On the contrary, at "high" rotation speed, the desiccant does not remain "long enough" in the process area, and it is still able to adsorb water when it enters the regeneration area. Thus, in both the "extreme" (very fast or slow rotation) conditions, the desiccant adsorption capacity is not well exploited, and therefore it is clear that there has to exist an optimal revolution speed, which minimizes the process air outlet humidity. Most important, this optimal speed can be predicted by the presented model.

Looking at the experiments a bit more in detail, it can be noted that we obtain good agreement between model and data in particular for expA and expB, where the maximum difference between simulation results and experimental data is less than 10%, and the optimal revolution speed is well predicted.

In the case of expC we conversely obtain slightly less precise results: in particular, the maximum error between data and simulation results is less than 20% and the optimal speed is not so well predicted. It is however worth noting that the expC data appear to possibly contain some outliers, which can be at least hypothetically detected by further looking at the particular operating conditions. The main difference between expC and the other experiments lies, in fact, in the process and regeneration areas dimensions. As shown in Tab. 5.1, in expA and expB the wheel is split by the clapboard in half, thus the process and regeneration areas are equal, while in expC the process area is 270°. Given the geometry of the experimental setup, it can be assumed that guaranteeing the same air flow velocity conditions in both cases (as the model assumes) is not trivial. One can thus suppose that the observed discrepancies are due to unmodelled variations in the air speed, and since the entity of the observed errors is compatible with the magnitude that those discrepancies can be supposed to have, still be convinced of the model validity.

6 Operation analysis

In chapter 5, the ability of the presented model to reproduce the inlet/outlet behavior of a DW unit, has been shown. This chapter is conversely devoted to using the same model fore a more detailed analysis of the internal operation of the wheel. In other words, the detailed modelling approach followed here has already shown capable of representing the wheel "seen from outside"; the aim of this chapter is to prove that such an approach is really representative also of the wheel "seen from inside". To this end, we first define a base case, and show the spatial distribution of some interesting quantities, e.g. temperature and humidity, referring to that case. Subsequently, a parametric analysis is performed to underline how physical parameters influence the wheel operation.

6.1 Base case

For the *base case* and the simulations shown later in this chapter, we refer to the same DW used for validate the model in chapter 5.

The base case has the features listed in Tab. 6.1.

airflow	T,in [°C]	X,in [g/kg]	area angle [°]	velocity [m/s]
process	30	15	180	1
regeneration	80	15	180	1

Table 6.1: Base case inlet air flows conditions.

6.2 Spatial distribution analysis

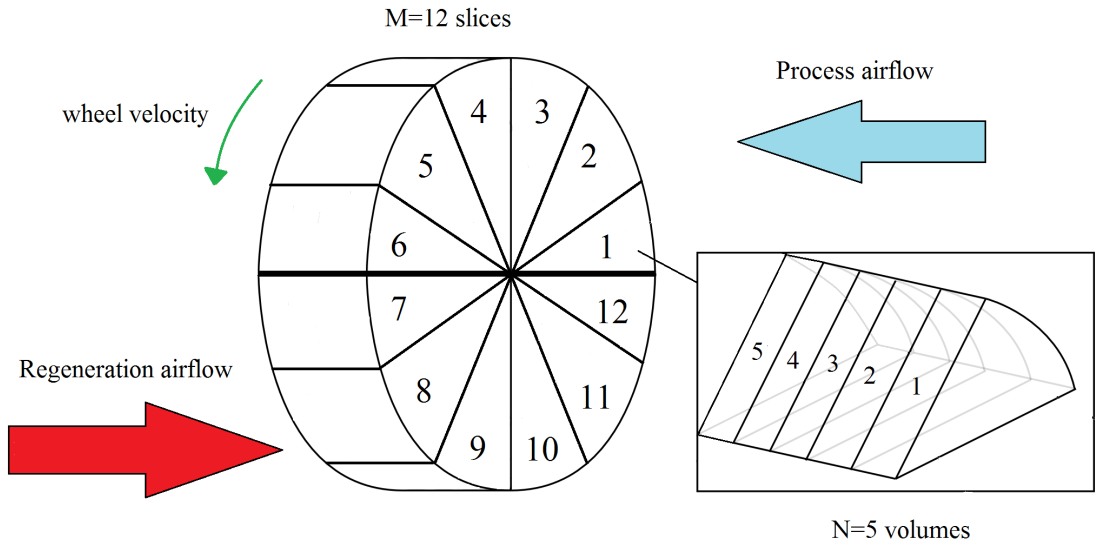

Figure 6.1: Spatial discretisation of the wheel.

In Fig. 6.1 the spatial discretisation of the wheel is shown. Here M=12 slices and N=5 volumes per slice were used for the simulations. The wheel is divided in half, maintaining the 6 upper slices (from 1 to 6) in the process area, and the lower 6 (from 7 to 12) in the regeneration area. Within each of the 12 slices, process air enters the wheel in volume 1 and exits from volume 5, while regeneration air enters in volume 5 and exits from volume 1. The wheel rotation is counterclockwise (see the arrow in Fig. 6.1 for the rotation direction assumed as positive).

To prove that the model provides a good representation of the DW behavior, the distribution of air temperature (Ta), desiccant material temperature (Tm), water content in the air (X) and in the desiccant (Xd) are shown in each volume (Fig. 6.2, Fig. 6.3, Fig. 6.4, Fig. 6.5) for a rotating speed of 10 rev/h.

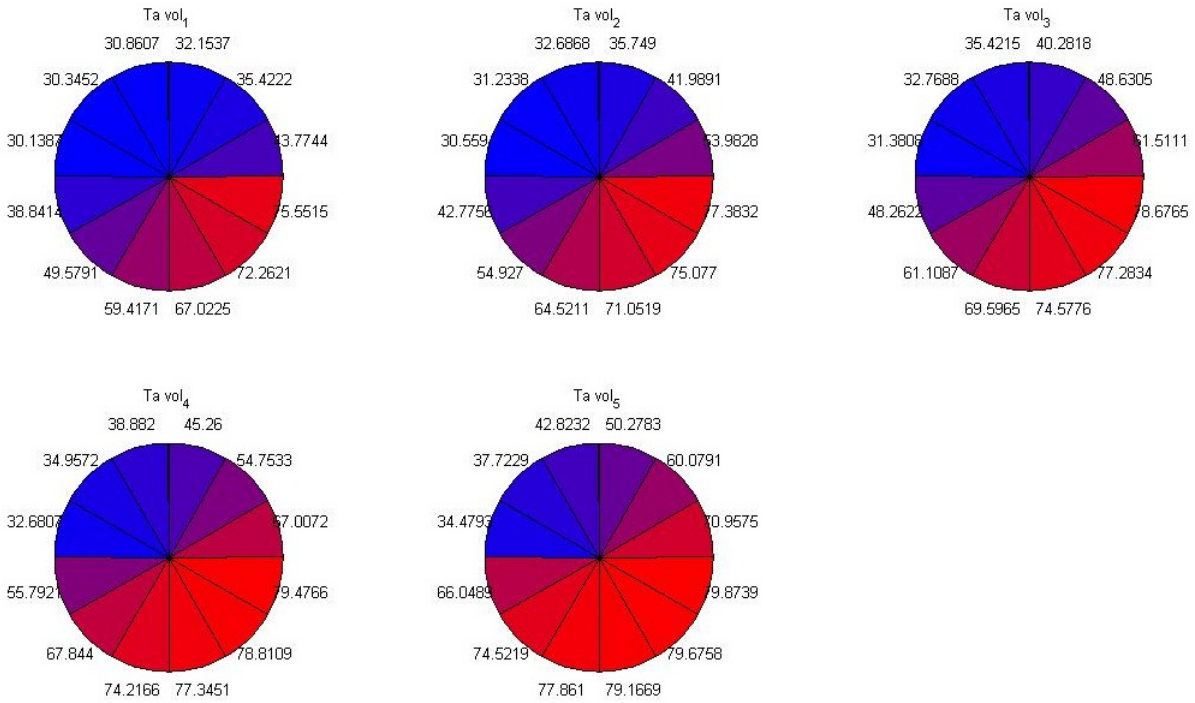

Figure 6.2: Air temperature.Spatial distribution.

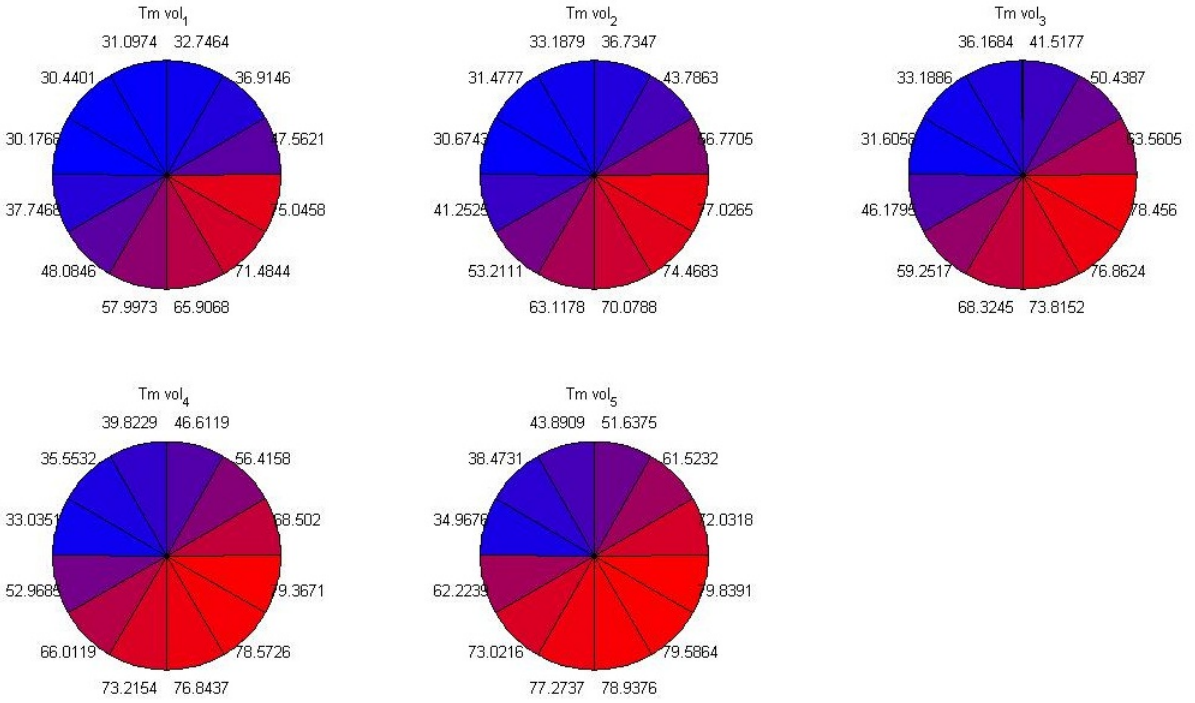

Figure 6.3: Desiccant material temperature. Spatial distribution.

In Fig. 6.2 and Fig. 6.3 the air streams and desiccant material temperatures are shown. The two temperatures differ up to at most 4°C in the boundary slices, thus between the process and the regeneration areas, and show the same trend.

First, we analyze the process area.

We start considering volume 1, that is directly connected with the inlet process air. The desiccant material, which is heated by the regeneration air, has a high temperature while entering the process area in slice 1. Process air stream temperature is influenced by desiccant condition entering the process area, and thus it is higher than the prescribed 30°C process temperature also in volume 1 of each slice. Both the mentioned temperatures decrease from slice 1 to slice 6, because the air stream cools down the desiccant material while said material flows in angular direction due to rotation. If we conversely analyze the axial direction, from volume 1 to volume 5 of the same slice, the same two temperatures increases.

Now we analyze the regeneration area.

If we consider volume 5 instead of volume 1, we can see a dual effect with respect to the process area just addressed. The desiccant material enters the regeneration area, in slice 7, at a low temperature referring to the air flow regeneration temperature of 80°C. Then the material is heated by the regeneration air, and both the considered temperatures increase from slice 6 to slice 12. In the axial direction, thus following the regeneration air stream direction, both temperature conversely decrease.

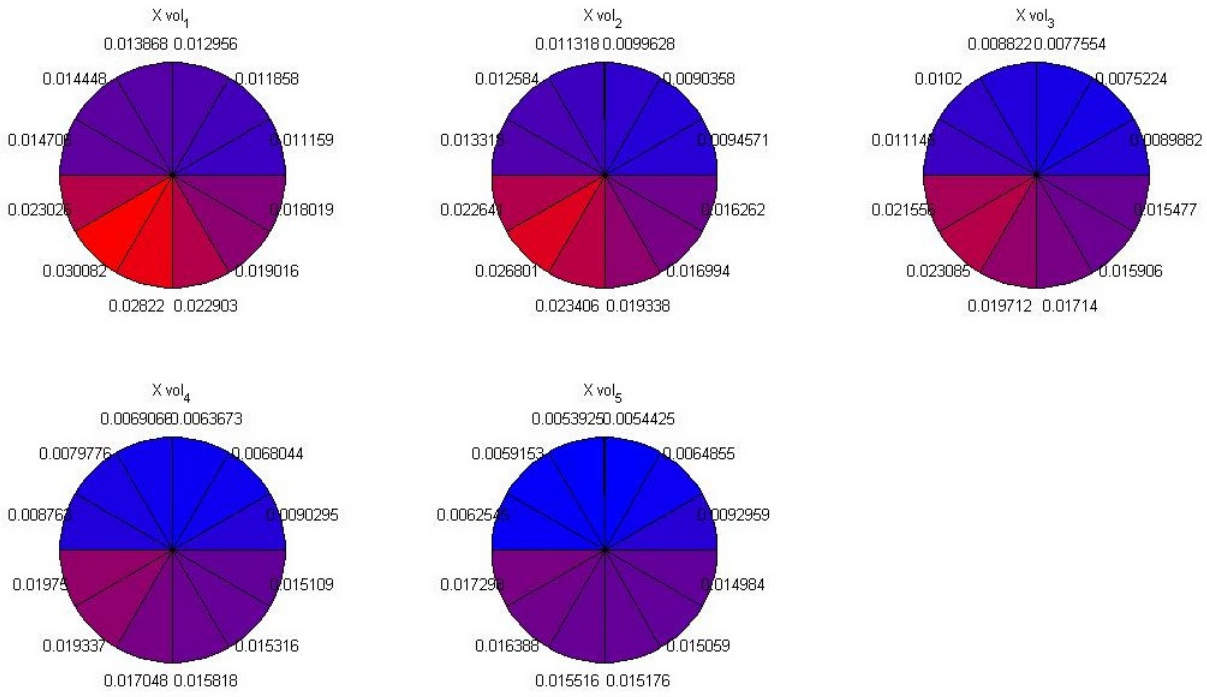

Figure 6.4: Water content in the air. Spatial distribution.

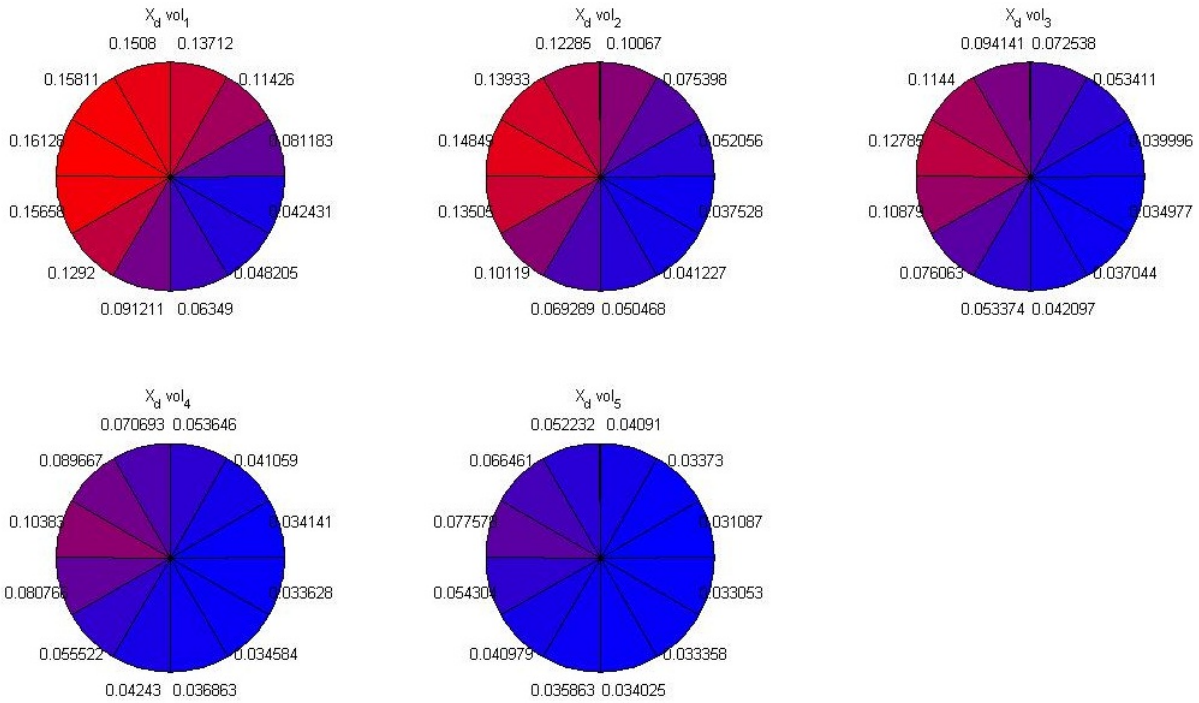

Figure 6.5: Water content in the desiccant material. Spatial distribution.

In Fig. 6.4 and Fig. 6.5 the air streams and desiccant material water contents are shown, to prove the good agreement between the model and the assumption made (and verified in chapter 5) on the wheel operation.

If we consider Fig. 6.4, we can see that the air water content decreases from volume 1 to volume 5 for process area slices, while it increases from volume 5 to 1 for the regeneration ones. Thus the process air is dehumidified, while the opposite happens to the regeneration air. If we consider volume 5, thus the outlet process air humidity, we can make the following statements. At the beginning of the adsorption period, from slice 1, the adsorption process is less effective because the desiccant material is still at high temperature, as said before and shown in Fig. 6.3. Then, at the end of the adsorption period, the desiccant increases its water content, as shown in Fig. 6.5, and its adsorption capacity decreases. Thus, the air humidity in the process area (from slice 1 to 6 of volume 5) first decreases and then increases, because the adsorption phenomenon is influenced by the desiccant water content and temperature. At the beginning (slice1) the effect of the temperature on the adsorption capacity is more relevant, while it is the desiccant water content at the end (slice 6). We can see the dual effect considering volume 1 in the regeneration area: from slice 7 to 12, air humidity first increases and then decreases.

Referring to Fig. 6.5, we notice that water content in the desiccant material is higher in volume 1 than in volume 5, in both the regeneration and the process area. This is because of the airflows' direction: process air releases water flowing from volume

1 to volume 5, while regeneration air brings water flowing from volume 5 to volume 1. Thus the water content in desiccant is greater at the process air inlet and at the regeneration air outlet, corresponding to volume 1.

6.3 Parametric analysis of performance

In this section a parametric analysis is carried out, referring to the base case illustrated in sec. 6.1. The wheel operation, as said in sec. 2.2, is influenced by some parameters. For the presented analysis we decided to change, one at time, the inlet conditions of airflows, and to show how these conditions affect the wheel behavior. In Fig. 6.6 and Fig. 6.7 the simulation results for outlet process air absolute humidity ($X_{pro,out}$), as a function of the wheel speed, are presented, and can be compared with Fig.6 in [7].

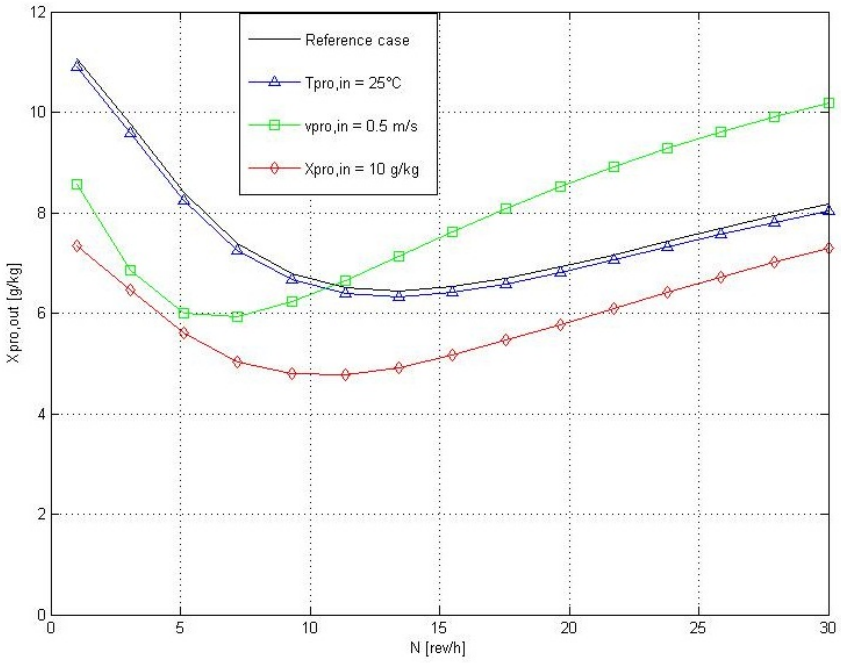

Figure 6.6: Outlet process air humidity versus rotating speed: influence of process air conditions.

Fig. 6.6 shows the results obtained in three simulations, varying the process airflow temperature, velocity and absolute humidity with respect to the base case.

- If the inlet process air temperature decreases (blue line) the relative air humidity becomes higher at constant absolute humidity. Thus the desiccant dehumidification capacity increases, and the process air exits the wheel with a lower amount of water. This effect is due to the higher capacity of the desiccant material of keeping water at high relative humidity as shown in sec. 2.2.1.

- If the process air velocity decreases (green line), at low rotating speed, also the outlet air relative humidity does. This is because the process air remains for a longer time inside the wheel. However, at high rotating speed, the dehumidification capacity decreases, because the reduced airflow takes more time to cool the desiccant material and to start the dehumidification process.
- If the inlet process air absolute humidity decreases (red line), quite obviously also the outlet process air humidity decreases.

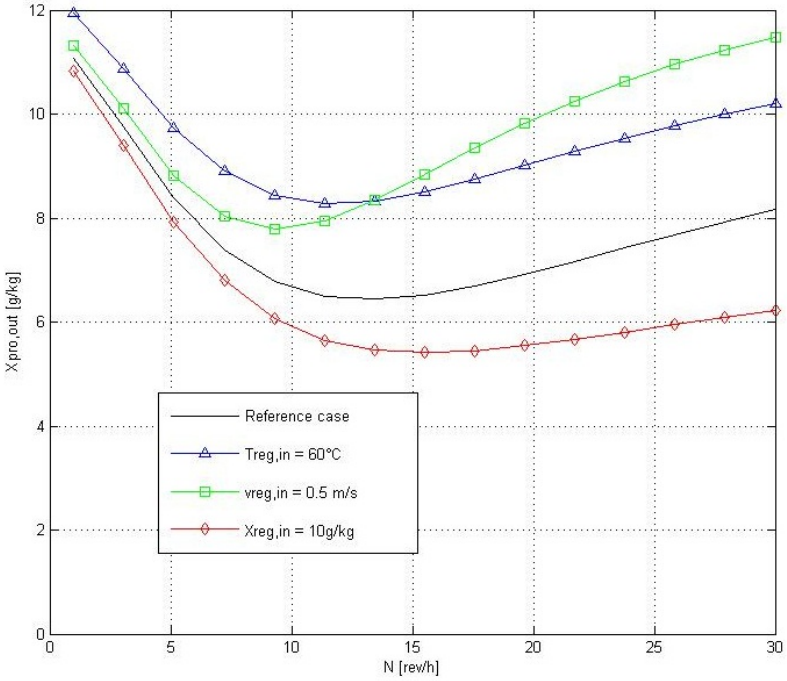

Figure 6.7: Outlet process air humidity versus rotating speed: influence of regeneration air conditions.

Fig. 6.7 is obtained changing the regeneration air flow temperature, velocity and absolute humidity, with respect to the base case.

- If the inlet regeneration air temperature decreases (blue line) the relative air humidity becomes higher at constant absolute humidity. The result is a lower dehumidification capacity, due to the reduced water mass transfer between the desiccant and the regeneration air.
- If the regeneration air velocity decreases (green line), the moisture removal from the desiccant material is less effective. This is because the regeneration air remains for a longer time inside the wheel, and therefore the dehumidification capacity of the wheel is lower.
- If the inlet regeneration air absolute humidity decreases (red line), the dehumidification capacity become higher. This effect is due to the higher water

mass transfer during the regeneration process, which leads to higher adsorption capacity.

7 System control and energy saving

As said in sec. 1.5, DWs are an interesting technology to improve the performance of AHUs in terms of energy saving. Thus, the DW model presented in this work, has been first validated, as shown in chapter 5, and then, it has been used for a system-level study, that is described in this chapter. The main purposes of this study are to show that the model is suitable for control design, and to prove the energy saving discussed in sec. 1.5. In this chapter, we first choose a representative operating context and the desired indoor air conditions. Then, we present a Modelica model of a standard AHU, and we introduce a simple control system for it. In the same operating conditions, a control system is then implemented also for a AHU based on a DW with the aim of obtaining the same HVAC operation required to the AHU without DW. Finally, the energy consumptions of the two models (without and with DW) are compared through simulation.

7.1 The considered scenario and the desired control behavior

In this section we present the operating conditions used for both the models, standard AHU and AHU with DW, and we establish the desired system control performances.

The chosen air conditions, in terms of humidity and temperature, are shown in Tab. 7.1. In the presented configurations, one third of the return air has to be recirculated. For the AHU with DW the operation speed of the wheel has been set at $3rev/hour$.

Air conditions	$X[g/kg]$	$T[°C]$
External ambient air	17	30
Indoor return air	15	27
Desired indoor air	13	26

Table 7.1: Air conditions

One of our work's purposes is to show the energy efficiency of a AHU with DW through simulation. Thus, we decide to compare standard AHU and AHU with DW

in the same operating conditions, as said before. It is worth noting, however, that the energy consumption is also affected by the performances of the control system. If we desire a higher-performances control, we have to spend more in terms of energy than if we use a control with lower performances. Therefore, we here define some desired control performances, as shown in Tab. 7.2, and we choose a control system that guarantees the system behavior at the boundary of such conditions. To specify said control performances, we refer to the temperature and humidity set point step variations, as shown in the followed section.

Control performance	desired value
maximum overshoot [%]	25
temperature 2% *settling time* [*sec*]	60
humidity 5% *settling time* [*sec*]	1800

Table 7.2: Desired control performances.

7.2 Control of a standard AHU

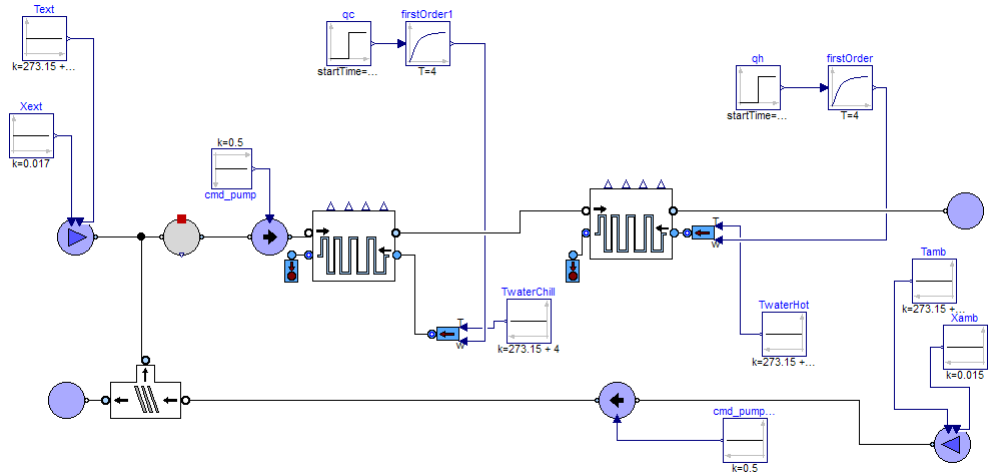

Figure 7.1: Standard AHU model in Modelica

The standard AHU model used here is shown in Fig. 7.1. The external ambient air, mixed with the recirculation air, passes through a cooling coil, in which it is cooled down considerably. Then it has to be heated before it can enter the indoor ambient at the desired conditions of humidity and temperature. To bring process air in such conditions, the control variables that we can use are the cooling (qc) and heating (qh) water mass flow rates. For the classical control system design, we need to know the system in terms of transfer functions. Thus, we make the following simulation:

we let the system reach an equilibrium state, and then we apply a step change to each control variable, as shown in Fig. 7.2 and Fig. 7.3.

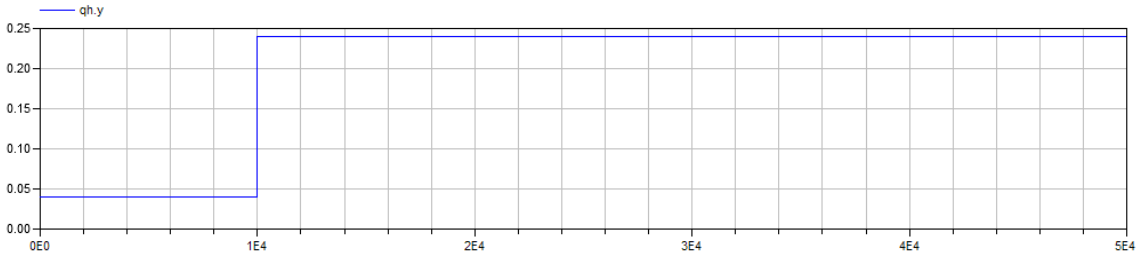

Figure 7.2: Step on heating water mass flow rate (qh).

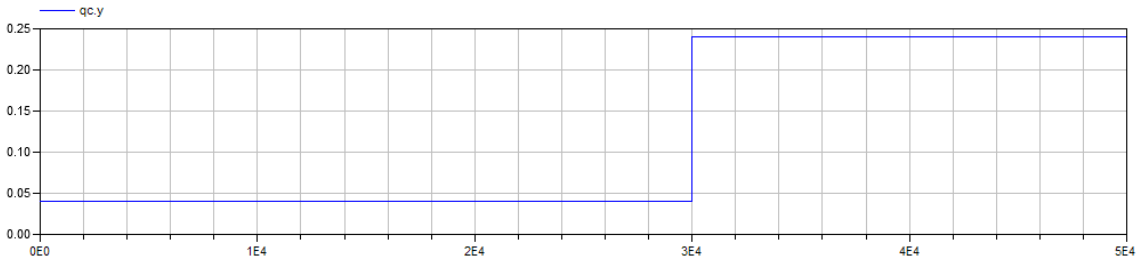

Figure 7.3: Step on cooling water mass flow rate (qc).

Watching the system responses, shown in Fig. 7.4 and Fig. 7.5, it is immediately clear that the system is triangular: *qh* does not affect the air humidity, but only the air temperature, while *qc* affects both the quantities.

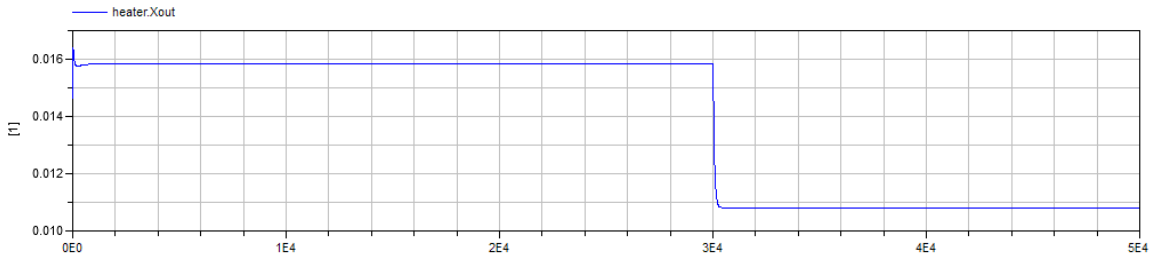

Figure 7.4: Air humidity (Xout) response.

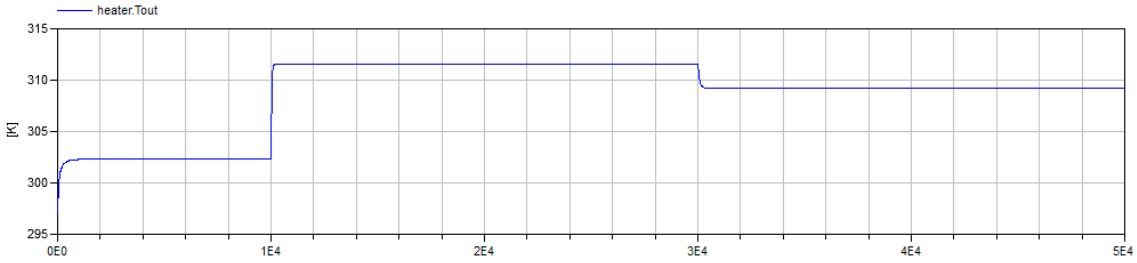

Figure 7.5: Air temperature (Tout) response.

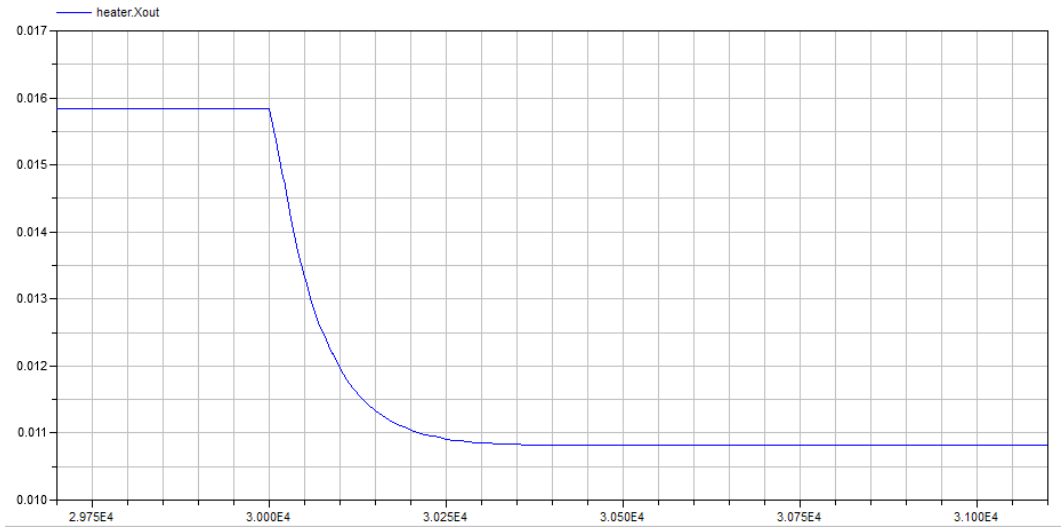

Figure 7.6: Air humidity (Xout) response.

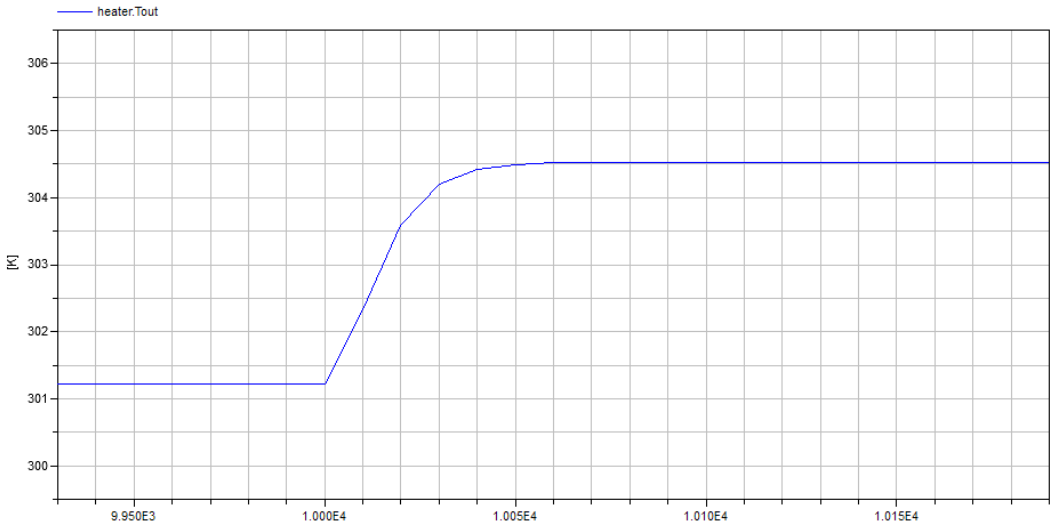

Figure 7.7: Air temperature (Tout) response.

With the simulation results, shown in Fig. 7.6 and Fig. 7.7, we can obtain the transfer functions which characterize the system using an empirical method. The result is shown in figure Fig. 7.8, where $G_{cx} = \frac{-0.021839}{1+60s}e^{-5s}$, $G_{ht} = \frac{14.56}{1+17.25s}e^{-4.25s}$ and $G_{ct} = \frac{-71.13}{1+88.5s}e^{-2.5s}$.

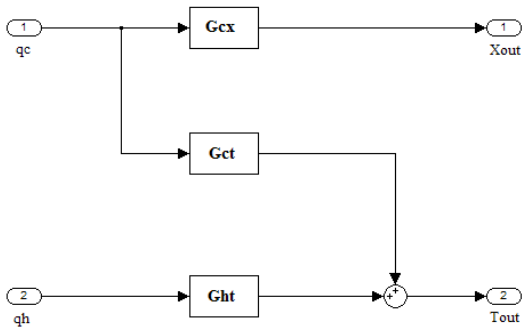

Figure 7.8: AHU block diagram.

The control purposes can be achieved using two PI controllers, as shown in Fig. 7.9. PI_X uses the control variable qc to control air humidity, while PI_T uses qh to control air temperature; both qc and qh depend on valves' opening and closure.

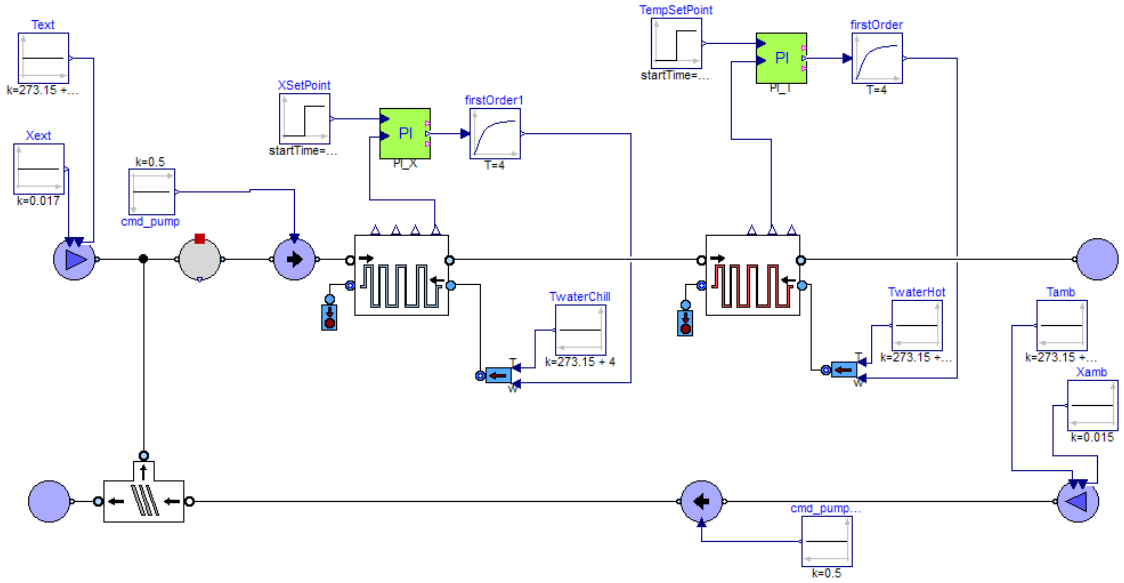

Figure 7.9: AHU control scheme.

The PIs parameters have been found with the use of an empirical method, based on the Internal Model Control (IMC) principle [15], and then with a some fine-

tuning based on simulations. The results of this procedure are shown in Tab. 7.3. This method was chosen because it seems to be a good choice in the case of model responses characterized by a dominant time constant and a delay, as in the present case.

Controller	Kp	Ti
PI_X	-5.8	60
PI_T	0.05	17

Table 7.3: PIs parameters.

The simulation results in Fig. 7.10, Fig. 7.11 and Fig. 7.12, show the behavior of the control system. Blue and red lines represent, respectively, the control set points, and the controlled variables responses ($Tout$ and $Xout$). Note the temperature scale in Fig. 7.12.

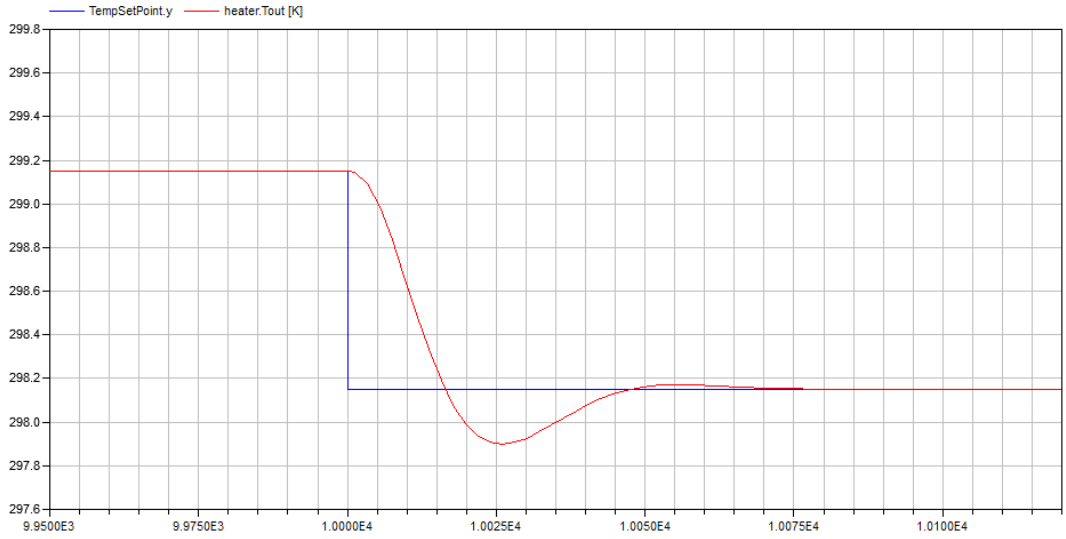

Figure 7.10: Step change in temperature set point and air temperature response.

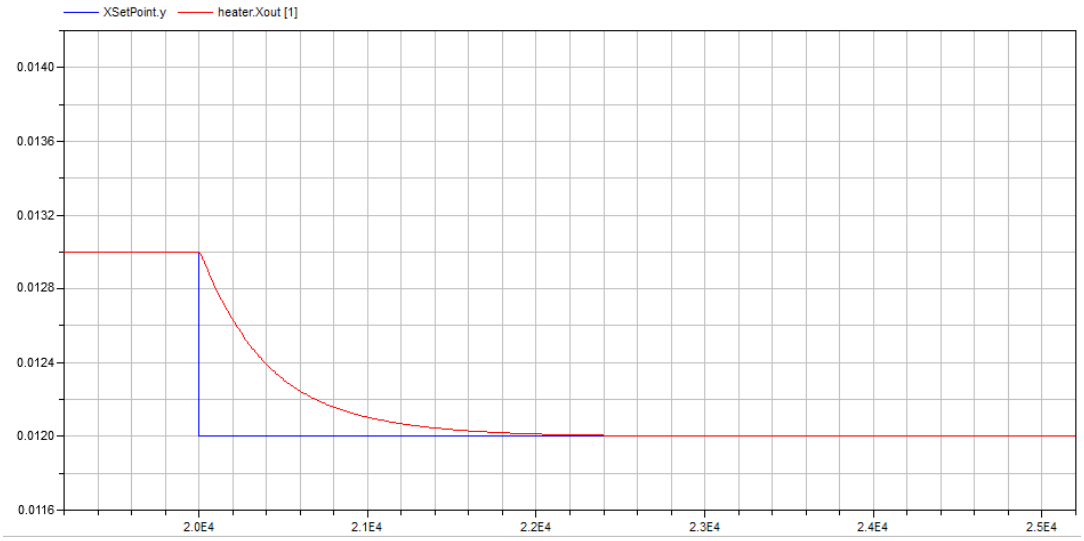

Figure 7.11: Step change in humidity set point and air humidity response.

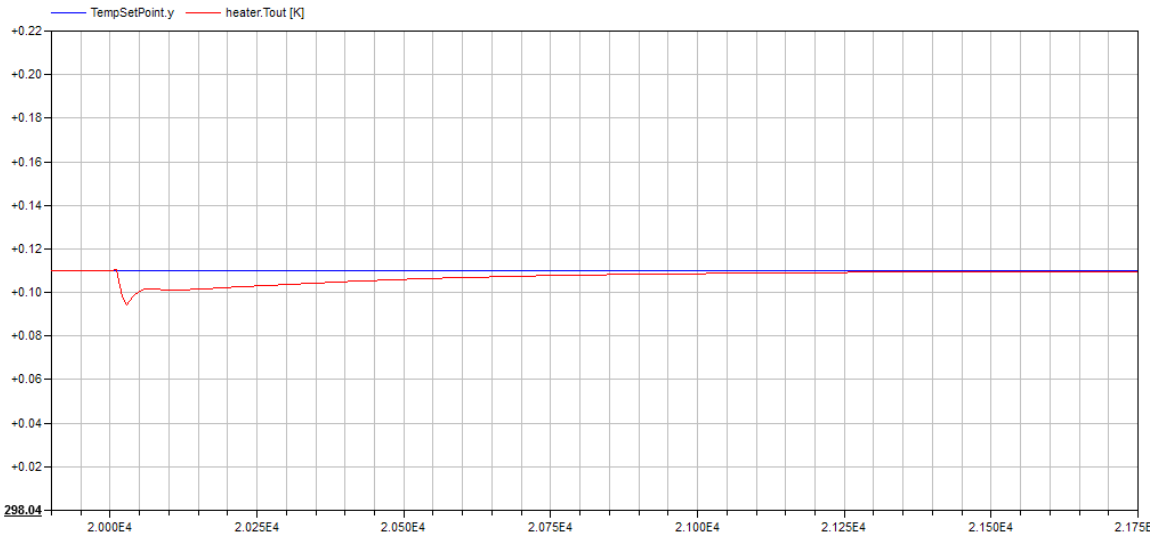

Figure 7.12: Air temperature variation due to the step of humidity set point.

Simulation results show that we can obtain a good set point tracking, which is among the main control purposes in HVAC systems. Both regulations satisfy the desired specifications listed in Tab. 7.2. $Xout$ response is slower than $Tout$ one, because of the desired control behavior.

It is worth noting that control parameters are chosen in order to obtain a "frequency separation" which allows the humidity control not to affect too much the $Tout$ behavior, as shown in Fig. 7.12.

7.3 Control of an AHU with DW

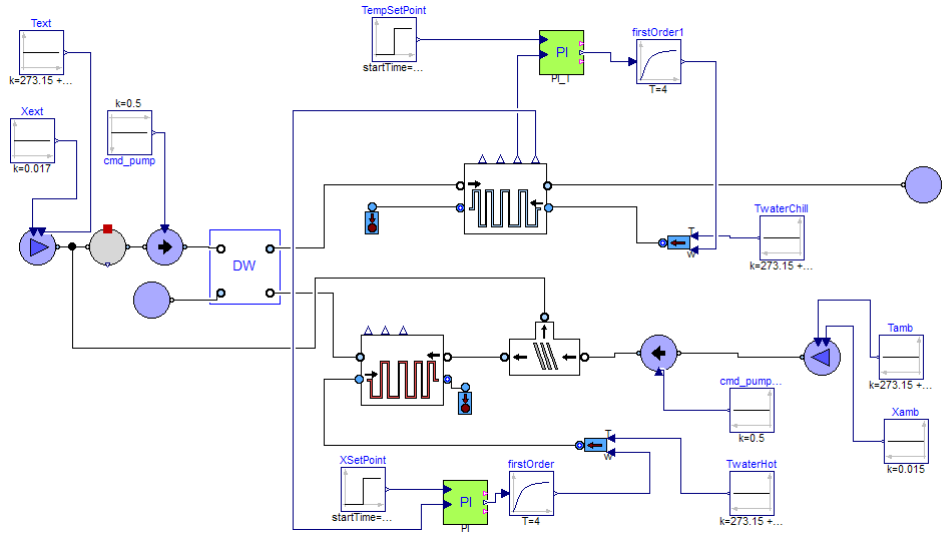

Figure 7.13: AHU with DW model in Modelica.

Fig. 7.13 shows a possible model of an AHU with DW, the only one used in this work for obvious space reasons, endowed with a control system. The external ambient air is mixed with the recirculation air, and then it passes through the wheel process area. In the DW, process air is dehumidified, until reaching the desired value, and heated. Then, a cooling coil cools the air, before it enters the internal ambient. Air from the indoor is split and used as recirculation air or as regeneration air, after being heated. The model has the same boundary conditions and results in the same control scenario as in the case of the standard AHU control (sec. 7.1).

For control system design, we follow the same steps illustrated in sec. 7.2. The system is still triangular, but in this case we have to use qh to control air humidity and qc to control air temperature. Referring to Fig. 7.14 the transfer functions are: $G_{hx} = \frac{-0.021839}{1+325.5s}e^{-189.5s}$, $G_{ct} = \frac{-71.72}{1+70.5s}e^{-3.1s}$ and $G_{ht} = \frac{43.06}{1+712.5s}e^{-400.5s}$.

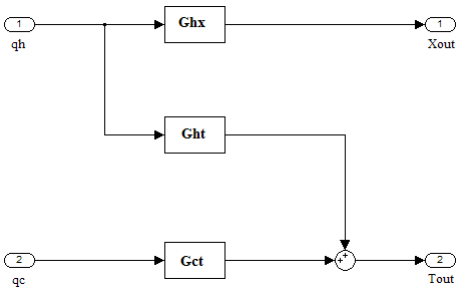

Figure 7.14: AHU with DW block diagram.

It is worth noting that the use of the DW introduces a relevant delay due to a higher-order dynamics, in the system. This dynamic can also be approximated with a first order model plus delay. In this case we found consistent delays, as shown in G_{hx} and G_{ht}. The wheel performs 3 $rev/hour$ and thus, the heat and moisture transport is quite slow. Therefore, the system control performances are limited by the system delay between the qh variation and the induced $Xout$ response. However, we can use the same control strategy, as shown for the standard AHU, and obtain good control results. The PIs parameters used in the model of an AHU with DW are shown in Tab. 7.4.

Controller	Kp	Ti
PI_X	-10	525
PI_T	-0.8	60

Table 7.4: PIs parameters.

To show the behavior of the control system, we present the results of a simulation in which the set point signals vary as in the case of the standard AHU simulation in the previous section. In Fig. 7.15, Fig. 7.16 and Fig. 7.17, blue and red lines represent respectively, the control Set Points, and the controlled variables responses ($Xout$ and $Tout$). Note the temperature scale in Fig. 7.17.

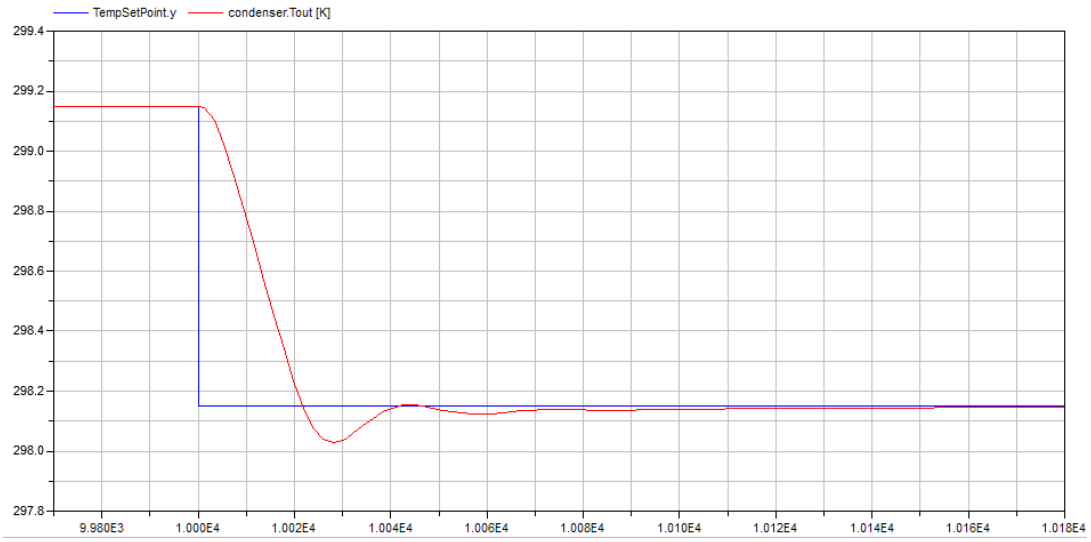

Figure 7.15: Step change in temperature set point and air temperature response.

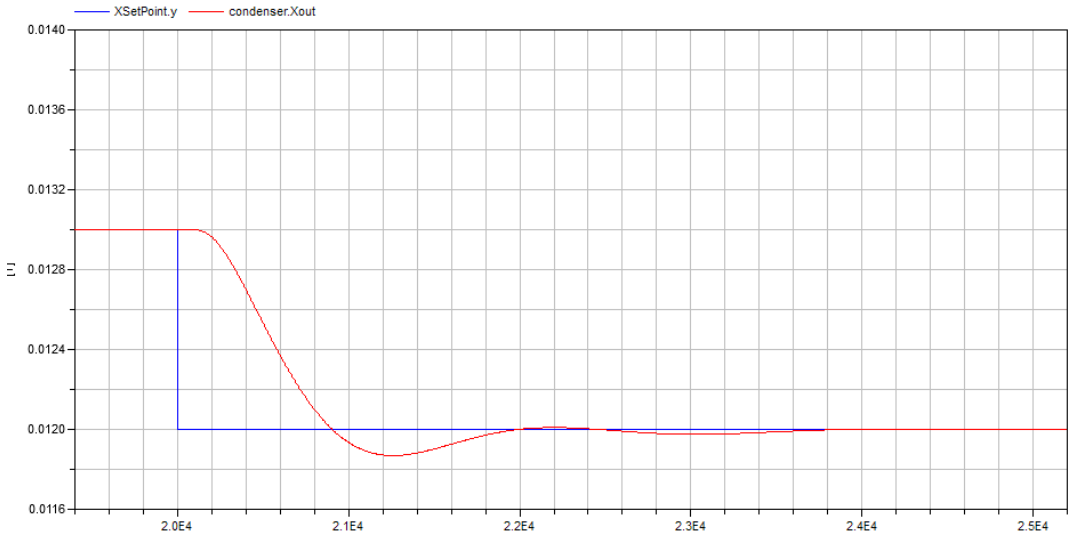

Figure 7.16: Step change in humidity set point and air humidity response.

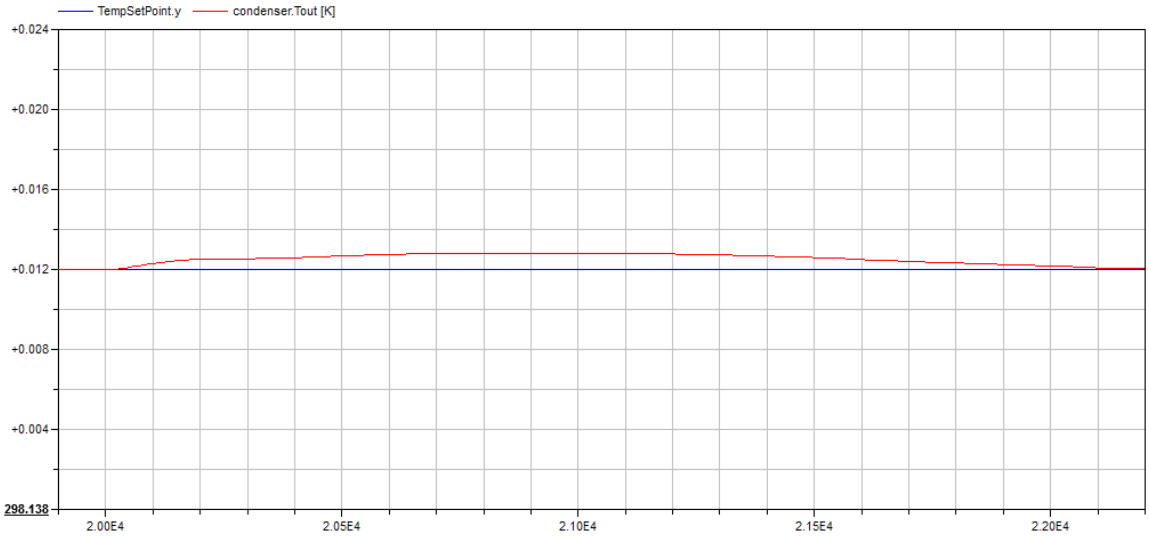

Figure 7.17: Air temperature variation due to the step of humidity set point.

Watching at Fig. 7.16, we can notice that the humidity response in "quite slow" as the system has a higher-order dynamic. With a PI controller, it is not possible to increase further the settling time performance, but with a different humidity controller we can do so, as shown later in sec. 7.5.2. However, the slow dynamic of $Xout$, even if of tens of minutes, is not a critical matter. We have to remember that the presented control system is used for human being comfort. For such a purpose, the control performances shown above are acceptable.

7.4 Comparison between standard AHU and AHU with DW

In this section, we compare the simulation results of the standard AHU model and the one with DW. First, the air temperature and humidity responses are shown together to prove the "similar" behavior of the two control systems. Then, the energy consumptions are compared to show the possible energy saving with the use of a DW solution.

7.4.1 Control systems behavior

As said in sec. 7.1, control systems' behaviors can be compared in terms of maximum overshoot and settling time. In order to appreciate this comparison, simulation results shown in sec. 7.2 and sec. 7.3 have been plotted together, and shown in Fig. 7.18 and Fig. 7.19.

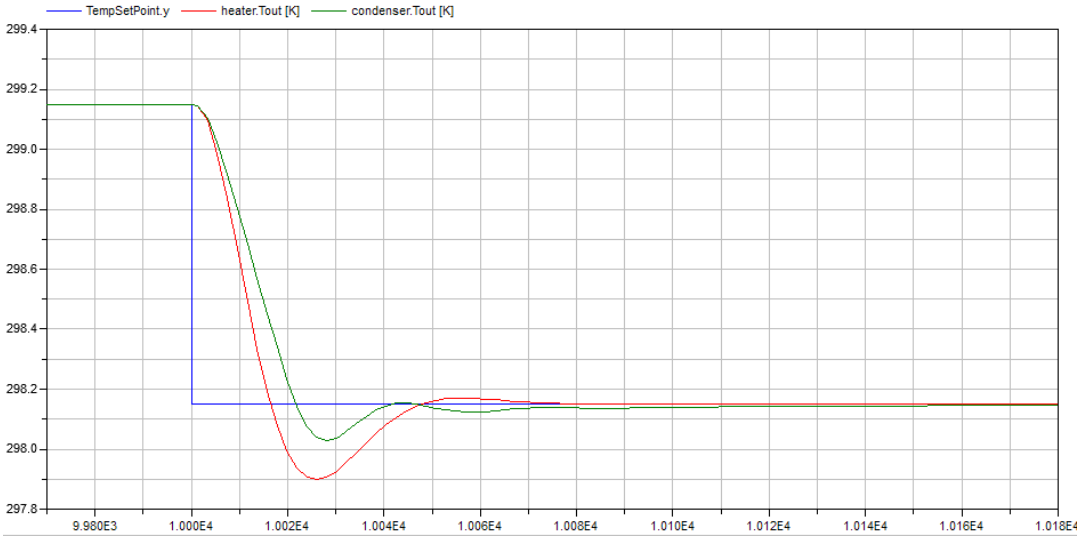

Figure 7.18: Step change in temperature set point (blue line) and air temperature response. Comparison between standard AHU (red line) and AHU with DW (green line).

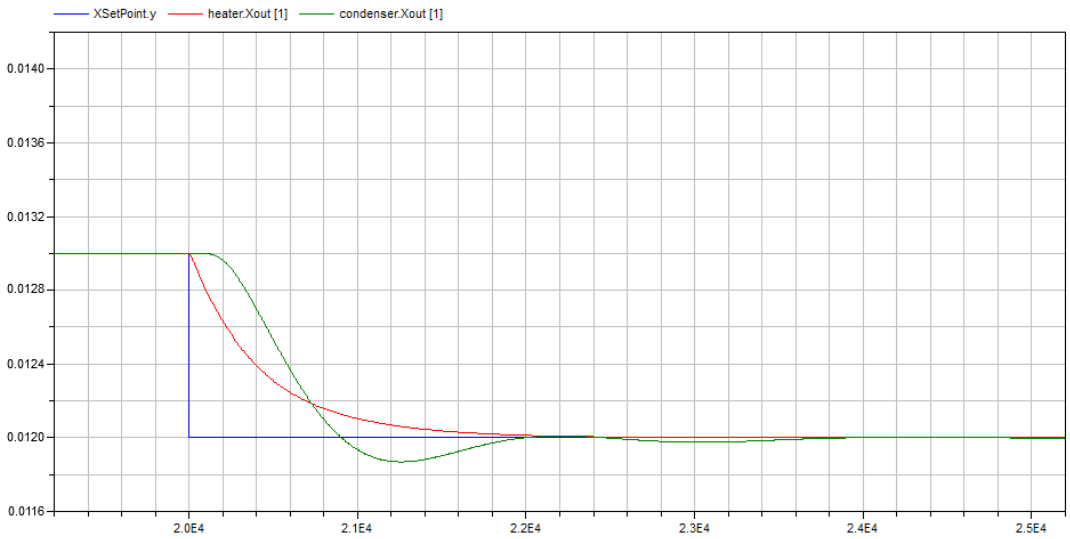

Figure 7.19: Step change in humidity set point and air humidity response. Comparison between standard AHU (red line) and AHU with DW (green line).

The comparison shows that the two control systems can be considered "equivalent" in terms of performances. Thus, the energy consumptions of the two models can be compared, as shown the next section.

7.4.2 Energy consumption

Once we show that we obtain a good control in both (standard AHU and AHU with DW) cases, and the control performances are similar, we can compare the energy consumption of the two (controlled) AHU models.

The *heating energy*, related to the heater operation, and the *cooling energy*, corresponding to the cooler/condenser operation, are shown in Fig. 7.20 and Fig. 7.21. These figures evidence that DW based solution (blue lines) requires less energy, especially if we consider the cooling. This result is not surprising if we consider that the cooling energy, in the case of standard AHU, refers to the energy used by the condenser. In that case, we require a lot of energy, because we need to pull down the air temperature considerably. This is because we want to dehumidify the air through condensation, thus the air has to be brought under its dew point temperature. In the case of AHU with DW, we do not need to reduce the process air temperature so much, because the air is dehumidified passing through the wheel, and condensation is not required.

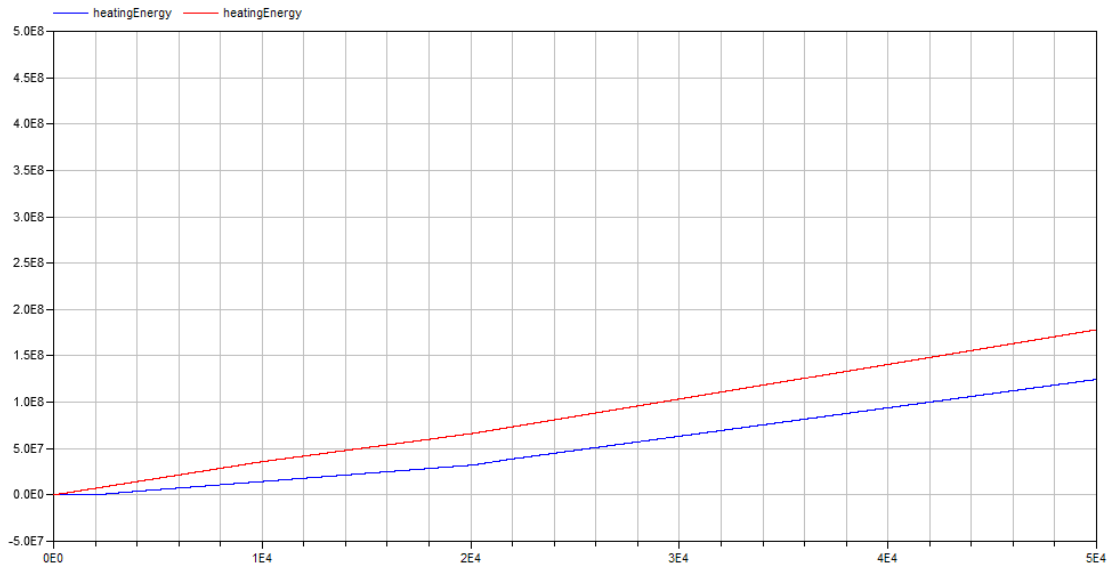

Figure 7.20: Heating energy consumption. Comparison between standard AHU (red line) and AHU with DW (blue line).

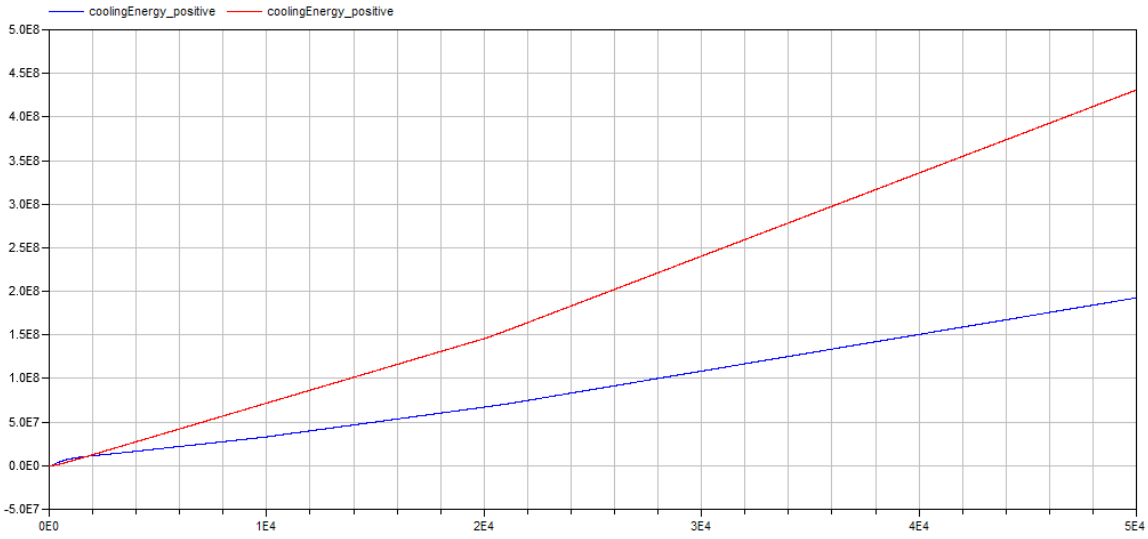

Figure 7.21: Cooling energy consumption. Comparison between standard AHU (red line) and AHU with DW (blue line).

In Tab. 7.5 the energy consumptions during the entire simulation period, 50000 sec ($\backsimeq$13.88 hours) are listed. The possible energy saving appear immediately clear and it is up to 42%.

Energy consumption	Standard AHU	AHU with DW
Cooling energy [kWh]	119.73	53.5
Heating energy [kWh]	49.13	43.7
Total energy [kWh]	168.86	97.2

Table 7.5: Energy consumptions. Comparison between standard AHU and AHU with DW.

In the case of an AHU with DW, we have to consider also the energy consumption of the engine used for the wheel rotation. This energy is however definitely small compared with the cooling and heating energies, thus it can be neglected in the energy consumption comparison between the two AHU solutions.

7.5 Control system performance

In this section, we spend a few words on the choice of the control systems performance. Comparing the temperature control requires with the humidity ones, in sec. 7.1, one can note that the settling time for humidity control is very long. In the case of an AHU with DW, it is clear that such a time is influenced by the higher order dynamic introduced by the wheel, as said in sec. 7.3. In a standard AHU, conversely, that effect does not appear, thus it seems reasonable that the control system can reach higher performances in terms of settling time. As said in sec. 7.1, the aim of this chapter is to perform an energy comparison between the two AHU configurations. Thus, we need the same control system performances for both the configurations. To obtain that, we chose a set of control specifications (in terms of overshoot and settling time of the set point response) feasible for both the standard AHU and that with the DW, and we tuned the controls of the two in such a way to best approach those specifications. Of course this means that no optimality was pursued for the two units individually, but rather a simulation setting was created where they are required to "do the same (reasonable) things", and the two energy consumptions for that operation are compared. In this section, we present a particular choice of PI_X parameters for the standard AHU that guarantees better performances and we show the energy consumption in that case.

The second topic of this section deals with the AHU with DW control. As said in sec. 7.3, with a PI controller, it is not possible to make faster the humidity response, but with a different controller, we can do something about it. Now, we want to present a simple PID controller that exploits this possibility.

7.5.1 Improvement of the standard AHU control

The control strategy and the PI_T parameters are the same as in sec. 7.2, but the PI_X parameters are different from the previous case, as shown in Tab. 7.6.

Controller	Kp	Ti
old PI_X	-5.8	60
new PI_X	-80	60

Table 7.6: PI_X parameters. Old and new solution.

In Fig. 7.22 the *Xout* behavior, with the new PI_X controller, is compared with the same signal in the case of standard AHU control illustrated in sec. 7.2. It is clear that with a different humidity controller, we can reduce the settling time significantly.

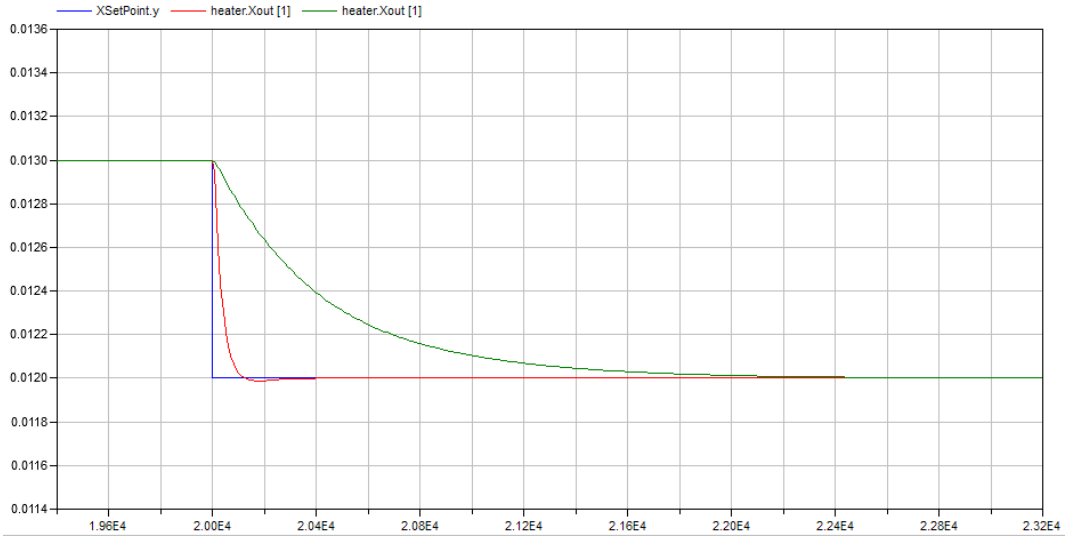

Figure 7.22: Step change in humidity set point (blue line) and air humidity response. Comparison between new PI_X (red line) and old PI_X (green line).

However, the better performance of the control system is paid for in terms of a greater coupling of the system, as shown in Fig. 7.23. This is clearly an undesired effect, but the results obtained herein seems to suggest that it can be considered a small drawback compared to the performance improvement on the humidity control. The matter surely deserves a deeper analysis, that is however deferred to future research.

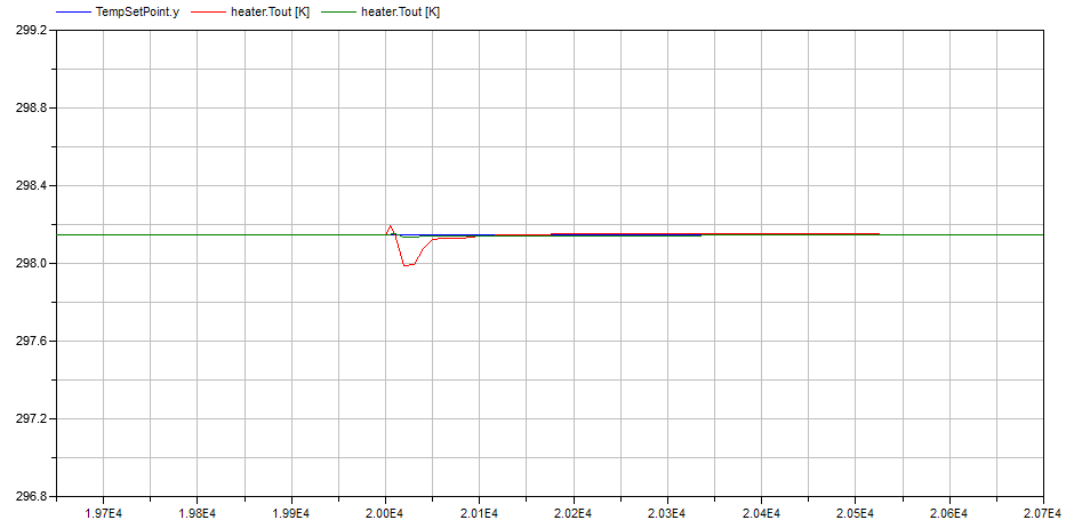

Figure 7.23: Air temperature variation due to the step of humidity set point. Comparison between new PI_X (red line) and old PI_X (green line).

As said before, the energy consumption depends also on the control system. If we desire a higher-performance control, we generally have to spend more in terms of energy. Fig. 7.24 and Fig. 7.25 show that the system configuration with the new PI_X parameters, is a little more energy demanding compared with that with the old PI_X parameters. The energy consumption in the reference period is shown in Tab. 7.7 for both cases. Based on the obtained results, we can confirm the energy saving of the DW solution as in the case of standard AHU with control performances closer to the real operation.

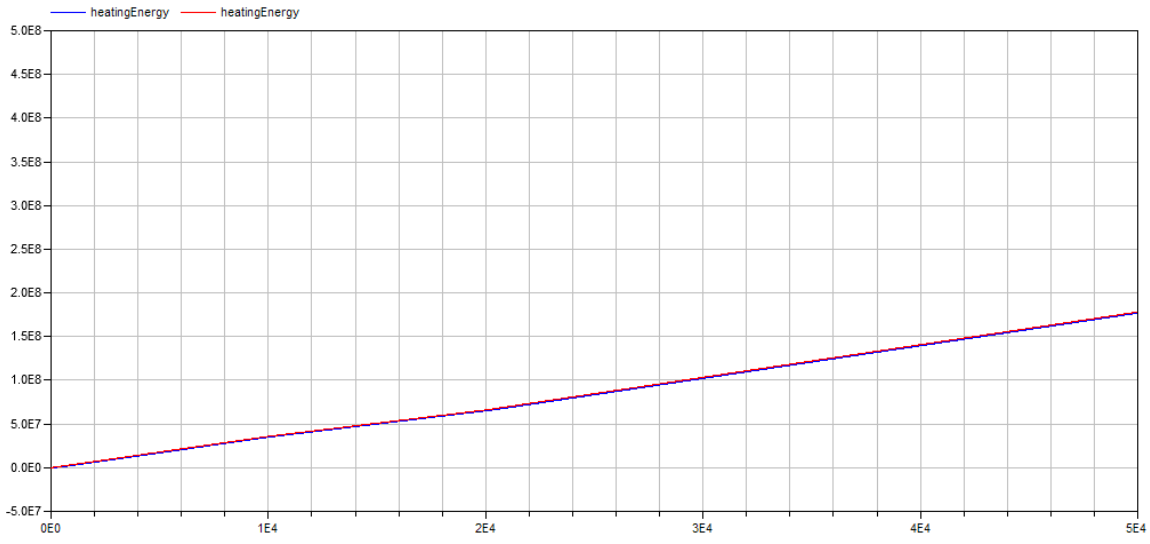

Figure 7.24: Heating energy consumption. Comparison between standard AHU with the old PI_X (blue line) and the one with the new PI_X (red line).

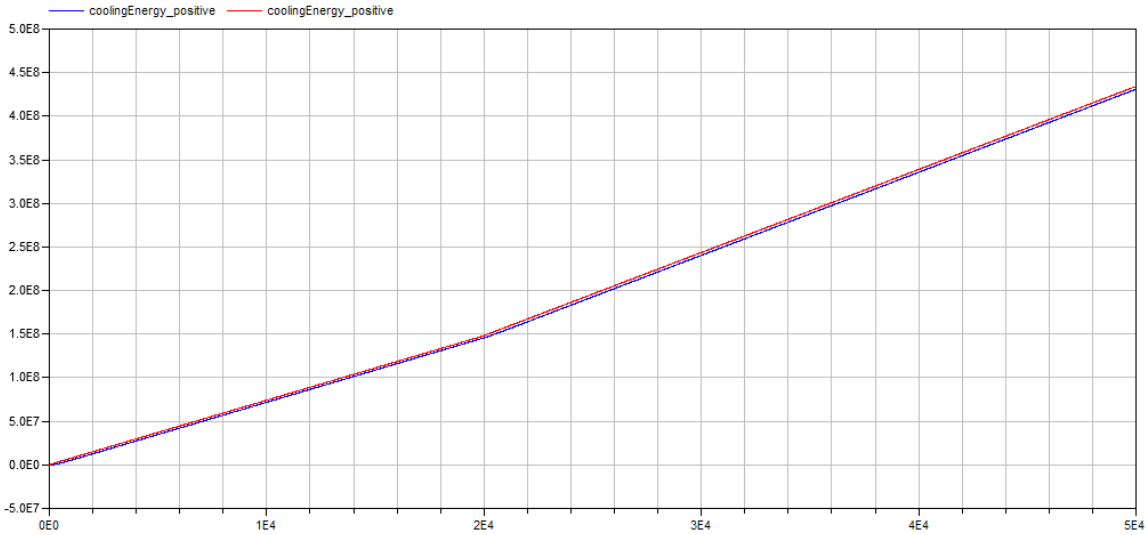

Figure 7.25: Cooling energy consumption. Comparison between standard AHU with the old PI_X (blue line) and the one with the new PI_X (red line).

Energy consumption	AHU with old PI_X	AHU with new PI_X
Cooling energy [kWh]	119.73	120.64
Heating energy [kWh]	49.13	49.5
Total energy [kWh]	168.86	170.14

Table 7.7: Energy consumptions. Comparison between standard AHU with old PI_X parameter and AHU with new PI_X parameter.

7.5.2 AHU with DW: PID controller

The control scheme adopted in this chapter requires the use of two PI controllers, one devoted to the temperature control, and the other to the humidity control. Such an approach proves suitable for the considered control purpose, but for a more general viewpoint, the system performances could be improved with different control schemes. It is not within the scope of the present work to analyze advanced control strategies, nevertheless we spend just a few words on a different humidity controller choice. We focus on the humidity control because it seems to be the one with the most critical behavior.

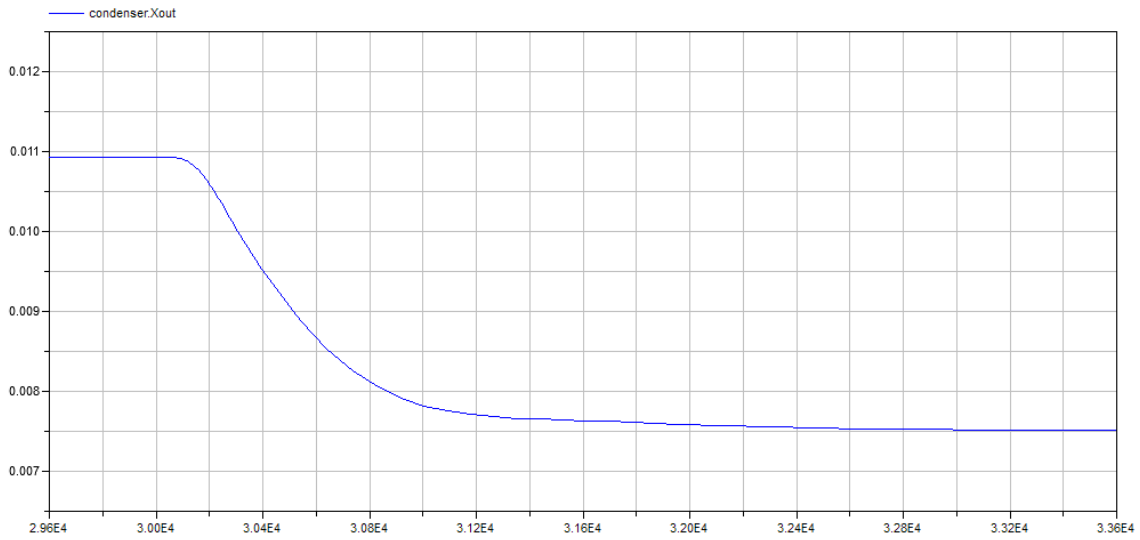

Figure 7.26: Air humidity (Xout) response.

When we dealt with the system identification in sec. 7.3, we approximated the system behavior with a first order plus delay model. This approach is simple and leads to a quite good controller choice. However, if we analyze more in detail the system humidity response (Fig. 7.26), this seems to be more like a response of a system with higher-order dynamics. Thus, we can try to approximate it with a second order dynamic, in order to use a PID controller. The use of derivative action allows to reduce the settling time; further, a PID controller is easily implemented in industrial applications. The PID parameters chosen for the new humidity controller, are listed in Tab. 7.8 (N represents the derivative filter ratio).

Controller	Kp	Ti	Td	N
PID_X	-35	550	130	200

Table 7.8: PID_X parameter.

Looking at the system humidity response, Fig. 7.27, the advantages are both a settling time and overshoot reduction as shown in Tab. 7.9.

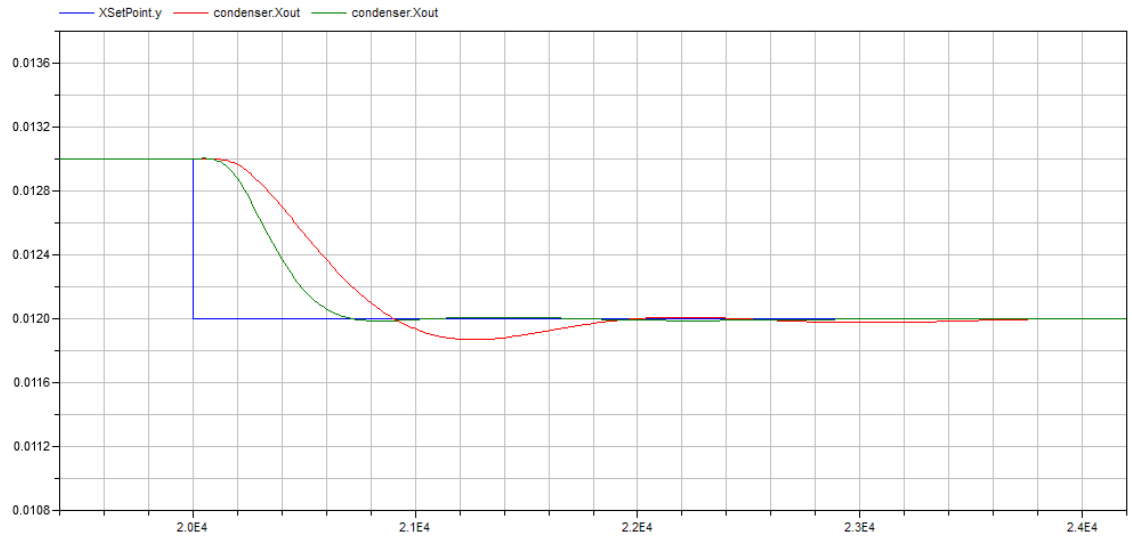

Figure 7.27: Step change in humidity set point (blue line) and air humidity response. Comparison between new PID_X (green line) and old PI_X (red line).

Humidity control performances	old PI_X	new PID_X
settling time 5% [*sec*]	1350	620
maximum overshoot [%]	7.52	1.37

Table 7.9: AHU with DW humidity performance. Comparison between new PID_X and old PI_X.

Obviously, the energy consumption is slightly increased, because of the increase in control system performances. However, the difference between the presented control scheme and that with two PI controllers, in terms of energy consumptions, is not so relevant, thus the obtained response improvements could be worth the expense, although dealing with such tradeoffs in a methodologically sound manner is outside of our scope.

8 Considerations on the wheel velocity

In the previous chapter, a comparison between the energy consumption of a standard AHU and an AHU with DW was presented. Thus, we proved the (considerable) energy saving that can be obtained with the use of a DW. In the control configuration, shown in the previous chapter, we used the heater water flow rate (q_h) to control process air humidity and the cooler water flow rate (q_c) to control the air temperature. The DW velocity (ω) was considered as a parameter. In this chapter, we investigate the possible use of ω as a control variable.

8.1 Investigation on the use of the wheel velocity as a control variable

If the reader focuses on the energy consumption shown in Fig. 7.20 and Fig. 7.21, it is clear that the energy saving is more relevant if we focus on the cooling energy. As said in sec. 7.4.2, the cooling energy in the case of AHU with DW, is related to the cooler operation. Thus, in the AHU, the cooler is the critical element if we consider the energy consumption. Further, it is worth noting that changing the wheel velocity affects the energy consumption of the AHU, but without a relevant effort in terms of wheel engine energy. For these reasons, the question appears legitimate, whether or not the use of ω as a control variable, instead of q_c, could be a good choice. Thus, the idea is to control process air temperature and humidity with ω and q_h. Incidentally, with this new control configuration, the use of the cooling coil is no more necessary.

First, we decided to choose some inlet process and regeneration air conditions and to investigate how the wheel velocity and inlet regeneration air temperature ($Treg, in$) affect the process air outlet conditions. Note that $Treg, in$ in the AHU scheme depends on q_h.

We performed a set of simulations with the wheel model used in chapter 5, and the inlet conditions and parameters in Tab. 8.1. We choose a range of variations for ω and $Treg, in$ and a step of variation for each parameter, as shown in Tab. 8.2.

simulation parameters	$Xpro, in[g/kg]$	$Xreg, in[g/kg]$	$Tpro, in[°C]$	$\frac{Apro}{Areg}[m^2/m^2]$
sim	16.0	15.0	30.0	1

Table 8.1: Setup parameters for simulations.

parameters	min value	max value	*step*
$\omega[rev/h]$	0.5	7	0.5
$Treg, in$ [°C]	40	100	10

Table 8.2: Range of variation and step for wheel velocity and regeneration air temperature.

Fig. 8.1 shows the simulation results by plotting $Xpro, out$ respect to $Tpro, out$. The curves represent the simulations with the same ω, and the dots on each curve represent different values of $Treg, in$ (ω increases from left to right and $Treg, in$ increases from top to bottom along each curve).

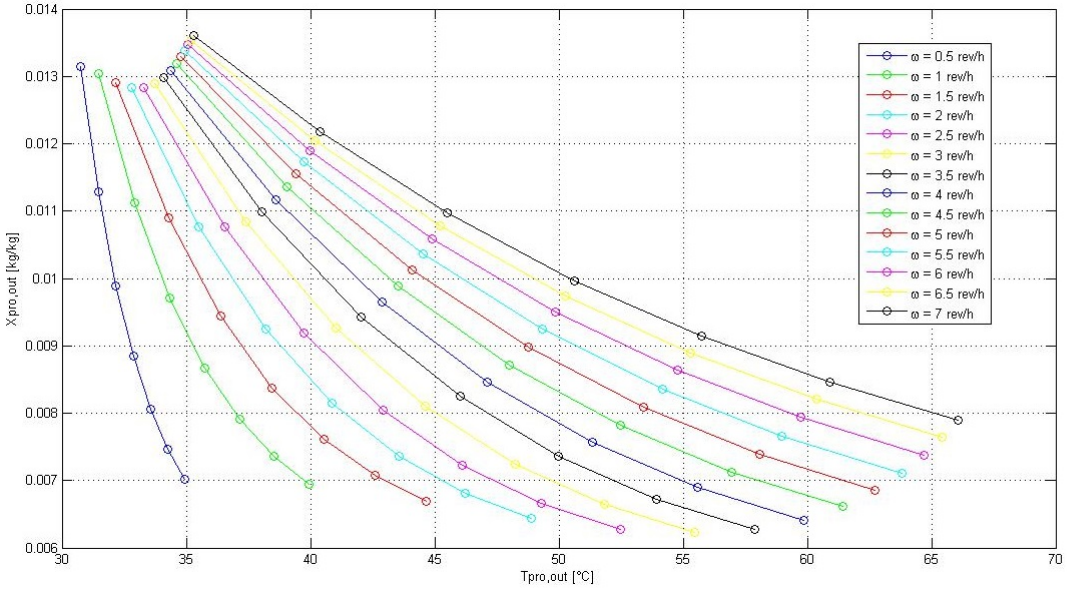

Figure 8.1: Operation range.

Observing Fig. 8.1, we can note that $Tpro, out$ is higher than 30°C for all combinations of ω and $Treg, in$. Recalling that $Tpro, in = 30$°C, it is clear that, if we want to dehumidify, the process air temperature always increases passing through the wheel. Thus, the proposed control scheme is not useful for our purposes (dehumidify and cool down the air). Taking into account the wheel operation, it is possible to implement such a control scheme only if we want to dehumidify and heat the process

air, thus when the external ambient air is "cold" and with a consistent moisture amount. This situation is most typical in winter, however could happen also in summer operation, e.g. in the nigh time and in the particular, but relevant, case of storms. In the situation just mentioned, the external ambient air temperature is lower than the required air temperature, and we need to dehumidify. A heater coluld be placed after the DW, and used to increase the process air temperature once it exits the wheel, and the cooler is switched off. Here, we propose to use the wheel velocity to increase the air temperature without using an additional heater.

8.2 Wheel velocity control

In order to better explain the considered situation, we present a simulation done with the same control scheme used in Fig. 7.13. We maintained the same indoor ambient air conditions, air temperature and humidity set points (Tab. 8.3), PIs' parameters and wheel velocity ($3rev/h$) as in sec. 7.3, while the external ambient air temperature and humidity follow the profiles shown in Fig. 8.2 and Fig. 8.3. Note that we considered a day long cycle for both air temperature and humidity. We decided to take into account the second day because of the startup effects.

airflow	*temperature* $[°C]$	*humidity* $[g/kg]$
indoor air	27	15
set point	26	13

Table 8.3: Simulation parameters.

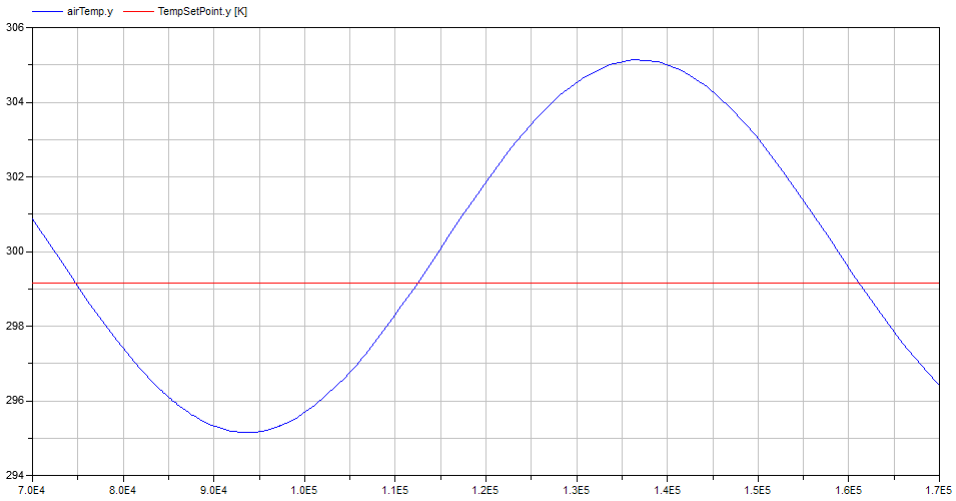

Figure 8.2: External ambient air temperature profile (blue line) and temperature set point (red line).

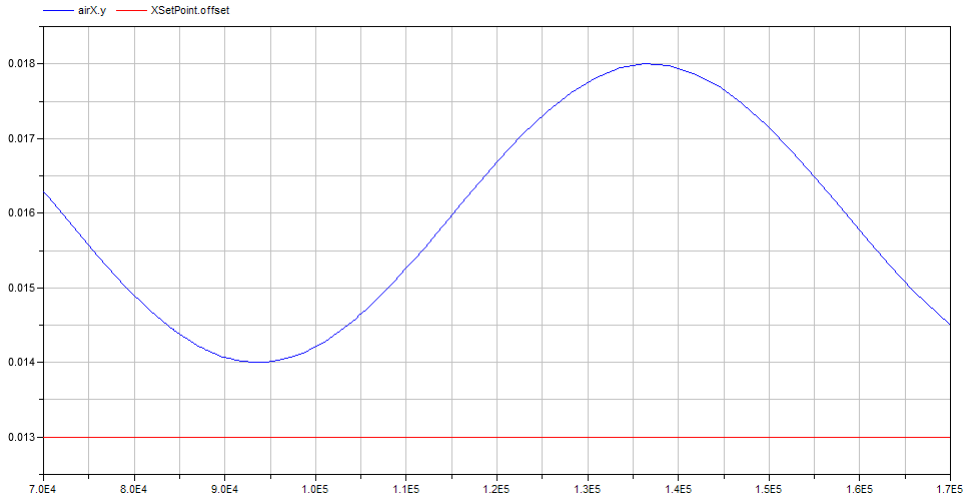

Figure 8.3: External ambient air humidity profile (blue line) and humidity set point (red line).

It is worth noting that the external ambient air temperature is lower than the set point during almost half a period, while the humidity is always higher than the set point. As said in sec. 8.1, the air temperature always increases passing through the wheel. It is clear that if, as in the presented scenario, the process air temperature does not grow enough to excede the set point temperature, we need to increase $Tpro, out$. In Fig. 8.4, we show the simulation results: during a relevant period, the desired air temperature could not be reached since $Tpro, out$ is lower than the set point. Therefore, to reach the desire temperature we should heat the air exits the wheel, but in the presented AHU configuration we have only a cooler after the DW and thus we can only switch it off.

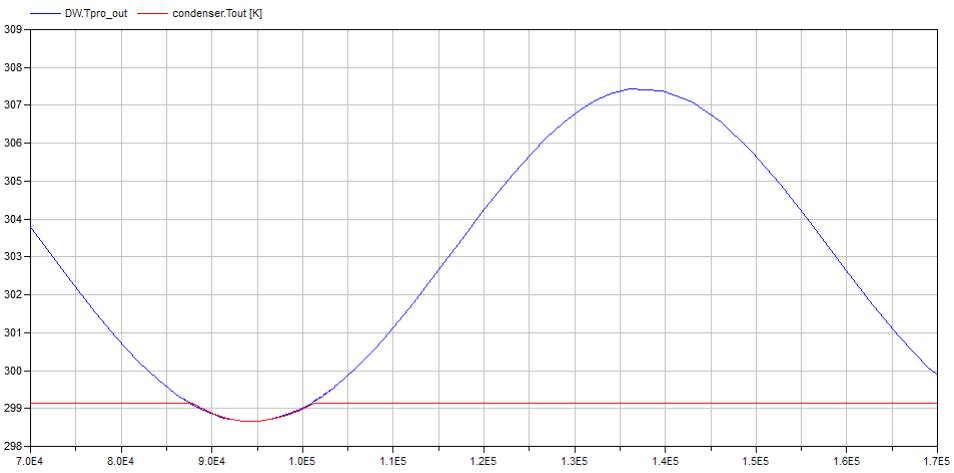

Figure 8.4: DW outlet process air temperature (blue line) and air temperature entering the room (red line).

It is clear that, to reach the desired air conditions, we need to keep $Tpro, out$ always higher than the required air temperature. For such a purpose, we added a PI controller that uses $Tpro, out$ as controlled variable, the wheel velocity as control variable and the same set point of the PI_T controller. A small offset can be added to the set point in order to maintain $Tpro, out$ a little bit higher than the required temperature. The control scheme is shown in Fig. 8.5.

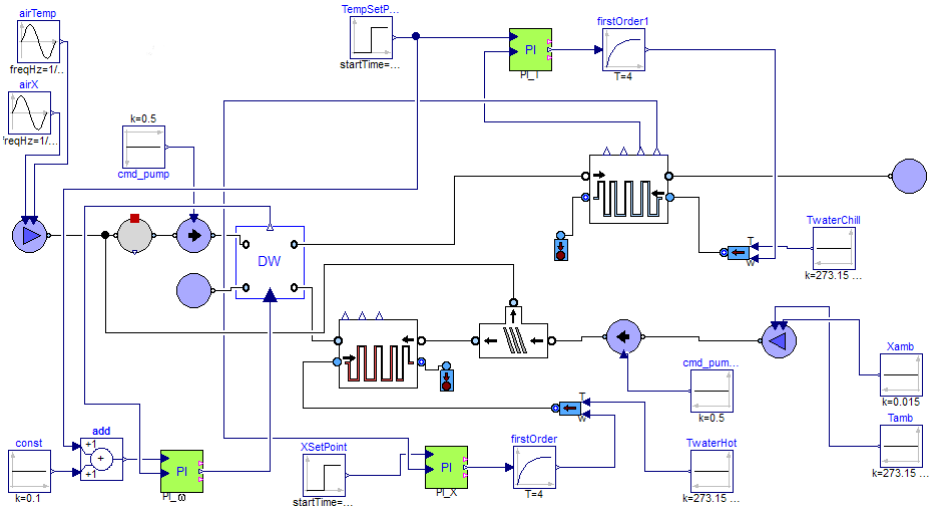

Figure 8.5: AHU with DW model. Wheel velocity control scheme.

The wheel velocity control has to operate only when $Tpro, out$ becomes cooler than the desired temperature set point. Thus, we introduced a minimum saturation level in the control signal. This minimum level must be chosen properly, and a possible method for that choice will be discussed in the next chapter. Obviously, even a maximum saturation value has to be set in order to maintain the wheel in the range of operation. We repeat the previous simulation with the outlined control scheme. In Tab. 8.4 we show the PI_ω parameters.

Controller	kp	Ti	$\omega\ min[rev/h]$	$\omega\ max\ [rev/h]$	$offset$
PI_ω	0.1	200	2	5	0

Table 8.4: PI_ω parameters.

In Fig. 8.6, one can note that $Tpro, out$ is kept as a higher value with respect to the set point for the entire simulation period. Thus, we can ensure the desire air temperature without the need of a post heating.

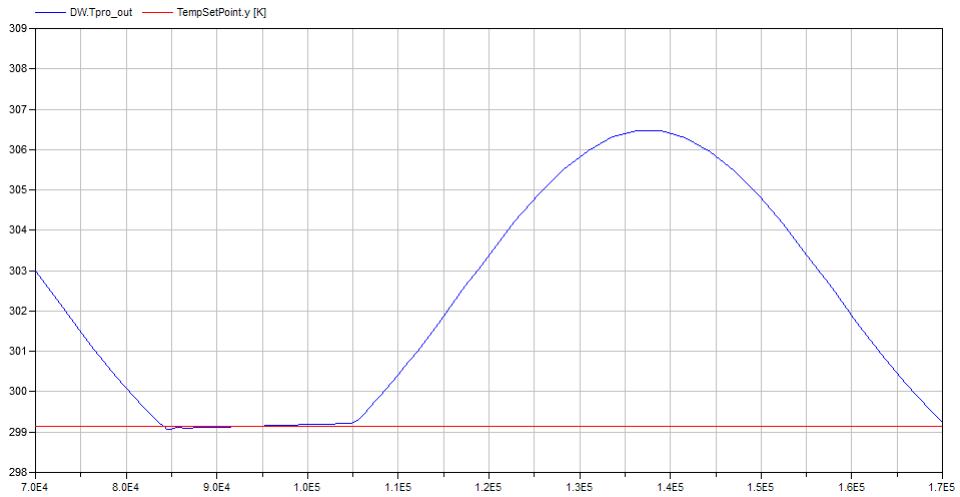

Figure 8.6: DW outlet process air temperature (blue line) and air temperature entering the room (red line).

The wheel velocity control works only when $Tpro, out$ tends to be lower than the desired set point, as shown in Fig. 8.7. When the velocity control is not necessary, the wheel speed is set at the low saturation value. The choice of this value is very important because the wheel operation depends on it for the most of time. Thus, this velocity has to be chosen to guarantee the best performances for the system. The considerations developed in the next chapter for the choice of the best wheel velocity, can be used also to determine this minimum value.

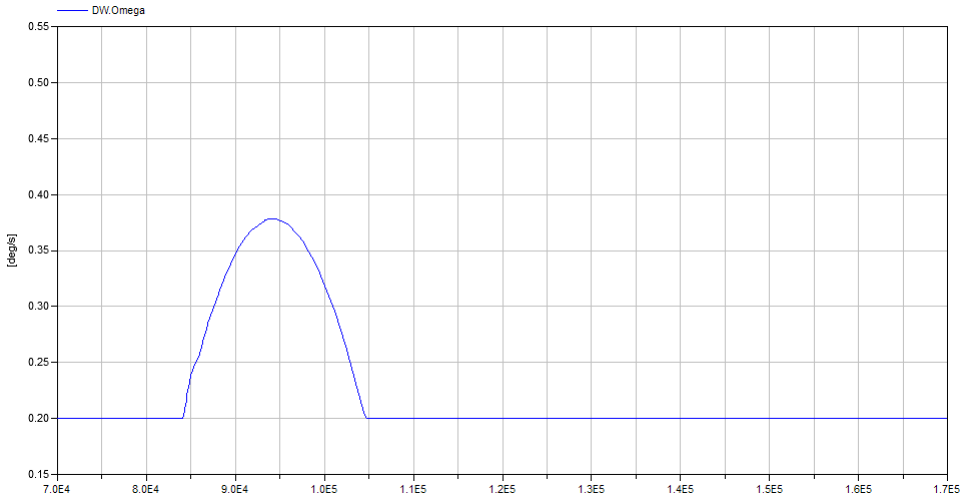

Figure 8.7: Wheel velocity.

9 Wheel velocity choice for energy saving

If we consider the DW operation mode in which we want to dehumidify and cool the process air, the control scheme adopted in chapter 7 is required. However, the choice of the wheel velocity could be made with different approaches. In this chapter, to give just an example of how the idea can be exploited, we pursue the energy saving policy.

9.1 Effect of the wheel velocity on the energy consumption

We focus on the energy consumption of the AHU, and we recall that the critical element is the cooler. Quite intuitively, the energy required by the cooler depends on its inlet air temperature. The higher the inlet air temperature is, the greater the energy consumption will be. The considered temperature depends on the wheel operation and corresponds to $Tpro, out$. Thus, if we succeed in reaching the desired $Xpro, out$ with the minimum $Tpro, out$, the energy consumption of the cooler will be the minimum possible.

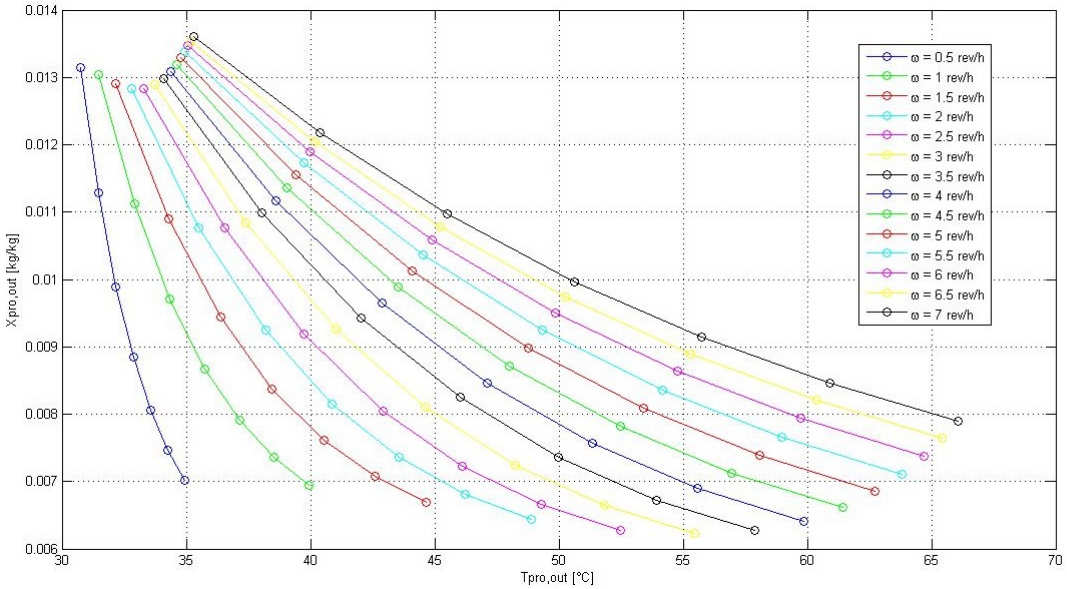

Figure 9.1: Operation range.

Referring to Fig. 8.1, that is here reported again in Fig. 9.1, we can observe that if we choose the lowest wheel velocity that permits to reach the desired air moisture content, the outlet process air temperature reaches the minimum value.

The same figure also shows another interesting result. The same value of $Xpro, out$ is reached for a different value of $Treg, in$ depending on the wheel velocity. For example, if we consider the curves with $\omega = 0.5\ rev/h$ and $\omega = 1\ rev/h$ the same value of $Xpro, out$ is reached for a greater $Treg, in$ in the case of $\omega = 0.5\ rev/h$. Thus, the choice of the minimum velocity results in the need of higher regeneration air temperature to reach the desired humidity value for the process air. The air entering the heater is considered at constant temperature, and obviously, to bring the regeneration air at a high temperature, the heater requires more energy.

Therefore, we have to consider two opposite effects that occur when reducing the wheel velocity: the decrease of cooling energy demand, and the increase of heating energy one.

In order to better visualize this effect, we show some simulation results dealing with the energy demand with respect to different wheel velocities. Fig. 9.2 shows the total energy consumption, while Fig. 9.3 separately shows the heating and cooling energy demand for the same simulations.

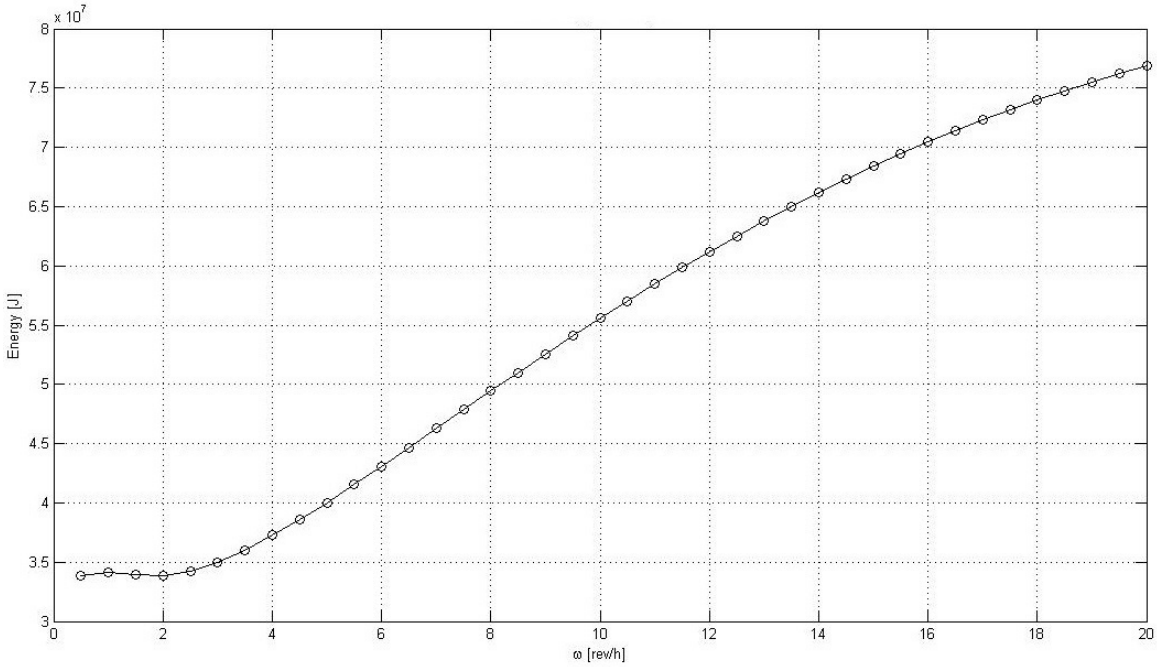

Figure 9.2: Total energy consumption.

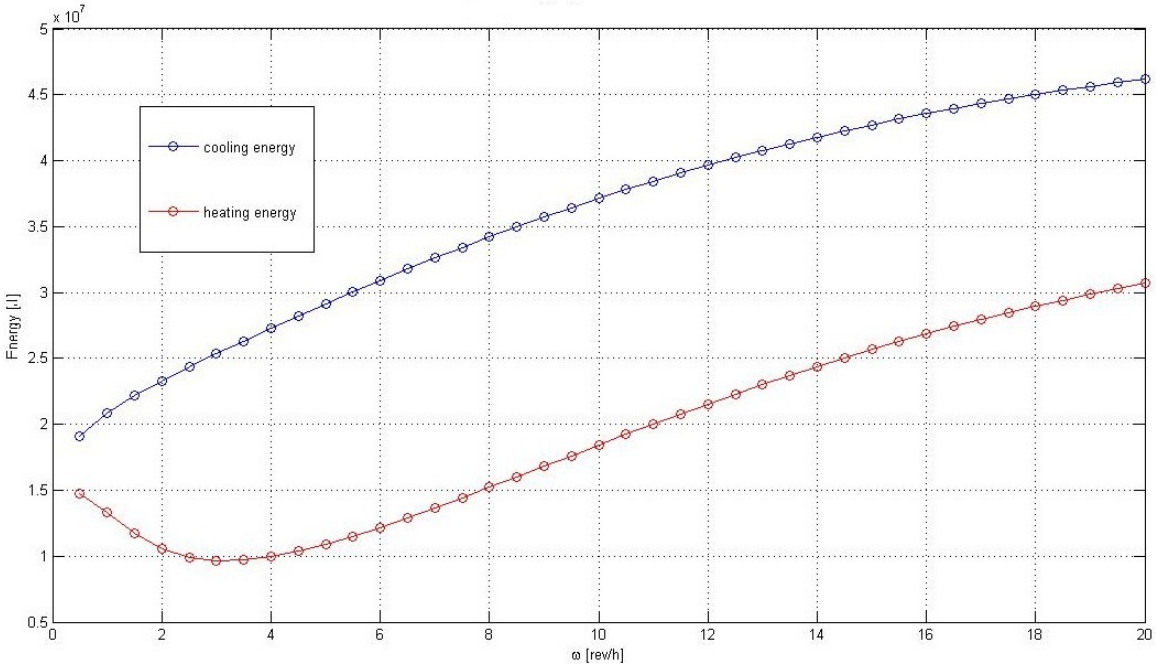

Figure 9.3: Heating and cooling energy consumption.

If we analyze the results, we can notice that the cooling energy has an increasing trend, while the heating energy has a minimum value near $\omega = 3\ rev/h$. For

$\omega < 3\ rev/h$ cooling energy increases while heating energy decreases. Thus, the total energy consumption, for low wheel velocity, results more or less constant. For higher wheel speed, conversely, both the energy consumptions increase with ω, thus the total energy consumption increases considerably.

Summarising, in any case, the previous considerations show that we can minimize the total energy consumption with an appropriate choose of the wheel velocity.

9.2 Total energy demand minimization

We performed some simulations, with the model shown in sec. 7.3, devoted to find the DW velocity that corresponds on the minimum of the AHU energy consumption. Note that the model includes the control scheme, and thus the system is in closed loop.

We decided here too, to define a base case, and two types of simulations. In the first type (type I), we took into account the external air conditions variations due to climate changes. Thus, we maintained the indoor air conditions and varied the external ambient air temperature and humidity. In the second type (type II) of simulations, we considered changes in the desired internal air conditions. Thus, we maintained as constant the external air conditions and varied the humidity and temperature set points.

The temperature and humidity values for external ambient air and controllers' set points, used in the base case and type I simulations, are shown in Tab. 9.1.

Simulation	$Xamb\ [g/kg]$	$Tamb$ [°C]	$Xset\ point\ [g/kg]$	$Tset\ point$ [°C]
base case	17.0	30	13.0	26
simA	**18.0**	30	13.0	26
simB	**16.0**	30	13.0	26
simC	17.0	**32**	13.0	26
simD	17.0	**28**	13.0	26

Table 9.1: Simulations parameters (type I).

Hereafter, we show each simulation result with two figures. In the first one, we show the total energy consumption and in the second one, we show a comparison between cooling and heating energy. Fig. 9.4 and Fig. 9.6 show the total energy consumptions depending on the wheel velocity. The first figure shows the simulations in which a change in the ambient humidity is performed, while the second one deals with simulations with a different ambient temperature, referring to the base case.

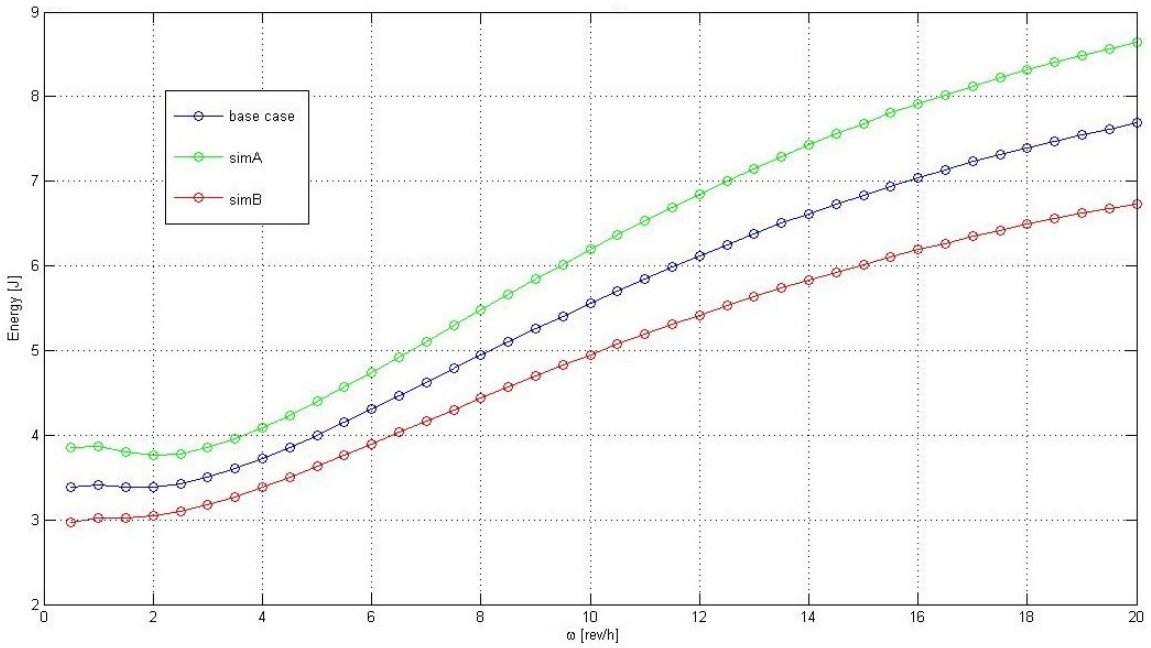

Figure 9.4: Total energy consumptions for simulations A and B.

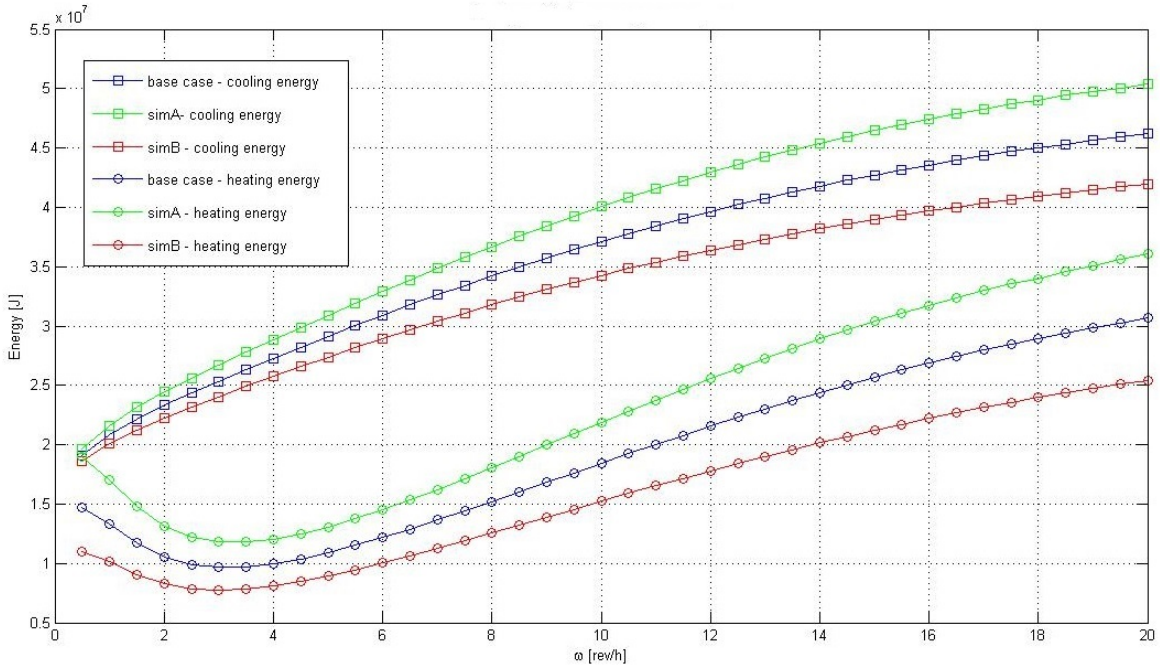

Figure 9.5: Cooling and heating energy consumptions for simulations A and B.

Watching at Fig. 9.5, we can also note that the heating energy is related to the dehumidification demand. If we desire a higher dehumidification, the trend of the

heating energy is more accentuated. Thus, the total energy consumption exhibits a minimum, that depends on the heating energy curve.

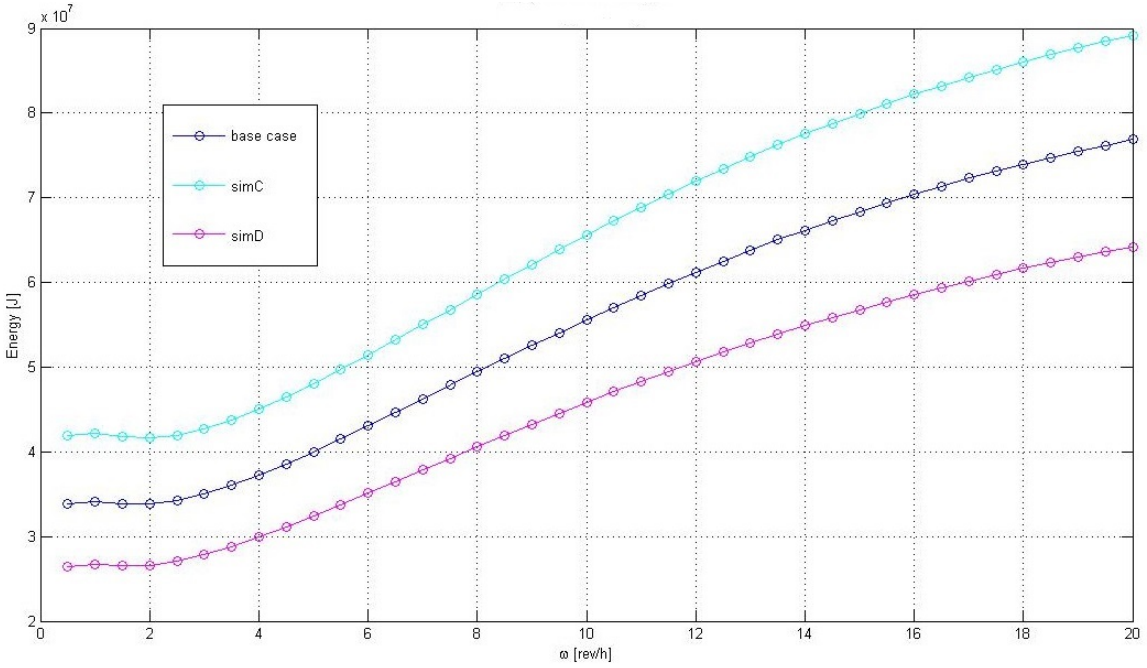

Figure 9.6: Total energy consumptions for simulations C and D.

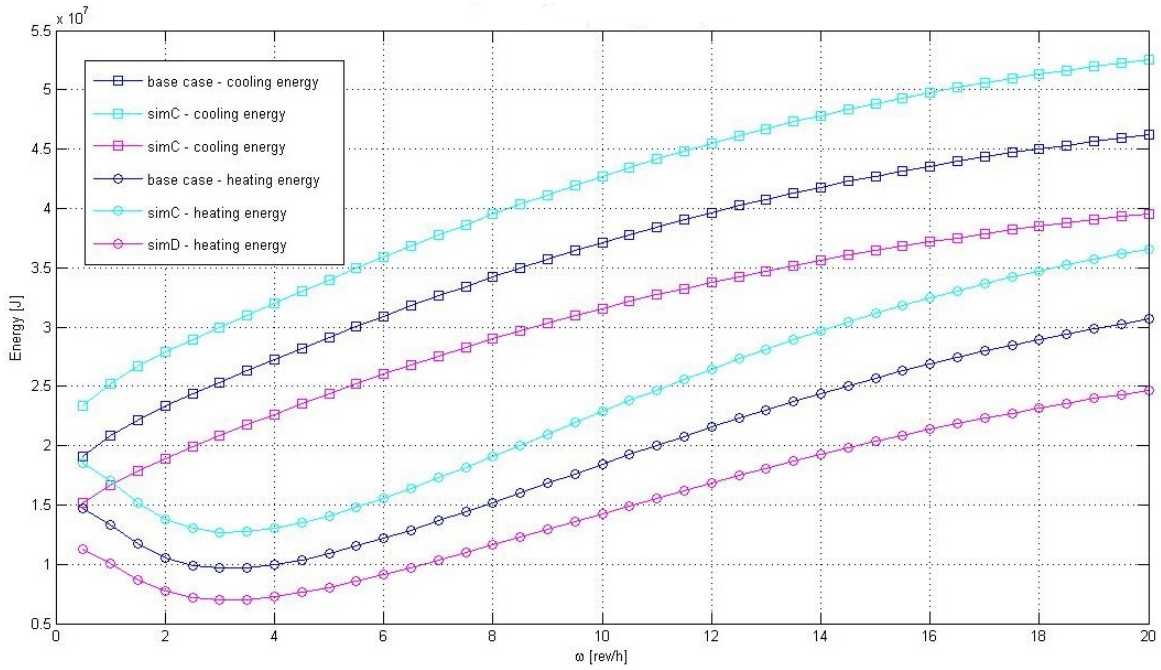

Figure 9.7: Cooling and heating energy consumptions for simulations C and D.

For $\omega < 2\ rev/h$ we have more or less the same total energy consumption for each simulation, but for greater value of ω we have a relevant increase in the consumption.

Therefore, a choice of DW velocity under $2\ rev/h$ seems to be the best for all possible ambient conditions changes around the considered scenario, that is represented by the base case.

Now, we analyze the second type of possible operating conditions changes. The temperature and humidity set points values, used in the base case and type II simulations, are shown in Tab. 9.2.

Simulation	$Xamb\ [g/kg]$	$Tamb$ [°C]	$Xset\ point\ [g/kg]$	$Tset\ point$ [°C]
base case	17.0	30	13.0	26
simE	17.0	30	**12.0**	26
simF	17.0	30	**14.0**	26
simG	17.0	30	13.0	**25**
simH	17.0	30	13.0	**27**

Table 9.2: Simulations parameters (type II).

Fig. 9.8 and Fig. 9.10 show the total energy consumption for these simulations. As said for type I simulations, for $\omega < 2\ rev/h$ we have more or less the same energy consumption for each simulation, but for greater values of ω we have a relevant increase in the energy demand, especially if we desire a greater dehumidification (simE). It is worth noting that if we desire a lower or higher air temperature, the consumption curves (simG and simH) differ from the base case only by a (practically constant) offset. This is because the temperature control does not involve directly the wheel operation, hence the increase of energy demand is due only to the cooling energy. Thus, in Fig. 9.11 we can see that the heating energy consumption is almost the same for the base case and for simulations G and H.

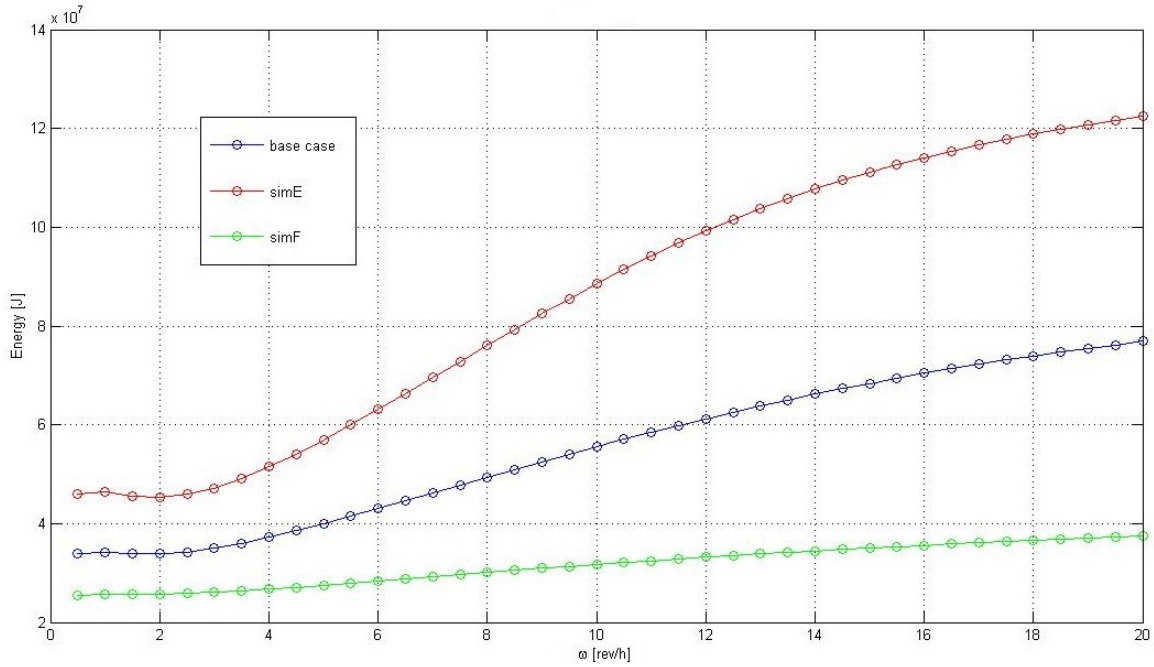

Figure 9.8: Total energy consumptions for simulations E and F.

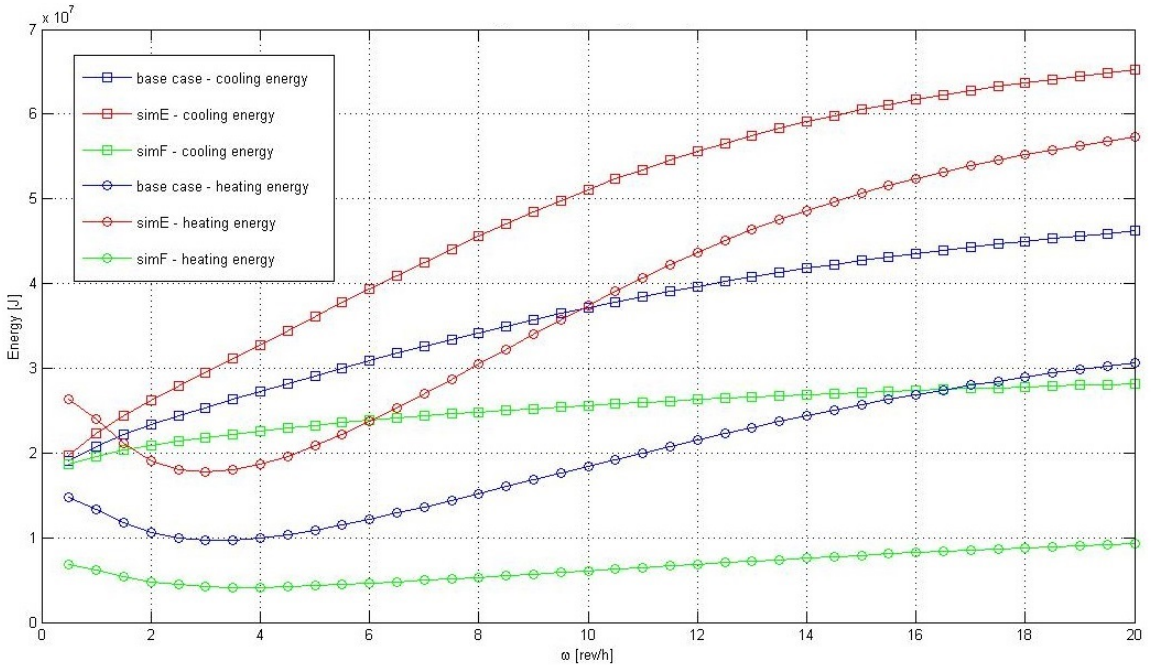

Figure 9.9: Cooling and heating energy consumptions for simulations E and F.

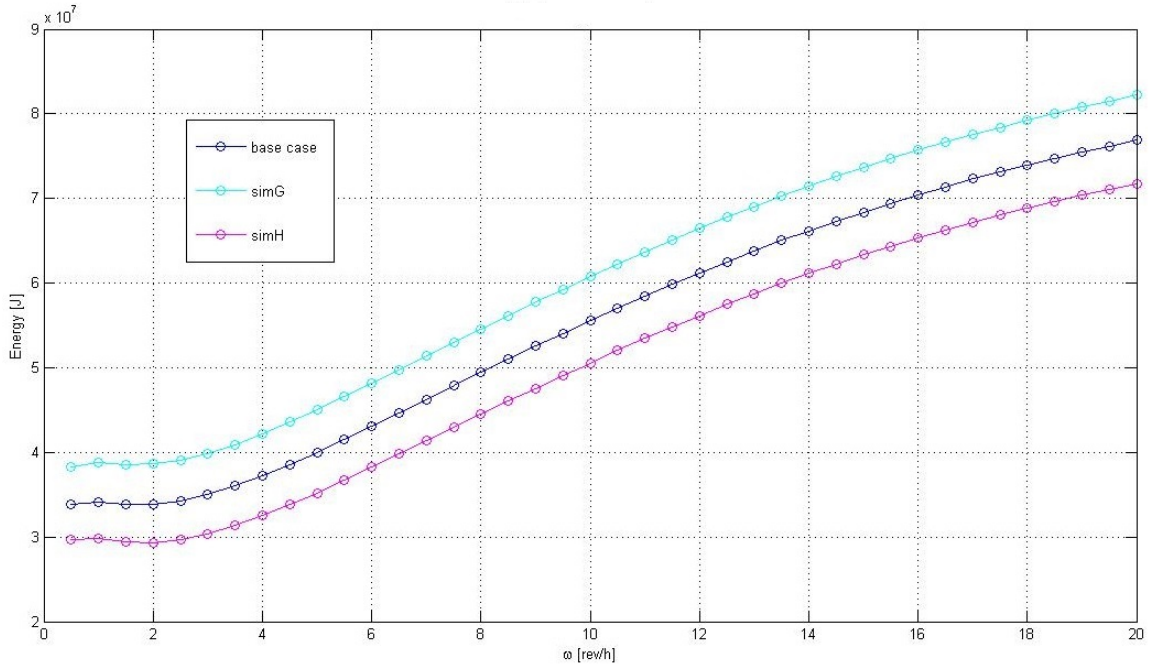

Figure 9.10: Total energy consumptions for simulations G and H.

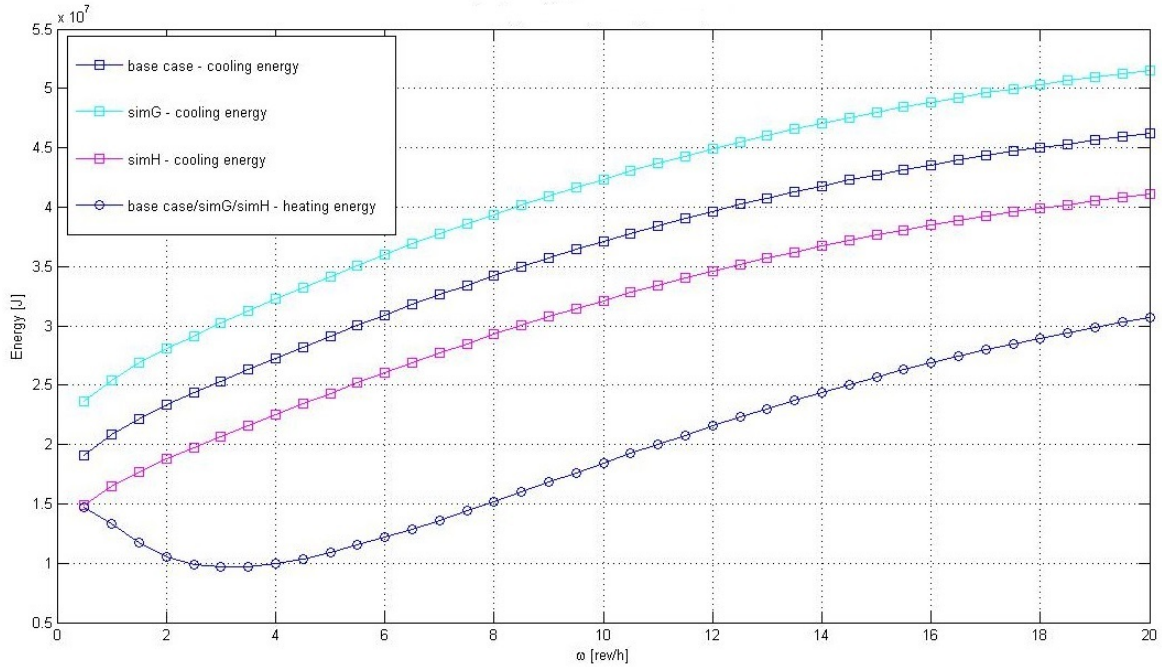

Figure 9.11: Cooling and heating energy consumptions for simulations G and H.

Referring to all the simulations, it seems reasonable to choose $\omega < 2\ rev/h$, in order to minimize the total energy consumption.

As said before, the minimization of the total energy is a way to take into account both the cooling and the heating consumptions depending on the wheel velocity. Another interesting choice could be the minimization of the cooling energy only in some operative conditions. This choice could be better, referring to the total energy minimization, if e.g. we can use the heat of recovery from other applications to regenerate the wheel. In the following section, we analyze the wheel velocity choice considering only the cooling energy.

9.3 Cooling energy demand minimization

Fig. 9.12, Fig. 9.13, Fig. 9.14 and Fig. 9.15 show the results of the simulations used in the previous section, concentrating however on the cooling energy. If we consider only the cooling energy demand, it is clear that the choice of the DW velocity as the minimum as possible is the right one. This assumption, mentioned before, when we deal with $Tpro, out$ minimization, is supported by the simulations results. If we use, for the wheel regeneration, a low temperature heat source, we have also to consider the feasibility of the process because reducing the wheel velocity, the regeneration air temperature demand increases.

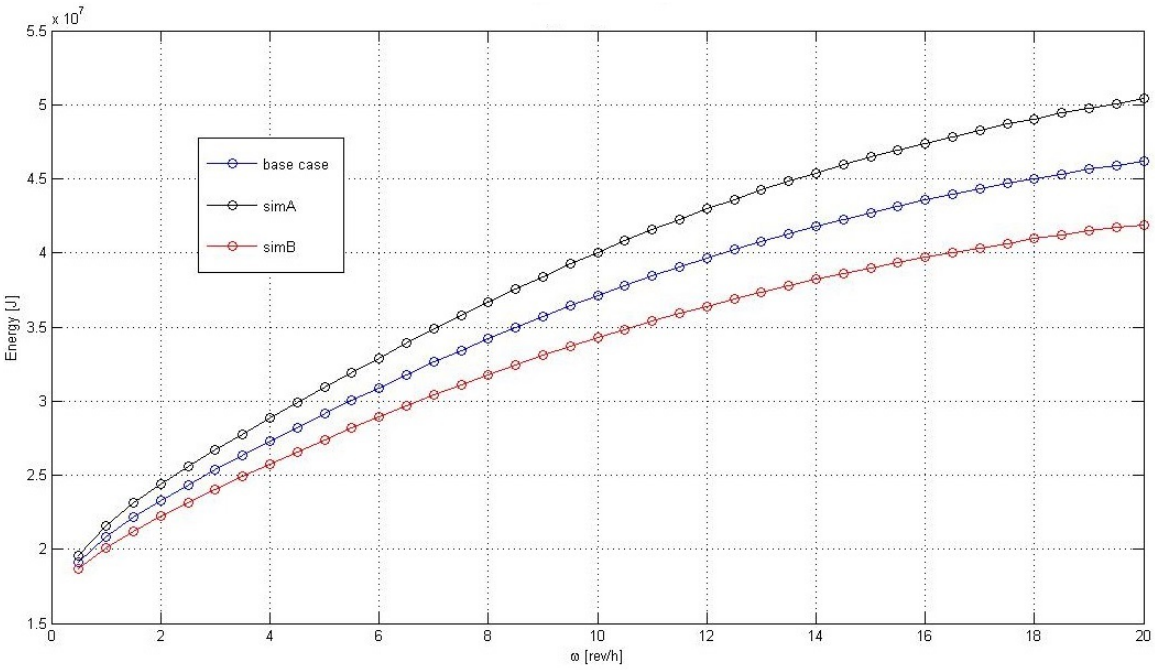

Figure 9.12: Cooling energy consumptions for simulations A and B.

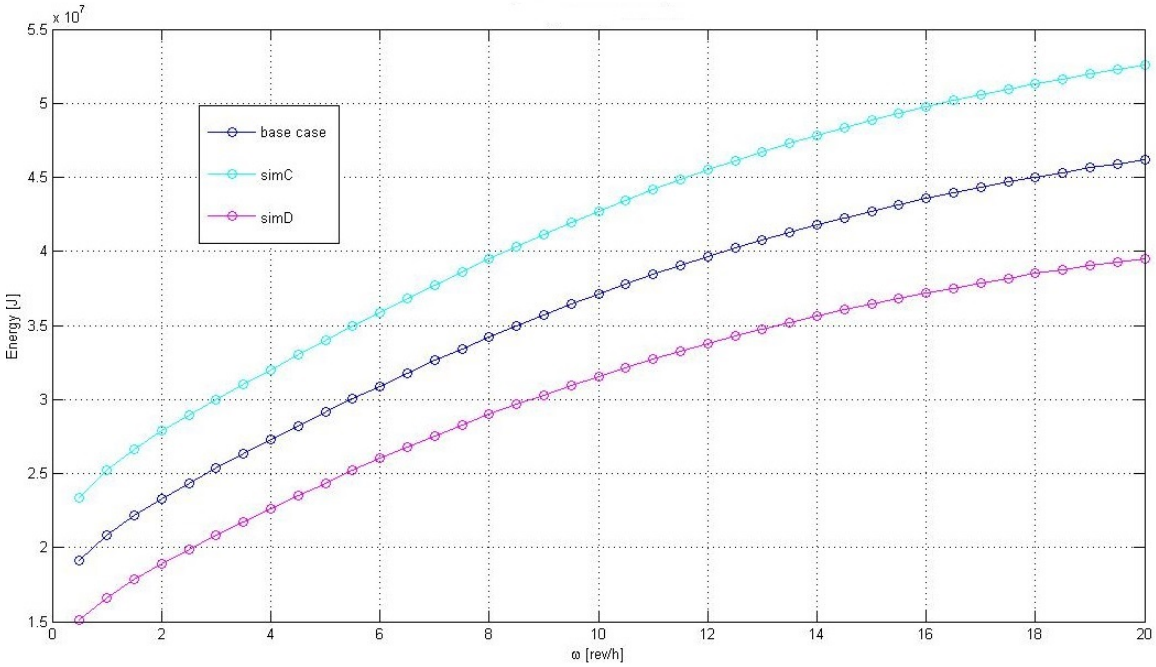

Figure 9.13: Cooling energy consumptions for simulations C and D.

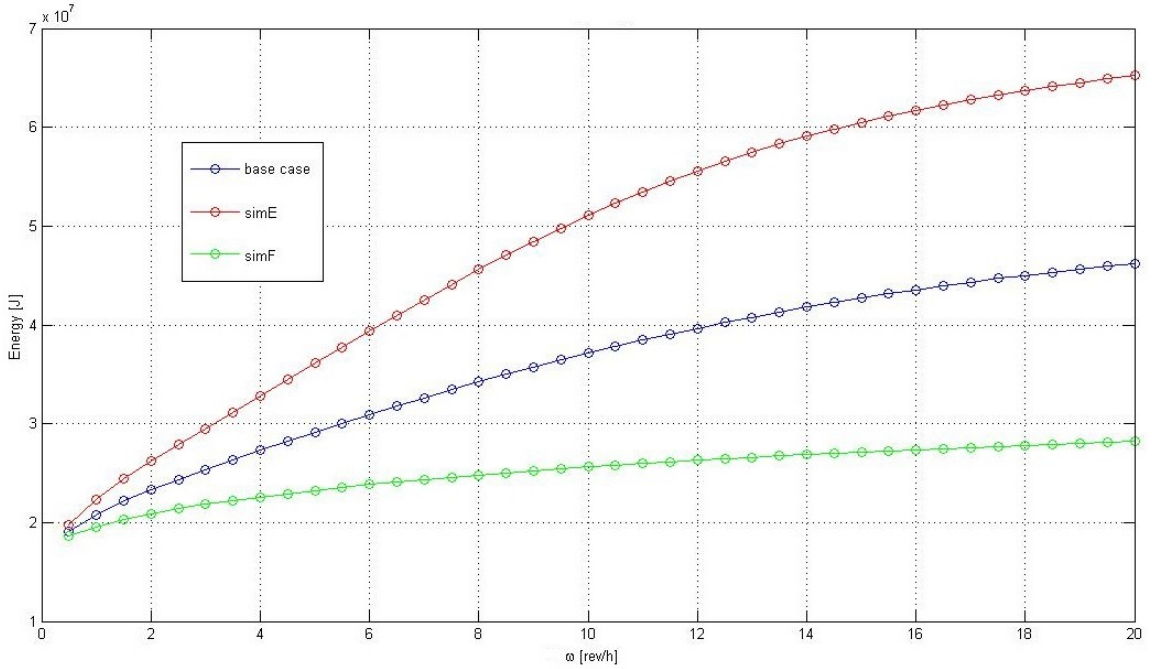

Figure 9.14: Cooling energy consumptions for simulations E and F.

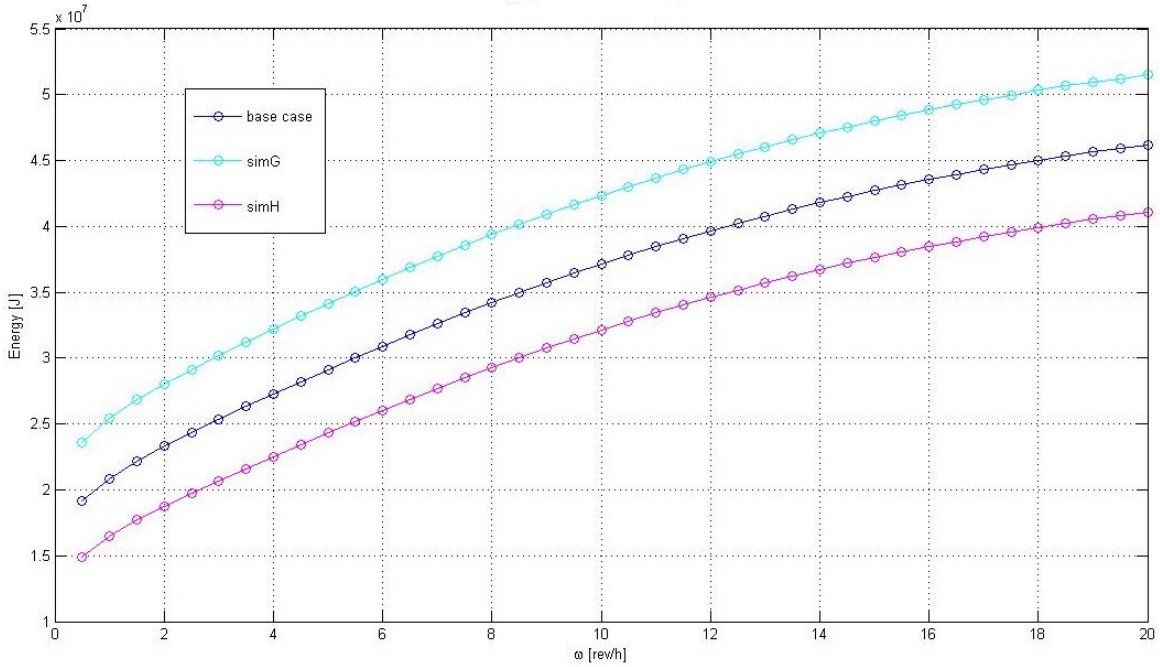

Figure 9.15: Cooling energy consumptions for simulations G and H.

9.4 System performances with different choice of wheel velocity

To conclude the chapter, we can show a (preliminary) investigation on whether a different choice of the wheel velocity affects the control system performances. To this end, we decided to make a simulation with $\omega = 0.5\ rev/h$. We choose such a value because it is the one, in the optimal operating range ($\omega < 2\ rev/h$), that is farthest from the value we used in sec. 7.3 ($\omega = 3\ rev/h$). We compare the system performances with $\omega = 3\ rev/h$ and $\omega = 0.5\ rev/h$ in terms of air humidity, Fig. 9.16, and and temperature responses, Fig. 9.17.

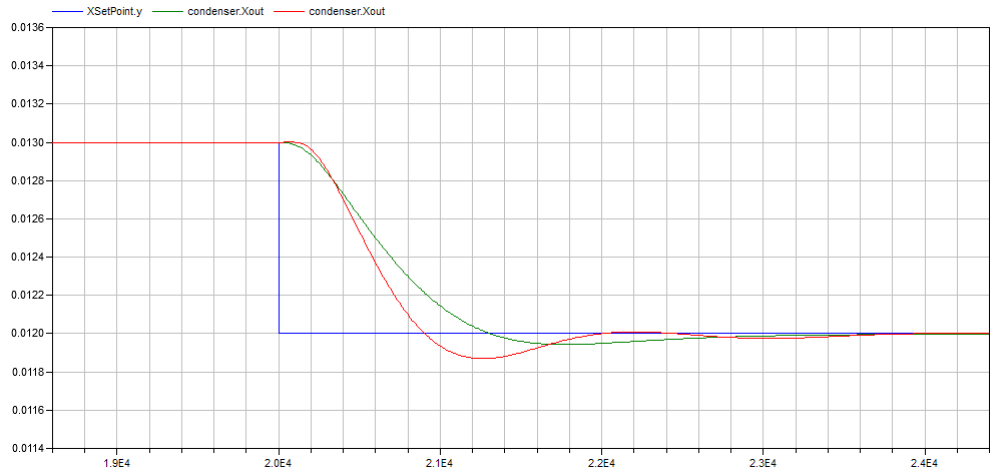

Figure 9.16: Step change in humidity set point and air humidity response. Comparison between AHU with DW: $\omega = 3\ rev/h$ (red line) and $\omega = 0.5\ rev/h$ (green line).

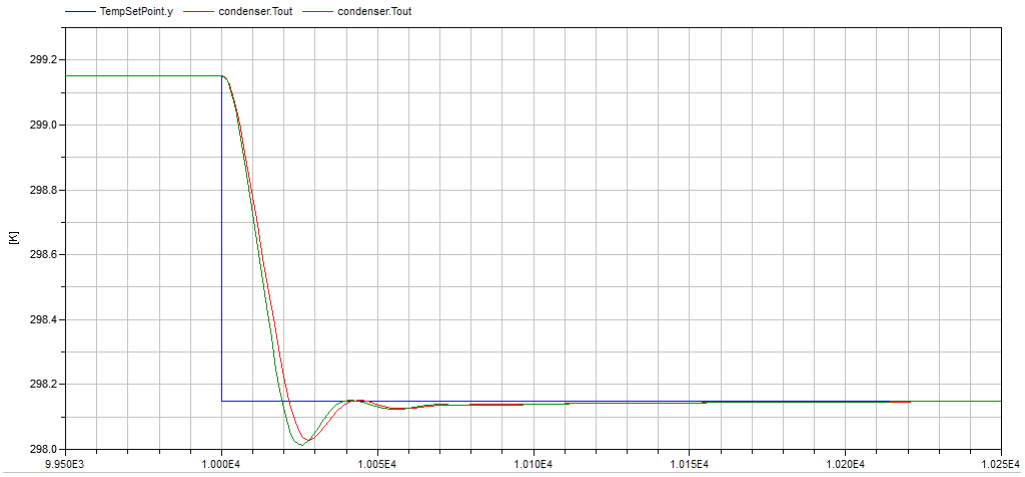

Figure 9.17: Step change in temperature set point and air temperature response. Comparison between AHU with DW: $\omega = 3\ rev/h$ (red line) and $\omega = 0.5\ rev/h$ (green line).

We can notice that the control system behavior is quite similar in both the cases, and the desired system performances are preserved. Thus, the use of a quite different wheel velocity affects the energy consumption without changing the system behavior significantly. In Fig. 9.18 and Fig. 9.19, the cooling and heating energy consumptions for the different DW velocities are shown. In Tab. 9.3, the energy consumptions during the entire simulation period of 50000 sec ($\backsimeq$13.88 hours) are listed. In extreme synthesis, although the matter requires further research as already stated, we can say that the total energy saving is confirmed by the simulations.

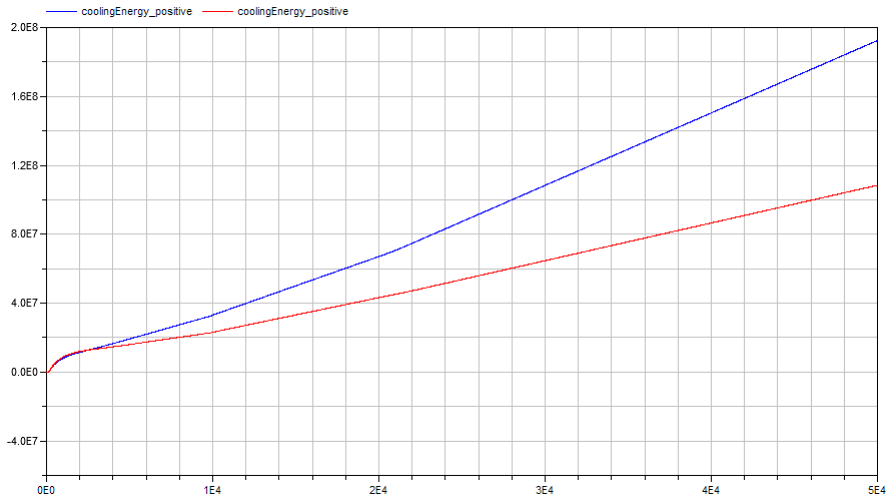

Figure 9.18: Cooling energy consumption. Comparison between AHU with DW: $\omega = 3\ rev/h$ (blue line) and $\omega = 0.5\ rev/h$ (red line).

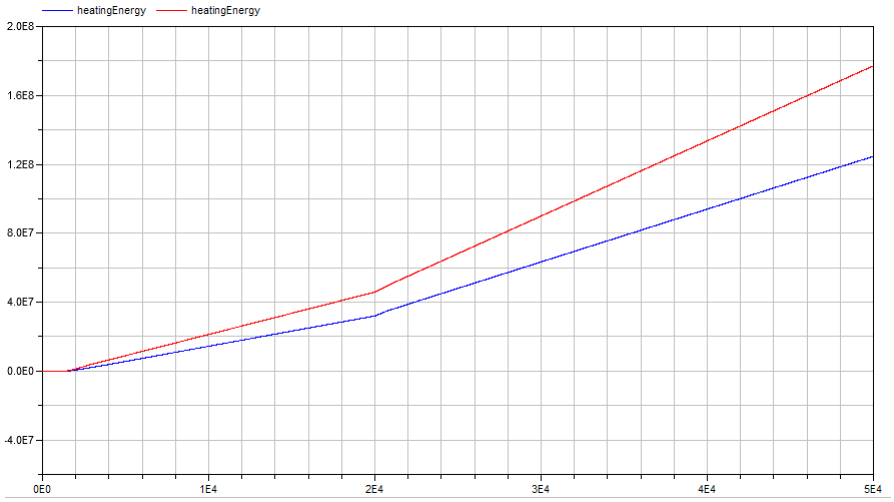

Figure 9.19: Heating energy consumption. Comparison between AHU with DW: $\omega = 3\ rev/h$ (blue line) and $\omega = 0.5\ rev/h$ (red line).

Energy consumption	$\omega = 3\ rev/h$	$\omega = 0.5\ rev/h$
Cooling energy [kWh]	53.5	30.1
Heating energy [kWh]	43.7	49.2
Total energy [kWh]	97.2	79.3

Table 9.3: Energy consumptions. Comparison between AHUs with DW.

10 Conclusions

In this dissertation, dynamic modelling and simulation of desiccant wheels were addressed. The presented work is part of a long-term research on energy efficiency in HVAC systems, and in that context, its primary goal is to investigate the dynamic behavior of desiccant wheels, particularly in a view to using such devices for energy efficiency improvements in air handling units.

To this end, first the theory of operation of desiccant wheels was analyzed (Capitolo 2), based on first-principle considerations and on a convenient review of related work, reported in Capitolo 3. A specific character of the reported analysis is its focus on dynamic models oriented to system-level studies, that apparently have to consider also the control system. As a result, in Capitolo 4, a dynamic model of a DW was proposed, and then validated in chapter 5. The presented model has an intermediate complexity with respect to the two main alternatives in the literature, and thus - as illustrated - it is suitable for our purposes. One of the main advantages of using the presented model is that the results can be easily interpreted, because of the physical meaning of the parameters. Further, also the choice of how to model the wheel motion brings some relevant advantages both in the efficiency of the model and the understanding of the simulation results. Thus, the model is suitable for both system-level studies and control purposes, and can also be integrated with others from different physical domain thanks to its OOM character.

In chapter 7, the focus was moved from the DW model to a wider context in which the model can be integrated, namely - to stick to the dissertation scope - that of an AHU for an HVAC system. We proposed some control schemes for both a standard AHU and an AHU with DW and we performed an energy consumption comparison, thus confirming the saving yielded by use of the DW based solution.

In chapter 8 we investigated some alternative (with respect to the traditional solutions) control approaches, specifically aimed - among the various and often conflicting possible objectives - at energy efficiency. The possibility and opportunity of using the DW velocity as a control variable was synthetically analyzed, and we also proposed a temperature control strategy using the DW velocity. Another approach, dealing with the wheel velocity, is shown in chapter 9 in which we proposed a method, devoted to minimize the energy consumption of the AHU, by choosing an appropriate value for the DW velocity.

Future research will be devoted to investigate case studies of higher complexity and different control approaches in a rigorous manner, with the aim to better exploit the model advantages in the context of energy efficiency and design optimization.

List of Figures

List of Tables

Bibliography

[1] A.Joos, G.Schmitz, and W.Casas. Enhancement of a modelica model of a desiccant wheel. *Modelica*, 2008.

[2] A.Kodama, M.Goto, and T.Hirose. Experimenatal study of optimal operation for a honeycomb adsorbent operated with thermal swing. *Journal of Chemical engineering of Japan*, 26:530–535, 1993.

[3] A.Kodama, T.Hirose M.Goto, and T.Kuma. temperature profile and optimal rotational speed of a honeycomb rotor adsorber operated with terma swing. *Journal of Chemical engineering of Japan*, 27:644–649, 1994.

[4] A.Kodama, T.Hirose M.Goto, and T.Kuma. Performance evaluations for a thermal swing honeycomb rotor using a humidity chart. *Journal of Chemical engineering of Japan*, 28:19–24, 1995.

[5] M.Goto A.Kodama, T.Hirayama, T.Hirose, and R.Critoph. The use of psychrometric charts for the potimisation of a thermal swing desiccant wheel. *Applied Thermal Energy*, 21(16):1657–1674, 2001.

[6] H.S. Al-Sharqawi and N.Lior. Effect of flow-duct geometry on solid desiccant dehumidification. *Ind. Eng. Chem. Res.*, 47:1569–1585, 2008.

[7] S. De Antonellis, C.M.Joppolo, and L.Molinaroli. Simulation, performance analysis and optimization of desiccant wheels. *Energy and Buildings*, 42:1386–1393, 2010.

[8] B.O.Glav. Air conditioning apparatus. Patent No.3,251,402, 1966.

[9] Y.Li D.La, Y.J. Dai, R.Z.Wang, and T.S.Ge. Technical development of rotary desiccant dehumidification and air conditioning: A review. *Renewable and Sustainable Energy Revuews*, 14:130–147, 2010.

[10] D.Murayama, K.Mitsumoto, and S.Yamamori Y.Takagi, Y.Iino. Smart grid ready bems adopting model-based hvac control for energy saving.

[11] J.J. Jurinak. *Open-cycle solid desiccant cooling. Component models and system simulation.* PhD thesis, University of Wisconsin, Madison, 1982.

[12] F.Butera M.Beccali, R.Guanella, and R.S.Adhikari. Simplified models for the performanche evaluation of desiccant wheel dehumidification. *International Journal of Energy Res*, 27(1):17–29, 2003.

[13] M.Bonvini and A.Leva. Modelling and control of desiccant wheel for energy-efficient air handling units.

[14] N.A.Pennington. Humidity changer for air conditioning. Patent No.2,700,537, 1955.

[15] I.Postlethwaite S.Skogestad. *Multivariable Feedback Control - Analysis and Design*. Wiley, 2005.

[16] Y.Li T.S.Ge, R.Z.Wang, and Y.J. Dai. A review of the mathematical models for predicting rotary desiccant wheel. *Renewable and Sustainable Energy Revuews*, 12:1485–1528, 2008.

[17] W.Casas, K.Prolb, and G.Schmitz. Modeling of desiccant assisted air conditioning systems. *Proceedings of the 4th International Modelica Conference*, 2005.

[18] A.L. London W.M. Kays. *Compact Heat-Exchangers*. third edition, 1984.